# Characterization of ACA-01 a Chemokine-binding Tick Evasin

Sayeeda Tasneem Chowdhury
*B.Pharm (Hon's), Ms. Pharm Tech*

A thesis submitted for the degree of Master of Philosophy (M. Phil) at
Monash University in 2020
Department of Biochemistry and Molecular Biology
Faculty of Medicine, Nursing and Health Sciences

**Abstract:**

Chemokines are mammalian proteins that regulate the migration of leukocytes, a central feature of inflammatory responses. Chemokines exert their activity by activation of G protein-coupled receptors (GPCRs) expressed on the target leukocytes. Inflammation is a natural response to injury. In the incidence of injury, chemokines recruit leukocytes from the blood to sites of infection or tissue damage. Chemokine receptors expressed on the leukocytes interact with more than one chemokine and vice versa. The complexity of the chemokine-receptor interaction network makes it difficult to engineer targeted drug therapy. However, in nature, ticks have the solution to this complexity. As a strategy to suppress the inflammatory responses of their mammalian hosts and thereby prolong their feeding and residence times, ticks have evolved the ability to produce salivary proteins, known as Evasins, which bind to host chemokines, blocking activation of chemokine receptors and preventing leukocyte migration. ACA-01 is an Evasin found in the tick species *Amblyomma cajanennense*, containing 8 cystine residues which form four intramolecular disulfide bonds. We aimed to establish that ACA-01 is a chemokine-binding protein and solve its crystal structure. An N-terminal SUMO-tag was used for the soluble expression of ACA-01 in an *E. coli* expression system. Analysis of the purified ACA-01 was conducted via ASEC and Mass Spectrometry (MS), the results of which suggested that ACA-01 may exist as a mixture of monomer and non-covalently bonded dimers. We report binding of ACA-01 to a panel of six CC chemokines using a Fluorescence Anisotropy (FA) assay. The interaction of ACA-01 was observed to be the strongest with CCL7/MCP-3 with an equilibrium dissociation constant ($K_d$) of 3 nM ($pK_d$ = 8.56 ± 0.26). After crystallization trials, we successfully obtained needles of ACA-01 protein crystals, the size of which was not sufficient to produce X-ray diffraction. However, the trial results will be extremely useful for future structure elucidation through optimization of the conditions in which the needles were formed. These studies will establish a foundation for developing ACA-01 as a potential anti-inflammatory therapeutic.

**Publications during enrolment**

1. Franck, C., Foster, S.R., Johansen-Leete, J., **Chowdhury, S**., Cielesh, M., Bhusal, R.P., Mackay, J.P., Larance, M., Stone, M.J. and Payne, R.J., 2020. Semisynthesis of an evasin from tick saliva reveals a critical role of tyrosine sulfation for chemokine binding and inhibition. Proceedings of the National Academy of Sciences, 117(23), pp.12657-12664.
2. **Chowdhury S**, Bhusal R, Stone M. J., Functional Analysis of ACA 01, A Novel Chemokine-Binding Tick Evasin. *Award Winners and Abstracts of the 33rd Annual Symposium of The Protein Society* 2019; 8(S1).
3. Bhusal, R.P., Eaton, J.R., **Chowdhury, S.T**., Power, C.A., Proudfoot, A.E., Stone, M.J. and Bhattacharya, S., 2020. Evasins: Tick salivary proteins that inhibit mammalian chemokines. *Trends in Biochemical Sciences*, 45(2), pp.108-122.

**Declaration**

This thesis is an original work of my research and contains no material which has been accepted for the award of any other degree or diploma at any university or equivalent institution and that, to the best of my knowledge and belief, this thesis contains no material previously published or written by another person, except where due reference is made in the text of the thesis.

Signature

Print Name: Sayeeda Tasneem Chowdhury

Date: 02 07 2020

**Acknowledgement**

I am starting in the name of Almighty who has given me every opportunity and good health to be able to finish this thesis for fulfillment of my MPhil degree.

I acknowledge the Traditional Custodians of the land on which I work and live, and recognise their continuing connection to land, water and community. I pay respect to Elders past, present and emerging.

This thesis would never have been possible without my son, Md. Imaan Benyameen Kabir, who has been an amazing child, always calm and composed. His demeanour has made this tough journey, of raising a child in addition to completing a degree single-handedly, a pleasant learning experience.

I am forever grateful to my main supervisor, Associate Professor Martin Stone, Department of Biochemistry and Molecular Biology, Faculty of Medicine, Nursing and Health Sciences, for giving me the opportunity to complete my thesis under his supervision. Thank you for all the advice, the kindness and support when it got tough for me. Your teaching skills and learning methods have helped me immensely and I am going to greatly value what you have taught me. I have never come across anyone so invested in research ethics and methodology as you are, and it is my absolute pleasure to have learned so much from you.

I cannot thank Professor Jacqueline Wilce enough, for her patience with me. When I started writing my thesis, it was far behind perfect, and you have worked so hard to give it the finesse it has today. Jackie, your simplistic style of explaining things, made it so much easier to understand the context. You never gave up on me, even when I was self-doubting. Your feedback has helped me becoming better at writing.

I want to express my love and gratitude for my father Late Chowdhury Mohammad Azizul Haque. The very short period we were together, he taught me everything that is right and had built my base as a human being. I would like to thank my mother, Shireen Chowdhury and my sister Assistant Professor Sayeeda Fahmee Chowdhury, who supported me through thick and thin. My sister has always motivated me when I was not at the top of my spirit.

I will forever be indebted to my best friend, Dr Rajib Majumder. He has been a rock during my research journey. Without him, I barely could have made it. I would like to mention the contribution of Dr. James Rundle in constantly keeping my mental health at check. I know it was his professional duty, but I would forever be indebted.

I would also like to thank Professor Matthew Wilce for providing me with advice when I needed; Dr Ram Bhusal, for his guidance regarding the expression of ACA-01; Dr Herman Lim, who offered me his laptop to finish writing my thesis; and Jenni Hayward, who helped me learn protein expression and purification when I first started; Cheng Huang (Enzo) for helping me with Mass Spectrometry.

I extend my gratitude to my cousin Dr. Silvia Zia, who is a blessing in my life. Utmost thanks to Dr Simon Foster, Pramod Aryal, Shankar Raj Devkota, Julie Sanchez, Baidaa Hirmiz for creating a pleasant working environment for me while I was working. I am grateful to my friends Shagufta Binte Zakir and Farhana Ahmed Shegufta for being there with me.

I would like to extend my thanks to Dr Sunshine Kamaloni and Associate Professor Priscilla Johanesen. They stood by me when I was at my low and they gave me the love and inspiration to move forward.

Lastly but not least thanks to Monash Graduate School and Faculty of Medicine Nursing and Health Sciences for awarding me the scholarships which has made it financially possible to have finished this thesis.

**Thesis Outline: Characterization of ACA 01- A Chemokine-Binding Novel Tick Evasin**

## Chapter 1: Introduction

1.1. Inflammation and Aetiology

1.2. Chemokines and its structure

1.3. Chemokine Receptor

1.4. Interactions between Chemokines and Chemokine Receptors

1.5. Evasins

1.6. Identification of Evasins from Numerous Tick Species

1.7. Classification and Nomenclature of Evasins

1.7.1. Class A Evasins

1.8. Evasin Structure and Receptor Binding Interaction

1.9. Evasins in disease models

1.10. Expression and purification of Evasins

1.11. Introduction to ACA-01 – a chemokine-binding novel tick Evasin

## Chapter 2: Materials and Methods

2.1. Media, Buffers and Solutions Chemokines

2.2. Bacterial Culture

2.2.1. Competent cell preparation

2.2.2. Transformation of DH5α and BL21 DE3

2.3. Protein Production and Purification

2.3.1. Expression and Harvest

2.3.2. Purification

2.4. Fluorescence Anisotropy Assay

2.4.1. Direct Binding Assay

2.4.2 Competitive Binding Assay

2.5. Stability Studies

2.5.1 Thermal Shift Assay

2.5.2 Crystallisation trials

# Chapter 1: Introduction

## 1.1. Inflammation and its Aetiology

Inflammation is the body's natural response to injury. The role of inflammation is more widely recognised both as a healing, restorative process, in addition to its aggressive role. Inflammation is considered as a sequence of events, from initiation of a response, through to the development of the basic signs such as *dolor* (pain), *rubor* (redness), *calor* (heat), *tumor* (swelling), and *function lesa* (loss of function), to healing and restoration of normal appearance and function of the tissue or organ (Punchard Neville, 2004).

Controlled inflammation including wound healing is usually self-limiting, however, uncontrolled regulation of any of the contributing factors can lead to abnormalities and ultimately, pathogenesis, for example, neoplastic progression. Inflammation can be largely divided into acute and chronic based on the length of response. Acute inflammation is the body's initial response to a sudden threat, including pathogen, infection or tissue damage. It involves the increased movement of leukocytes to the site of inflammation (Han, 2005). Chronic or prolonged inflammation has similar features to that of acute inflammation but over prolonged and repeated stages. A progressive change in the type of cells present at the site of inflammation is noticed in chronic inflammation which generates the simultaneous destruction and repair of the tissue. A certain number of diseases can be caused by chronic inflammation such as atherosclerosis, rheumatoid arthritis (RA), diabetes, allergies, hay fever, asthma, periodontitis and even cancer.

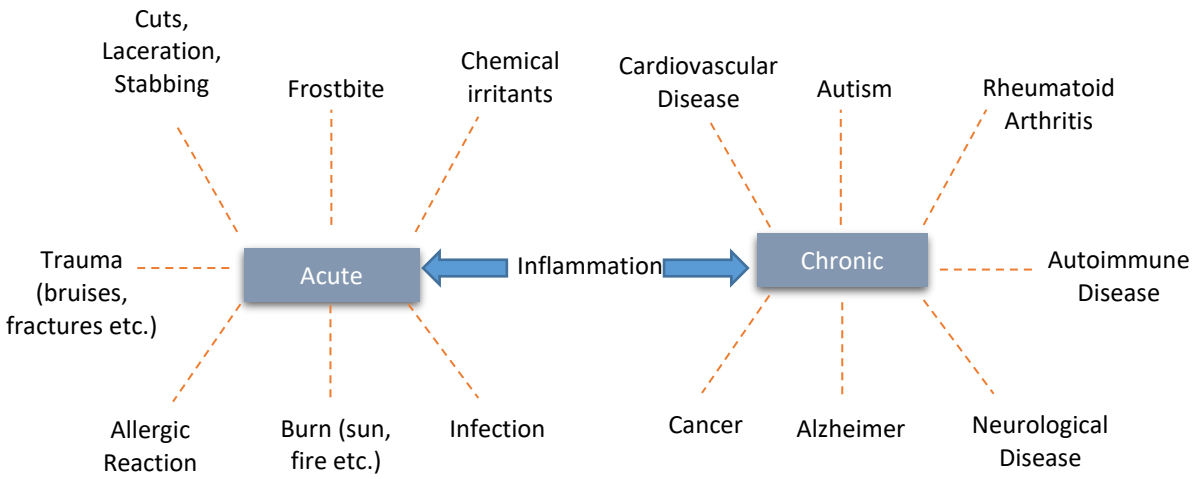


**Figure 1: Responses and related diseases to acute and chronic inflammation.** Inflammation can be divided into acute and chronic; acute inflammation occurs due conditions including allergic reactions, infections, while chronic inflammation leads to diseases including autoimmune disease, cancer.

The mechanism of inflammation involves chemokine-mediated leukocyte recruitment, which is a cascade of five steps including adhesion, capture, rolling, slow rolling, firm

adhesion, transmigration followed by extravasation of the leukocyte. Thus, leukocytes can exert their effects on the inflamed site. Blocking any of these steps can severely reduce leukocyte accumulation in the tissue which implies that each of these five steps appears to be necessary for effective leukocyte recruitment (Figure 2). These steps do not occur one after another, however, they represent the sequence of events from the perspective of each leukocyte. At any given moment, capture, rolling, slow rolling, firm adhesion and transmigration all happen simultaneously, involving different leukocytes in the same micro vessels.

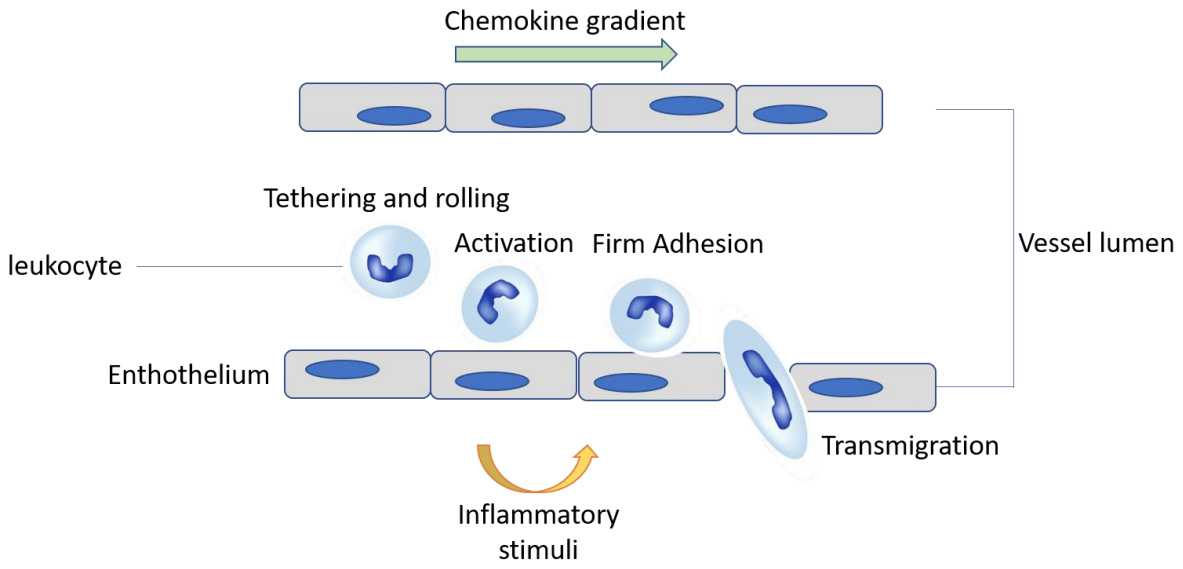


**Figure 2: Simplified illustration of the inflammatory cascade showing chemokine-mediated migration of leukocytes.** Inflammation involves a sequence of events which necessary for effective leukocyte recruitment - capture, rolling, slow rolling, firm adhesion and transmigration. (Wittchen, 2009)

Many of the common cancers are caused by years of chronic inflammation; examples include lung carcinoma, which is often caused by cigarette smoking leading to inflammation; adenocarcinoma of the esophagus, which is commonly caused by inflammation due to gastroesophageal reflux; and colon cancers, which are often associated with chronic inflammatory bowel disease; colonization of the stomach by *Helicobacter pylori*, may lead to gastric cancer and lymphoma. For many of these inflammation-associated cancers, the initiating influence remains unknown; but for others, infectious etiologies have been identified (Steven, 2005).

It is now known that inflammation plays a vital role in tumour progression and many cancers occur from sites of infection, chronic irritation and inflammation. Pro-inflammatory molecules including chemokines are incorporated by the tumor cells for invasion. These findings can be used for the development of anti-inflammatory approaches to cancer therapy (Coussens 2002).

## 1.2. Chemokines and their structures

During the incidence of an injury or infection by a pathogen, pro-inflammatory molecules, known as chemokines are expressed and secreted by the affected cells. Chemokines are a family of ~50 small cytokines, typically ~18 kDa and stabilised by two disulfide bonds, which mediate inflammatory responses by binding to chemokine receptors that are expressed on the surfaces of the leukocytes. Humans express more than 40 chemokines and many additional gene variants, splice variants, and truncated or otherwise post-translationally modified forms (Stone, 2017).

Injured or infected cells respond by secreting chemokines, which then accumulate at the endothelial cell and extracellular matrix glycosaminoglycans (GAGs) as a mechanism for chemokine localization which allows them to provide directional signals for migrating cells. Initially, leukocytes "roll" along the endothelium and once they encounter GAG-immobilized chemokines, the engagement of chemokines with their G-protein coupled receptors (GPCRs) on the leukocytes leads to leukocyte arrest through activation of integrins. Further interactions between chemokines and receptors cause the leukocytes to extravasate through endothelial cells into the surrounding tissue along chemokine gradients (Figure 2) (González-Motos, 2016).

Chemokines are classified into four main subfamilies: CXC, CC, $CX_3C$ and XC. Classification is based on the spacing between the two N-terminal Cys residues, into two major families (CC and CXC) and two minor families ($CX_3CL$ and XCL) (Zlotnik, 2012). CXC chemokines can be further subdivided based on the presence (ELR+) or absence (ELR-) of the Glu-Leu-Arg sequence near the N terminus. This sequence defines selectivity for the neutrophil receptors CXCR1 and CXCR2 (Bachelerie, 2014).

Chemokines can also be categorized based on their homeostatic versus inflammatory functions (Crump, 1997). All of these chemokines exert their biological functional through their interactions with G protein-coupled receptors (GPCRs), also known as chemokine receptors, which are selectively found on the surfaces of their target cells.

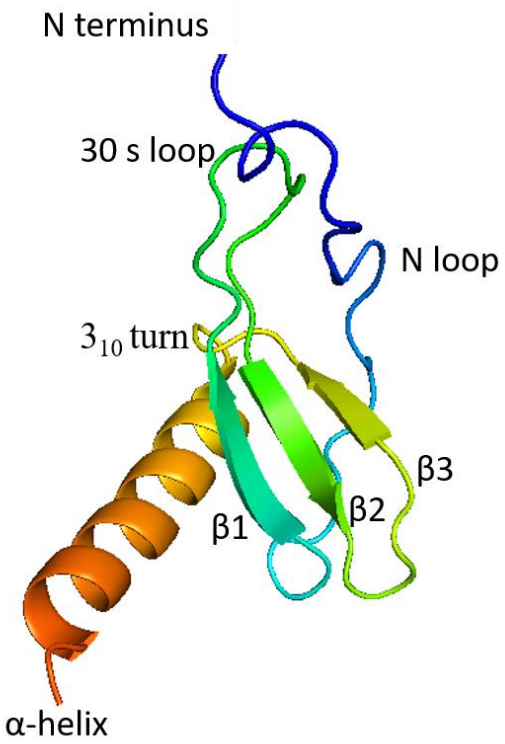


**Figure 3: Topology of a typical chemokine (CCL8) illustrating the significant secondary structure**. (PDB code 1ESR) The ribbon representation of a typical chemokine structure showing a flexible N-terminus, followed by N-loop, a β10-turn and a triple-stranded antiparallel β-sheet covered by a C-terminal α-helix .

A typical chemokine structure consists of a highly flexible N-terminus, followed by an irregularly structured region (N-loop), a $\beta_{10}$-turn and a triple-stranded antiparallel β-sheet covered by a C-terminal α-helix. There are also 2 disulfide bonds formed by 4 conserved cysteine residues in each chemokine, however in some chemokines, such as HCC-2, have an additional disulfide bond. The first cysteine residue (N-terminus) of the sequence is linked to the third one (30s loop) and the second cysteine residue (N-terminus) binds to the fourth one ($\beta_3$ strand) to form the disulfide bridges.

### 1.3.Chemokine Receptors

The chemokine receptors are known as GPCR (G-protein coupled receptor), which consists of a seven transmembrane-spanning α-helix structure (Lodowski, 2009). Figure 4 shows a typical chemokine receptor, consisting of an extracellular N-terminus, seven transmembrane α-helices connected by three extracellular and three intracellular loops (ICL), and a C-terminus that is located in the cytoplasm (Pawig, 2015).

Chemokine receptors are expressed differentially on leukocytes (Moser, 2001); for example, CCR3 is expressed exclusively on eosinophils and basophils, whereas CCR2 is expressed primarily on monocytes. Human chemokines can form a complex array of selectivity for human chemokine receptors. Therefore, a variety of leukocytes can be selectively recruited during inflammation, since they are able to express the specific chemokine receptors capable of binding to the chemokines produced by different inflamed tissues. Chemokine receptors are classified based on the family of chemokines to which they predominantly bind (e.g., CXCR1 is CXC chemokine receptor-1) and are differentially expressed on various types of leukocytes (Bhusal, 2020).

GCPRs are highly dynamic machines that can be activated through a variety of signals, apparently making the chemokine network multivariate. It is evident that chemokines targeting the same receptor can display significant bias through different efficiencies in activating their receptor towards a specific pathway which supports the observed changes in leukocyte migration (Moser, 2001).

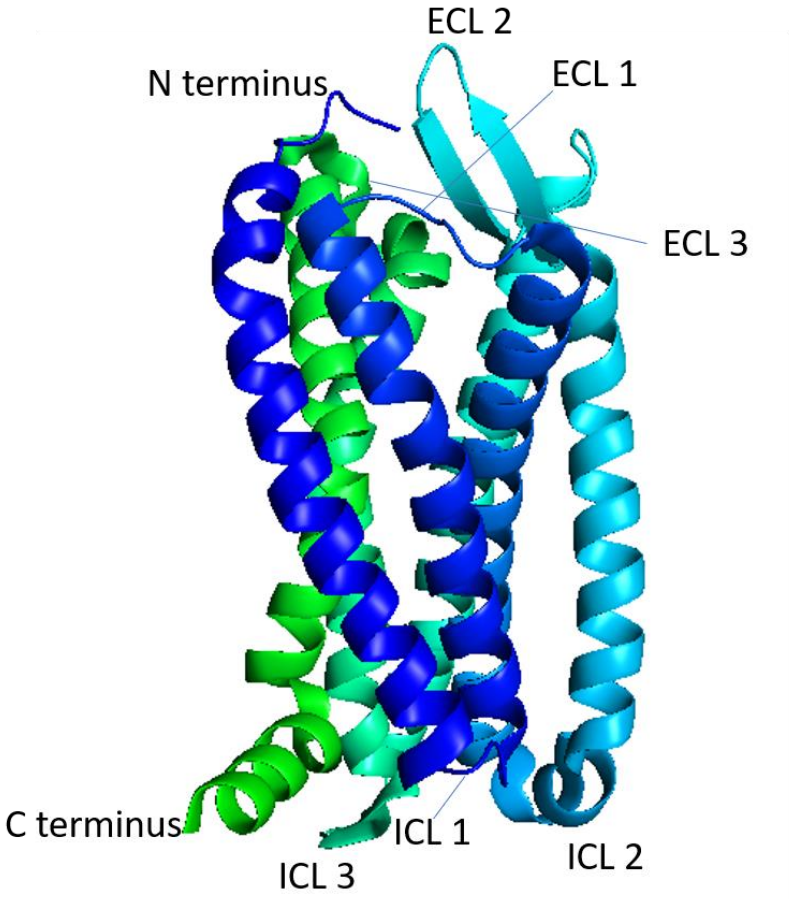


**Fig 4: Topology of a typical chemokine receptor (CXCR4) illustrating the significant regions for interaction**. (PDB code 4MBS) The figure shows ribbon representation of the chemokine receptor CXCR4 which includes an extracellular N-terminus, seven transmembrane α-helices connected by three extracellular (ECL) and three intracellular loops (ICL), and a C-terminus that protrudes to the cytoplasm.

## 1.4.Interactions between Chemokines and Chemokine Receptors

Chemokines are known to interact with the extracellular domains of their cognate GPCR receptors (Griffith, 2014). Several chemokines bind to the same receptor and vice versa. Some chemokines exhibit their selectivity in their binding to receptors, whereas others are more indiscriminate. In addition to the commonly known chemokines receptors, there are five atypical chemokine receptors (ACKRs), which are expressed on various cell types and are not G protein-coupled but respond to chemokines by similar recruitment of β-arrestins and internalization, thus removing chemokines from circulation (Figure 6).

The complexity of the chemokine signalling network is explained by a two-site model which describes the conserved mechanism of chemokine interaction with chemokine receptors. The two-site model suggests that the flexible, negatively charged N-terminus of the chemokine receptor is involved in the initial binding interaction to the positively charged N-loop and β2-β3 turn of the chemokine (Figure 5). Subsequently, a second interaction between the chemokine N-terminus and the receptor transmembrane domain is then required for triggering intracellular signalling. Most chemokines bind and activate several receptors and could either be agonists or antagonists of chemokine receptors. Similarly, most chemokine receptors respond to multiple chemokine ligands (Stone 2017).

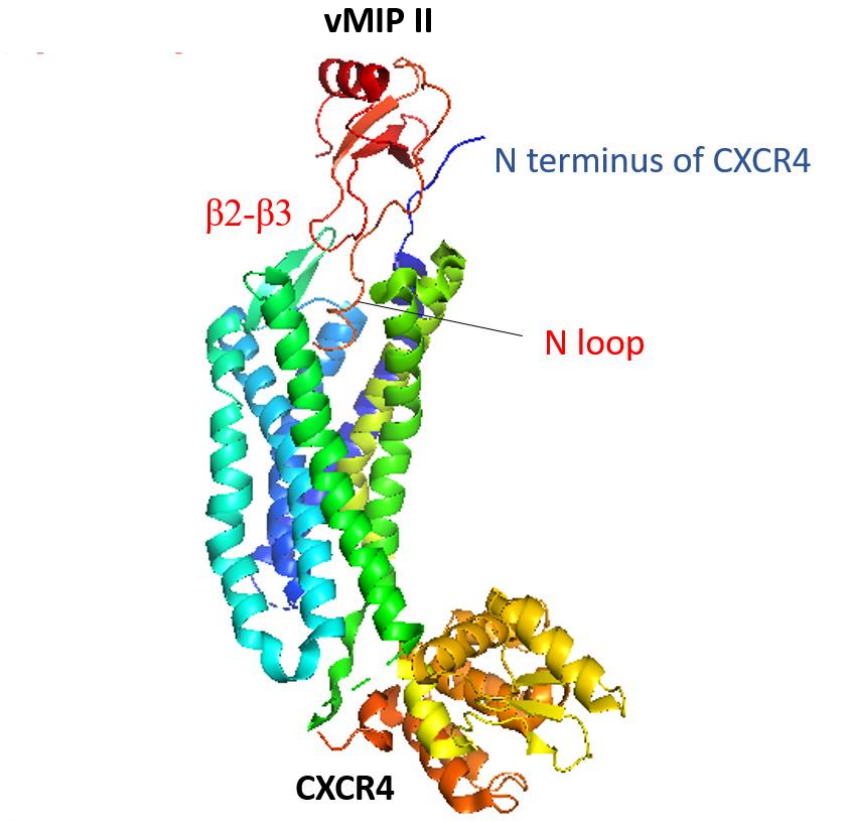


**Figure 5. Structural basis of chemokine-receptor recognition.** Ribbon representation of the receptor CXCR4 bound to vMIP II (PDB code 4RWS) with transmembrane helices coloured indigo (I), blue (II), sky blue (III), cyan (IV), green (V), dark green (VI), and yellowish green (VII). vMIP II is showed in red which interacts with the receptor through all the residues of the chemokine N terminus and N loop. CXCR4 N terminus interacts with the N loop and its $\beta_3$ strand.

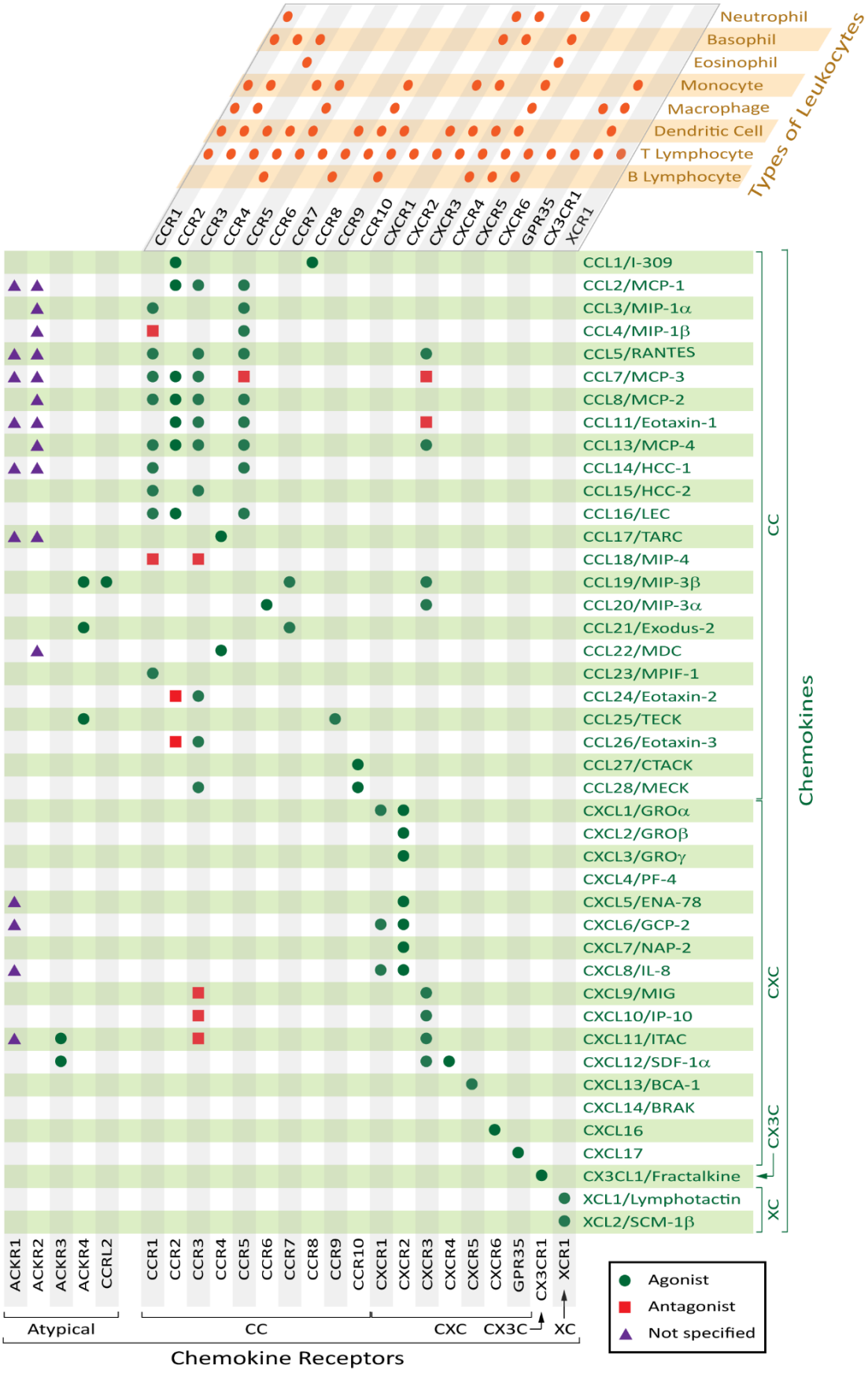


**Figure 6: Chemokines, Chemokine Receptors, and Leukocytes** (Bhusal *et al.*, 2020). The selectivity of human chemokines (listed on the right in green) for conventional

chemokine receptors (listed at top and bottom in black) and atypical chemokines receptors (listed at bottom left in black) is shown in the green and grey grid. Chemokine–ligand pairs are categorized as listed in the International Union of Basic and Clinical Pharmacology (IUPHAR) Guide to Pharmacology (http://www.guidetopharmacology.org/) (agonists, green circles; antagonists, red squares; not specified, purple triangles). The expression of conventional chemokine receptors on different types of leukocytes (listed top right in orange) is shown in the orange and gray grid; further details, including expression patterns on subtypes of leukocytes (especially T cells) and non-hematopoietic cells, are presented in. Abbreviations for chemokine nonsystematic names: BCA, B cell-attracting chemokine; BRAK, breast- and kidney-expressed chemokine; CTACK, cutaneous T cell-attracting chemokine; ENA, epithelial cell-derived neutrophilactivating peptide; GCP, granulocyte chemotactic protein; GRO, growth-regulated oncogene; HCC, hemofiltrate CC chemokine; IL, interleukin; IP, interferon γ-induced protein; ITAC, interferon-inducible T cell α chemoattractant; LEC, liver-expressed chemokine; NAP, neutrophil-activating peptide; MCP, monocyte chemotactic protein; MDC, macrophage-derived chemokine; MECK, mucosae-associated epithelial chemokine; MIG, monokine induced by γ-interferon; MIP, macrophage inflammatory protein; MPIF, myeloid progenitor inhibitory factor 1; PF, platelet factor; RANTES, regulated on activation, normal T cell expressed and secreted; SCM, single cysteine motif; SDF, stromal cell-derived factor; TARC, thymus- and activation-regulated chemokine; TECK, thymus-expressed chemokine.

Several published structures of chemokines bound to receptor fragments (Millard, 2014; Skelton, 1999; Veldkamp, 2008) have confirmed two vital aspects of the popular "two-site model" for chemokine-receptor interactions. Initially, the N-terminal region of the receptor binds to a shallow groove formed by the N-loop and $\beta_3$-strand of the cognate chemokine. While, the otherwise disordered chemokine N-terminus in the free chemokine, binds to a site buried within the receptor transmembrane helical bundle, thus undergoing induced fit to the receptor. The two-site model suggests that both these aspects of the interaction occur sequentially as two separate steps, thus, representing initial binding and subsequent activation. The structural basis of transmembrane signalling however still remains unclear since there is no reported structure for a chemokine-receptor complex in the activated state. Nevertheless, a shotgun mutagenesis study of CXCR4 has identified a network of interactions likely to participate in signal transmission during receptor activation (Ludeman, 2014).

Targeting the chemokine-receptors for potential anti-inflammatory drug delivery is .is challenging due to the complex nature of the interaction between chemokine and chemokine-receptors. For example, targeting CXCR3 for treatment of atherosceloris is difficult because it binds to CXCL9, CXCL10 and CXCL11 (refer to Table 1), and these chemokines also interact with CXCR7.

However, ticks have developed a strategic method to inhibit chemokine- receptor interactions. Tick saliva contains a cocktail of chemokine-binding proteins, called Evasins, which inhibit chemokines from binding to its receptors. Evasins are therefore valuable anti-inflammatory proteins for potential future therapeutic applications.

### 1.5.Evasins:

Ticks and other blood-sucking parasites can feed from several hours to several days, without being noticed or felt. What makes them unnoticed has brought into the limelight the presence of anti-inflammatory molecules in tick saliva. Some of these molecules possess anti-chemokine activity and thereby assist the tick to evade the host immune response. Recently, the Proudfoot lab (Merck Serono, Switzerland) has successfully applied a cloning approach and a cross-linking assay to generate a library of clones where each clone expresses one chemokine binding protein, and characterized the proteins responsible for this anti-chemokine activity in the tick species *Rhipicephalus sanguineus* (RSA). These tick chemokine-binding proteins were named “Evasins” (Frauenschuh, 2007).

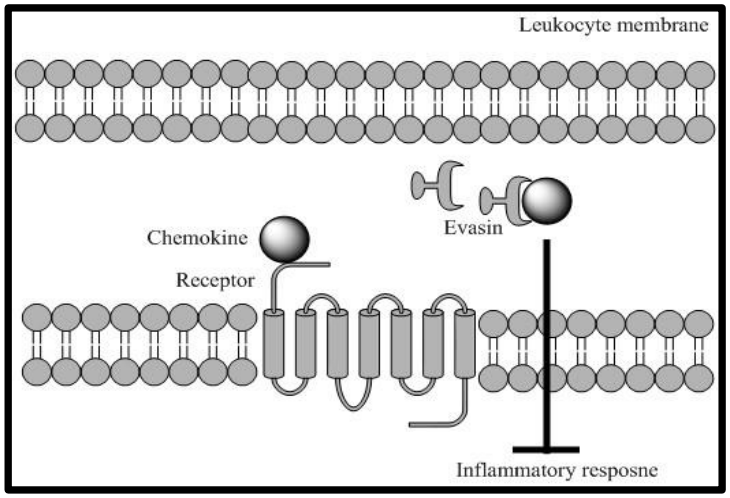


**Figure 7: Mechanism of inflammatory response and how Evasin binding to the chemokine receptors block the response.** When Evasins bind to chemokine, it inhibits the chemokine-receptor interaction and thereby inhibiting an inflamamtory response.

## 1.6.Identification of Evasins from Numerous Tick Species

*Singh et al.* and *Hayward et al.*, employed bioinformatics and experimental studies to identify and characterize new Evasin proteins. Singh *et al* used psiBLAST to identify over 350 sequences with homology to Evasin sequences in publicly available transcriptome datasets from prostriate and metastriate ticks (Singh 2017). These sequences were then cloned into a yeast surface display vector to generate a library of putative Evasins expressed on the surface of yeast, which was then screened against fluorescently labelled CC chemokines to identify chemokine-binding Evasins. Using this technology, 26 Evasin sequences homologous to Evasin-1 and -4 were identified, tens of which were produced recobinantly using HEK293 cells and then purified and characterised. Using a combination of biolayer interferometry these proteins were shown to bind and neutralize multiple chemokines in vitro (Singh 2017).

In a separate study, the Stone laboratory used sequence similarity searches to identify more than 250 sequences homologous to Evasin-1 and -4 in publicly accessible databases and locally obtained transcriptomes (Hayward, 2017). These putative Evasin sequences included numerous tick species from the genera *Rhipicephalus, Amblyomma,* and *Ixodes.* Of these sequences, nine were successfully expressed using an *E. coli* expression system; eight of these were shown to bind to various CC chemokines and four representative

Evasins were demonstrated to inhibit chemokine signaling in cell-based receptor activation assays. Two of the Evasins identified in this study (ACA-01 and RPU-01) (Hayward 2017) were identical to two Evasins reported by the Eaton *et al.* (P974_AMBCA and P467_RHIPU, respectively) (Eaton, 2018).

## 1.7. Classification and Nomenclature of Evasins

Taking into account the bioinformatic studies above were based on sequence similarity to *R. sanguineus* Evasin-1, -3, and -4, it is not surprising that the new Evasins (and putative Evasins) identified fall into two sequence families: those with high sequence similarity to *R. sanguineus* Evasin-1 and -4 (defined here as Class A Evasins) and those with high sequence similarity to *R. sanguineus* Evasin-3 (Class B Evasins). In light of the recent increase in the number of known Evasins, it was important to develop a consistent nomenclature of these proteins.

Therefore, Bhusal and Chowdhury *et al.* reported that each validated (chemokine-binding) Evasin protein sequence should be given a unique name, consisting of the prefix 'EVA- ', to designate the protein as an Evasin, followed by the identifier defined in the first publication in which that protein was demonstrated to be a chemokine-binding Evasin. For example, *R. sanguineus* Evasin-1 (Frauenschuh 2007) would be designated simply EVA-1, whereas the protein reported first as P974_AMBCA (Singh, 2017) and subsequently as ACA-01 (Hayward, 2017) would be designated EVA-P974; we have dropped the original species-specific suffix '_AMBCA', which is not required for unique identification of this sequence. Table 1 and 2 list the published systematic names for all Evasins validated to date, along with their previous designations.

### 1.7.1. Class A Evasins

**Protein Sequence Features**

To date, 21 proteins with significant sequence identity to EVA-1 and -4 have been validated as chemokine-binding proteins shown in Table 1a (Bhusal, 2020). Their

sequences (89–126 amino acid residues) are aligned in Figure 8A and their phylogenetic tree and pairwise identity matrix are shown in Figure 8B. Pairwise sequence identities among these Evasins range from 15% to 97% (average 31.1%). Nine of these sequences have <30% identity to both EVA-1 and -4, indicating substantial divergence from the earliest identified Evasins. The sequence alignment highlights several conserved features of the Class A Evasins. Eight cysteine residues that form four intramolecular **disulfide bonds** in the structure of EVA-1 (*vide infra*) are strictly conserved, except for three sequences from the genus *Ixodus*, which are missing the fifth and eighth cysteines, a disulfide pair. (Hayward, 2017). The strong conservation of the Cys residues suggests common disulfide-bonded architecture and protein fold. In addition, two glycine residues are completely conserved.

The Class A Evasin sequences indicate that these proteins are likely to undergo various post-translational modifications. All Evasin sequences contain an N-terminal signal peptide (not shown in Figure 8 that is cleaved off during secretion (Deruaz 2007, Frauenschuh 2007). Twenty-one of the 24 sequences contain at least one tyrosine residue in the N-terminal region in highly acidic sequence environments (2–6 Asp or Glu in the preceding six and following three residues). This type of sequence motif in secreted proteins is highly indicative of a tyrosine sulfation site (Stone, 2009; Stone, 2015). Moreover, tyrosine sulfation is a common post-translational modification of chemokine receptors, known to enhance their binding affinity and modify their selectivity for cognate chemokines (Ludeman, 2014). A recently accepted study in collaboration with Richard Payne's group at Sydney University shows the evidence that tyrosine sulfation of Evasins can also modulate its chemokine binding (Franck, C., et al. (2020). This provides an interesting example of evolutionary convergence and molecular mimicry.

Another conserved post-translational modification of Class A Evasins is N-glycosylation. The verified sequences each contain several potential N-glycosylation sites (Asn-Xaa-Ser or Asn-Xaa-Thr; Xaa indicates any amino acid), consistent with the early characterization studies. Several Class A Evasins also contain potential O-glycosylation sites (Singh, 2017)

(a)

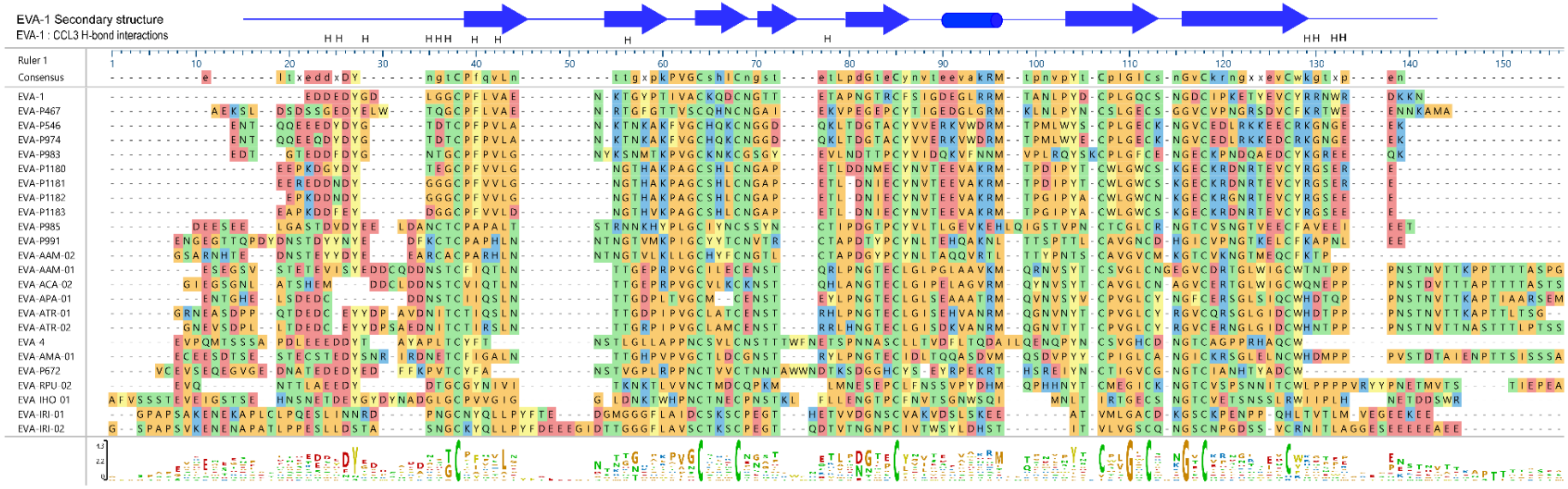
EVA-1 Secondary structure
EVA-1 : CCL3 H-bond interactions
Ruler 1
Consensus
EVA-1
EVA-P467
EVA-P546
EVA-P974
EVA-P983
EVA-P1180
EVA-P1181
EVA-P1182
EVA-P1183
EVA-P985
EVA-P991
EVA-P1243
EVA-AAM-01
EVA-AAM-02
EVA-ACA-02
EVA-APA-01
EVA-ATR-01
EVA-ATR-02
EVA 4
EVA-AMA-01
EVA-P672
EVA-RPU-02
EVA IHO 01
EVA-IRI-01
EVA-IRI-02

(b)

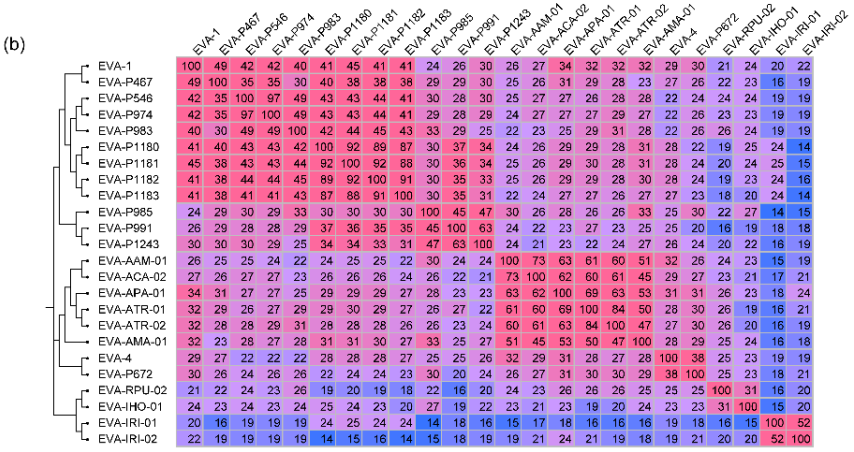
EVA-1 100 49 42 42 40 41 45 41 41 24 26 30 26 27 34 32 32 32 29 30 21 24 20 22
EVA-P467 49 100 35 35 30 40 38 38 38 29 29 30 25 26 31 29 28 23 27 26 22 23 16 19
EVA-P546 42 35 100 97 49 43 43 44 41 30 28 30 25 27 27 26 28 28 22 24 24 24 19 19
EVA-P974 42 35 97 100 49 43 43 44 41 29 28 29 24 27 27 27 29 27 22 26 23 23 19 19
EVA-P983 40 30 49 49 100 42 44 45 43 33 29 25 22 23 25 29 31 28 22 26 26 24 19 19
EVA-P1180 41 40 43 43 42 100 92 89 87 30 37 34 24 26 29 29 28 31 28 22 19 25 24 14
EVA-P1181 45 38 43 43 44 92 100 92 88 30 36 34 25 26 29 30 28 31 28 24 20 24 25 15
EVA-P1182 41 38 44 44 45 89 92 100 91 30 35 33 25 26 29 29 28 30 28 24 19 23 24 16
EVA-P1183 41 38 41 41 43 87 88 91 100 30 35 31 22 24 27 27 26 27 27 23 18 20 24 14
EVA-P985 24 29 30 29 33 30 30 30 30 100 45 47 30 26 28 26 26 33 25 30 22 27 14 15
EVA-P991 26 29 28 28 29 37 36 35 35 45 100 63 24 22 23 27 23 25 25 20 16 19 18 18
EVA-P1243 30 30 30 29 25 34 34 33 31 47 63 100 24 21 23 22 24 27 26 24 20 22 16 19
EVA-AAM-01 26 25 25 24 22 24 25 25 22 30 24 24 100 73 63 61 60 51 32 26 24 23 15 19
EVA-ACA-02 27 26 27 27 23 26 26 26 24 26 22 21 73 100 62 60 61 45 29 27 23 21 17 21
EVA-APA-01 34 31 27 27 25 29 29 29 27 28 23 23 63 62 100 69 63 53 31 31 26 23 18 24
EVA-ATR-01 32 29 26 27 29 29 30 29 27 26 27 22 61 60 69 100 84 50 28 30 26 19 16 21
EVA-ATR-02 32 28 28 29 31 28 28 28 26 26 23 24 60 61 63 84 100 47 27 30 26 20 16 19
EVA-AMA-01 32 23 28 27 28 31 31 30 27 33 25 27 51 45 53 50 47 100 28 29 25 24 16 18
EVA-4 29 27 22 22 22 28 28 28 27 25 25 26 32 29 31 28 27 28 100 38 25 23 19 19
EVA-P672 30 26 24 26 26 22 24 24 23 30 20 24 26 27 31 30 30 29 38 100 25 23 18 21
EVA-RPU-02 21 22 24 23 26 19 20 19 18 22 16 20 24 23 26 26 26 25 25 25 100 31 16 20
EVA-IHO-01 24 23 24 23 24 25 24 23 20 27 19 22 23 21 23 19 20 24 23 23 31 100 15 20
EVA-IRI-01 20 16 19 19 19 24 25 24 24 14 18 16 15 17 18 16 16 16 19 18 16 15 100 52
EVA-IRI-02 22 19 19 19 19 14 15 16 14 15 18 19 19 21 24 21 19 18 19 21 20 20 52 100

**Figure 8: Sequence Alignments, Phylogenetic Tree and Pairwise Identity Matrix of Class A Evasins.** (a) Sequence alignment of all validated Class A Evasins with proposed nomenclature. The consensus sequence (above alignment) and sequence logo (below alignment) show that eight cysteine residues (green) are conserved (except for two missing Cys residues in the bottom 3 sequences) and two glycine residues are completely conserved across the family. The secondary structure of EVA-1 (PDB ID: 3FPR) and EVA-1 residues forming hydrogen bond interactions with CCL3 (in PDB ID: 3FP), analysed by PDBSum, are presented at the top of the alignment. The alignment was performed using MAFFT, with default parameters, in the program DNASTAR Navigator 15. Amino acid residues are colour coded by physicochemical properties. (b) Phylogenetic tree (left side) and pairwise identity matrix of all validated Class A Evasins. Pairwise identities between sequences were calculated using MAFFT and are color-coded on a continuous scale from rose (high identity) to blue (low identity). The phylogenetic tree was generated on FigTree v1.4.3 using the alignment data from MAFFT. Figure taken from (Bhusal and Chowdhury, 2020)

**Table 1: Systematic Nomenclature for Class A Evasins**

| Systematic Name | Class | Tick Species[1] | Previous Name(s) and Reference(s) |
|---|---|---|---|
| EVA-1 | A | *R. sanguineus* | Evasin-1 (Deruaz, 2008) |
| EVA-4 | A | *R. sanguineus* | Evasin-4 (Déruaz, 2013) |
| EVA-P467 | A | *R. pulchellus* | P467_RHIPU (Singh, 2017), RPU-01 (Hayward, 2017) |
| EVA-P546 | A | *A. cajennense* | P546-AMBCA (Singh, 2017) |
| EVA-P672 | A | *R. pulchellus* | P672_RHIPU (Eaton, 2018) |
| EVA-P974 | A | *A. cajennense* | P974-AMBCA (Singh, 2017), ACA-01 (Hayward, 2017) |
| EVA-P983 | A | *A. cajennense* | P983-AMBCA (Singh, 2017) |
| EVA-P985 | A | *A. parvum* | P985-AMBPA (Singh, 2017), APA-01 (Hayward, 2017) |
| EVA-P991 | A | *A. cajennense* | P991_AMBCA (Singh, 2017) |
| EVA-P1180 | A | *A. triste* | P1180-AMBTR (Singh, 2017) |
| EVA-P1181 | A | *A. maculatum* | P1181-AMBMA (Singh, 2017) |
| EVA-P1182 | A | *A. maculatum* | P1182-AMBMA (Singh, 2017)(3) |
| EVA-P1183 | A | *A. triste* | P1183-AMBTR (Singh, 2017) |
| EVA-AAM-01 | A | *A. americanum* | AAM-01 (Hayward, 2017) |
| EVA-AAM-02 | A | *A. americanum* | AAM-02 (Hayward, 2017), P1243 (Alenazi, 2018) |
| EVA-ACA-02 | A | *A. cajennense* | ACA-02 (Hayward, 2017) |
| EVA-AMA-01 | A | *A. maculatum* | AMA-01 (Hayward, 2017) |
| EVA-ATR-02 | A | *A. triste* | ATR-02 (Hayward, 2017) |
| EVA-IHO-01 | A | *I. holocyclus* | IHO-01 (Hayward, 2017) |
| EVA-IRI-01 | A | *I. ricinus* | IRI-01 (Hayward, 2017) |
| EVA-RPU-02 | A | *R. pulchellus* | RPU-02 (Hayward, 2017) |

**Table 2: Systematic Nomenclature for Class B Evasins**

| Systematic Name | Class | Tick Species[1] | Previous Name(s) and Reference(s) |
|---|---|---|---|
| EVA-3 | B | *R. sanguineus* | Evasin-3(Deruaz, 2008), EVA3_RHISA (4) |
| EVA-P1174 | B | *I. ricinus* | P1174_IXORI (Lee, 2019) |
| EVA-P1170 | B | *I. ricinus* | P1170_IXORI (Lee, 2019) |
| EVA-P1132 | B | *I. ricinus* | P1132_IXORI (Lee, 2019) |
| EVA-P1172 | B | *I. ricinus* | P1172_IXORI (Lee, 2019) |
| EVA-P1162 | B | *I. ricinus* | P1162_IXORI (Lee, 2019) |
| EVA-P1168 | B | *I. ricinus* | P1168_IXORI (Lee, 2019) |
| EVA-P1166 | B | *I. ricinus* | P1166_IXORI (Lee, 2019) |
| EVA-P1229 | B | *I. ricinus* | P1229_IXORI (Lee, 2019) |
| EVA-P1156 | B | *I. ricinus* | P1156_IXORI (Lee, 2019) |
| EVA-P1128 | B | *I. ricinus* | P1128_IXORI (Lee, 2019) |
| EVA-P1127 | B | *I. ricinus* | P1127_IXORI (Lee, 2019) |
| EVA-P1134 | B | *I. ricinus* | P1134_IXORI (Lee, 2019) |
| EVA-P1096 | B | *I. ricinus* | P1096_IXORI (Lee, 2019)) |
| EVA-P1095 | B | *I. ricinus* | P1095_IXORI (Lee, 2019) |
| EVA-P1142 | B | *A. cajennense* | P1142_AMBCA (Lee, 2019) |
| EVA-P1126 | B | *A. cajennense* | P1126_AMBCA (Lee, 2019) |
| EVA-P1124 | B | *I. ricinus* | P1124_IXORI (Lee, 2019) |
| EVA-P1104 | B | *I. ricinus* | P1104_IXORI (Lee, 2019) |
| EVA-P1100 | B | *I. ricinus* | P1100_IXORI (Lee, 2019) |
| EVA-P1080 | B | *I. ricinus* | P1080_IXORI (Lee, 2019) |
| EVA-P1078 | B | *I. ricinus* | P1078_IXORI (Lee, 2019) |
| EVA-P1074 | B | *I. ricinus* | P1074_IXORI (Lee, 2019) |
| EVA-P1090 | B | *I. ricinus* | P1090_IXORI (Lee, 2019) |
| EVA-P942 | B | *I. ricinus* | P942_IXORI (Lee, 2019) |
| EVA-P675 | B | *I. ricinus* | P675_IXORI (Lee, 2019) |
| EVA-P1086 | B | *I. ricinus* | P1086_IXORI (Lee, 2019) |
| EVA-P1077 | B | *I. ricinus* | P1077_IXORI (Lee, 2019) |
| EVA-P458 | B | *I. ricinus* | P458_IXORI (Lee, 2019) |

[1]*R, Rhipicephalus; A, Amblyomma; I, Ixodes*.

## 1.8.Evasin Structure and Receptor Binding Interaction:

### *1.8.1. Structure of EVA-1:*

The Evasins from *Rhipicephalus sanguineus* are small proteins (8-11 kDa) of a similar size to their chemokine binding partners. The structure of EVA-1 both free and in complex with the chemokine CCL3 reveals a novel fold (Figure 9A-B) (Dias, 2009). The structural basis for the inhibition of chemokine activity by EVA-1 is explained by the conformation of the Evasin:chemokine complex. When bound by the Evasin, the chemokine N-terminus and N-loop are sequestered and therefore no longer free to interact with receptors on leukocytes to promote chemotaxis.

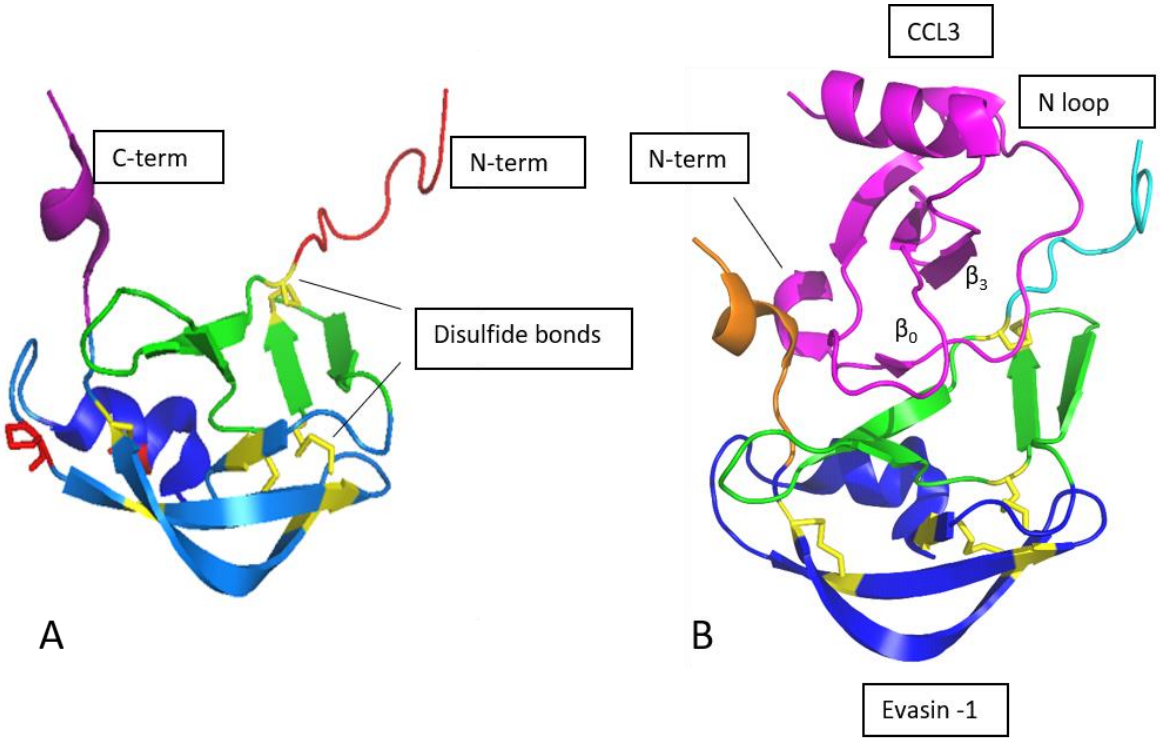


**Figure 9. Structure of the Complex between EVA-1 and CCL3.** (A) Ribbon representation of one protomer of non-glycosylated Evasin-1 (PDB ID: 3FPR) : The base of the structure formed by the three β-sheets (β5, β6 and β7 strands) and the α-helix, in blue; the first β-sheet (β1 and β2 strands) and second β-sheet (β3 and β4 strands), in green; the N-terminal region in red; the C-terminal region in magenta; and cysteine residues and disulfide bonds (sticks) in yellow. (B) Structure of the Complex between Evasin-1 and CCL3. CCL3 (magenta) bound to Evasin-1.

### *1.8.2. Structure of EVA-3:*

The 3-D structure of EVA-3 has initially been solved by Deruaz *et al*. and was refined as an asymmetric dimer containing a cystine knot. Recently, NMR analysis was conducted to confirm the protein structure (Denisov 2019). Figure 10 shows that each promoter of EVA-3 consists of a 'knottin' cystine topology, which consists of a single layer β-sheet linked by two long loops, connected by three disulfide bonds, one of which passes through the loop formed by the other two disulfides. The knottin topology is expected to be retained across the Class B Evasins based on the conservation of Cys residues and modelling studies (Lee 2019). The cystine knot is important in increasing the the structural, proteolytic, and chemical stability of these proteins, enhancing their potential clinical utility (Senthilkumar 2017). The five loop segments in knottins mediate protein interactions and can be engineered for development as diagnostic and therapeutic agents. The Class B Evasins represent the first knottin family isolated from ticks. They are also the first chemokine-binding knottins reported.

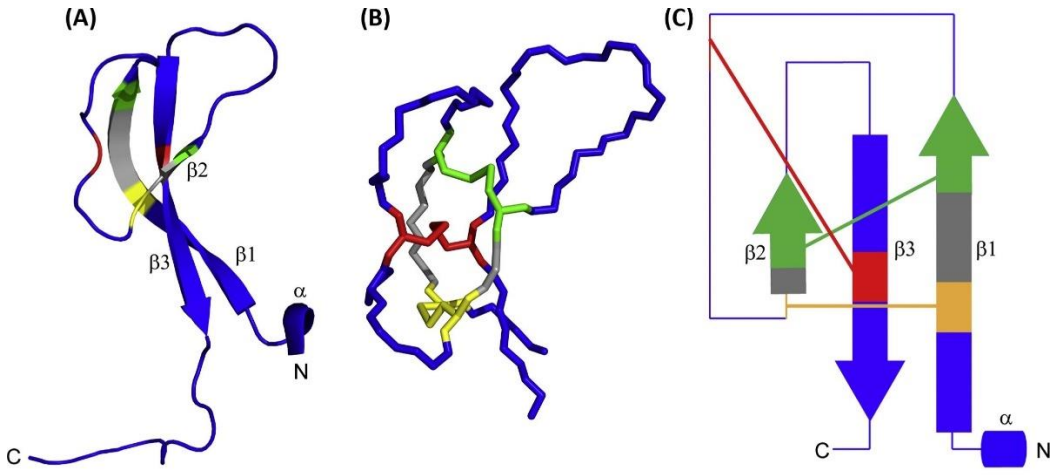


**Figure 10: 'Knottin' Cystine Knot Topology of EVA-3 structure.**

A) Ribbon representation of one protomer of EVA-3 (PDB ID: 6I3). Pairs of cysteines that form disulfide bonds (Cys-21 and Cys-37; Cys-26 and Cys-39; Cys-33 and Cys-50) are shown in different colors (yellow, green, and red, respectively). Other residues within the macrocycle created by the first two disulfide bonds are shown in gray. (B) EVA-3 structure, colored as in (A), showing the protein backbone and Cys side chains. This view highlights the third (red) disulfide bond passing through the macrocycle created by the first two (yellow and green) disulfide bonds. (C) Topology diagram showing β-strands as arrows and the α-helix as a cylinder, with coloring corresponding to (A) and (B) (Figure taken from Bhusal *et al.*, 2019).

## 1.9.Evasins in disease models:

In a study by *Bonvin et al.,* Evasin-1, -3 and -4 have all shown efficacy in vivo in several disease models. Evasin-1 reduced neutrophil recruitment induced by CCL3 in a peritoneal cell recruitment assay in a dose-dependent manner. In mice, CCR1 is highly expressed on neutrophils, resulting in its strong recruitment in response to CCL3. On the other hand, neutrophil recruitment in mice is also mediated by CXCR2 ligands, as it is in the human system. Thus, in accordance with its ability to inhibit neutrophil infiltration, Evasin-1 showed good efficacy in reducing fibrosis, which follows neutrophil infiltration into the lung after bleomycin administration, and also reduced the mortality observed in this model (Russo, 2011).

Evasin-3 was effective in several neutrophil-dependent disease models (Bonvin 2016) Antigen-induced arthritis (AIA), induced by intradermal administration of mouse BSA, is highly neutrophil dependent. In AIA, disease symptoms were significantly decreased by the administration of Evasin-3. In another neutrophil-mediated scenario, ischemic reperfusion injury, both Evasin-1 and Evasin-3 were effective, but Evasin-3 was shown to be more efficacious, indicating that the CXCR2 ligands play a predominant role in this model. On the other hand, only Evasin-1 and not Evasin-3 was effective in inhibiting the first wave of dendritic cell recruitment to the site of infection with Leishmania major, since it is mediated by neutrophil-secreted CCL3 (Amanda, 2016).

In line with the broad selectivity profile and inhibitory activity of Evasin -4 against several CC chemokines known to have proinflammatory activity, it was shown to be effective in reducing post-infarction myocardial injury and remodelling (Braunersreuther, 2013). Because of its broad CC chemokine-binding spectrum, Evasin-4 was considered the most suitable Evasin for development as a possible therapeutic candidate. However, it is well known that small proteins have a very short half-life in vivo and are not orally available, which means that for chronic indications, they would have to be injected with a frequency that is not convenient for patients.

## 1.10. Expression and purification of Evasins:

Dias *et al.,* first reported Baculovirus production of Evasin-1 (Dias 2009). *Spodoptera frugiperda* (Sf9) cells were transfected and the recombinant virus was amplified using standard methods. Evasin-1 was expressed using the baculovirus system in insect cells. Through the baculovirus system, they obtained soluble expression of both the glycosylated and non-glycosylated protein. After purification, the glycosylated protein was found to be heterogeneous comprising of different species of glycosylated protein, which was confirmed by isoelectric focusing, while the non-glycosylated protein showed a single band on SDS-PAGE, but the isoelectric focusing revealed two major bands, which were separated in the anionic exchange (Q-Resource) step. The two fractions were analysed by N-terminal sequencing and mass spectrometry, which revealed that they had molecular masses of 11286 Da and 11362 Da, respectively. The difference in 76 Da was not further explained in the report.

Deruaz *et al.* (2013), *Singh et al.* (2017), and Bonvin *et al.* (2016) all reported expression and purification of Evasins in HEK 293 cells. Hayward *et al.* (2017), first reported *E. coli* expression of Evasins, where C-terminal $His_6$-tagged candidate Evasins expressed in inclusion bodies. A standard chromatographic protocol was used for purification; however, the proteins were not characterized prior to Fluorescent Anisotropy assay to determine chemokine binding activity of the candidate evasins. .

## 1.11. Introduction to ACA-01:

ACA-01 is a Class A $C_8$-Evasin from the species *Amblyomma cajennense.* According to the published nomenclature of Evasins, ACA-01 is now designated EVA-P974. We have variously called it ACA-01, ACA801, or EVA-ACA801 and Singh *et al*., originally called it P974_AMBCA. However, for the convenience of this thesis, we will regard it as ACA-01.

As described in section 1.6, previously Jenni Hayward, from our lab and later Singh *et al.,* worked on the identification of putative Evasin sequences through bioinformatics research. The analysis considered the conserved features of putative Evasin-like sequences, in which the conservation of the number and spacing of cysteine residues was perhaps the most striking pattern observed. Generally, candidates from the genera

*Rhipicephalus* and *Amblyomma* had all 8 core cysteines, while candidates from genus Ixodes appeared to have only 6, missing the 5$^{th}$ and 8$^{th}$ cysteine residues (Figure 8a).

The sequence of ACA-01 contains the motif:

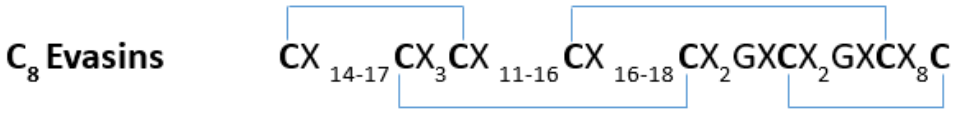


Since ACA-01 contains the same C-8 motif as Class A Evasins, we were interested to characterize ACA-01 as a model Evasin for all the other Class A Evasins. In addition to this, from the previous studies screening nine candidate Evasins for their expression, reported by Hayward *et al.,* ACA-01 expressed reasonably compared to all other candidate Evasins. However, ACA-01 was expressed in inclusion bodies and had very poor yield. This encouraged us to work with ACA-01 to find a suitable expression system for soluble expression of ACA-01. Once we obtained pure ACA-01, we planned to study its binding to chemokines. We were also interested to elucidate the 3-D crystal structure of ACA-01 since there has not been any report on structural studies of ACA-01 to date.

Therefore, for the purpose of this thesis, the overall objective was:

Characterization of ACA 01- A Chemokine-Binding Novel Tick Evasin

**Aim 1: Expression, Purification, Characterization of ACA-01**

*A.* Expression and Purification of ACA-01 using a $His_6$-ACA-01 construct.

*B.* Quality control of purified ACA-01 by SDS-PAGE, Analytical Size Exclusion Chromatography and Mass Spectrometry.

*C.* Expression and Purification of ACA-01 using $His_6$-SUMO-ACA-01 construct for soluble expression of ACA-01.

*D.* Quality control of purified ACA-01 by SDS-PAGE, Analytical Size Exclusion Chromatography and Mass Spectrometry.

**Aim 2: Chemokine Binding Studies of ACA-01:**

*A.* Analysis of chemokine-binding by ACA-01 through a Fluorescent Anisotropy Assay

*B.* Direct Binding Assay to determine fluorescent peptide binding to chemokines

*C.* Competitive Binding Assay to determine displacement of fluorescent peptide bound to chemokines by ACA-01

**Aim 3: Trials for Structure Determination of ACA-01**

*A.* Perform stability studies to determine the condition in which ACA-01 is most stable.

*B.* Perform Crystallization trials of ACA-01

*C.* Obtain Preliminary data from crystal trials of ACA-01

# Chapter 2: Materials and Methods

## 2.1. Media, Buffers and Solutions

**LB media (1 L):** 10 g tryptone, 5 g peptone (yeast extract), 10 g NaCl, 1 ml of 1 M NaOH

**LB plates:** 15 ml of LB media containing 0.23 g agar

**Kanamycin:** 30 μg/ml final concentration

**IPTG (Isopropyl ß-D-1-thiogalactopyranoside):** 1 mM final concentration unless optimized.

**Lysis buffer:** 20 mM Tris.HCl, pH 8.5, 500 mM NaCl, 5 mM imidazole, 5% (v/v) Glycerol

**Inclusion body wash buffer:** 20 mM Tris.HCl, pH 8.5, 500 mM NaCl, 5 mM imidazole, 0.5 % (v/v) TX-100, 2 mM DTT

**Refolding buffer:** 20 mM Tris. HCl, pH 8.0, 400 mM NaCl, 2.0 mM reduced glutathione (GSH), 0.5 mM oxidised glutathione (GSSG)

**Immobilized Metal Affinity Chromnatography (IMAC) denaturing load buffer:** 6 M Gdn.HCl, 20 mM Tris, pH 8.0, 20 mM imidazole and 20 mM β-mercaptoethanol (β-ME)

**IMAC denaturing elution buffer:** 6 M Gdn.HCl, 20 mM Tris, pH 8.0, 200 mM imidazole, 20 mM β-ME

**Phosphate Buffered Saline (PBS):** 137 mM NaCl, 2.7 mM KCl, 10 mM $Na_2HPO_4$, 1.8 mM $KH_2PO_4$.

**Ulp1 protease:** Produced in-house and stored at -20 $^oC$ .

**HisTrap column buffers:**

i. Buffer A: 20 mM Tris.HCl, pH 8.0, 500 mM NaCl, 20 mM imidazole
ii. Buffer B: 20 mM Tris.HCl, pH 8.0, 500 mM NaCl, 200 mM imidazole
iii. HisTrap stripping buffer: 20 mM $NaH_2PO_4$, 0.5 M NaCl, 50 mM EDTA, 5% (v/v) Glycerol

**Preparative Size Exclusion Chromatography (PSEC) buffer:** 10 mM HEPES, pH 7.4, 150 mM NaCl, 5% (v/v) Glycerol

**Analytical Size Exclusion Chromatography (ASEC) buffer:** 0.1 M $NaH_2PO_4$ (pH 7.5)

**SDS-PAGE solutions:**

i. Running gel buffer: 1.5 M Tris.HCl, pH 8.8
ii. Stacking gel buffer: 0.5 M Tris.HCl, pH 6.8
iii. Tank buffer: 0.025 M Tris.HCl, 0.192 M glycine, 3.5 mM SDS
iv. Gel drying solution: 4 % (v/v) glycerol, 30 % (v/v) EtOH
v. Non-reducing loading dye (2X): 0.5 M Tris.HCl, pH 6.8, 2.5 ml glycerol, 0.5 % (w/v) bromophenol blue, 10 % (w/v) SDS
vi. Reducing loading dye (2X): 0.5 M Tris.HCl, pH 6.8, 2.5 ml glycerol, 0.5 % (w/v) bromophenol blue, 10 % (w/v) SDS, 0.5 ml β-ME
vii. Coomassie Staining Solution: 0.1% Coomassie Brilliant Blue R-250, 50% methanol and 10% glacial acetic acid
viii. Coomassie De-staining Solution: 40% methanol and 10% glacial acetic acid.

**Bacterial Strains:** BL21 DE3 for expression of protein

**$His_6$-SUMO-ACA-01 in pET28a** from Genescript.

Chemokines CCL11/eotaxin-1, CCL24/eotaxin-2, CCL26/eotaxin-3, CCL/2/MCP-1, CCL8/MCP-2 and CCL7/MCP-3 were obtained from peprotech.

**SYPRO™ Orange Dye:** 5,000X Concentrate in DMSO from Merck.

## 2.2. Bacterial Culture

### 2.2.1. Competent cell preparation

Competent cells were prepared as follows: A single colony from a plate of freshly grown cells, DH5α or BL21 (DE3), was selected and transferred into 5 ml of LB media. Cells were grown at 37 °C overnight. 2 ml of this overnight culture was used to inoculate 200 ml of LB media in a 500 ml flask. The cells were grown at 37 °C, 180 rpm until the $OD_{600}$ reached ~0.3-0.35. Cells were then harvested by centrifugation at 3000 g for 5 min at 4 $^oC$. The pellet was resuspended gently in 50 ml of 0.1 M $CaCl_2$ (sterile-filtered and chilled on ice), followed by incubation on ice for 20 minutes. Cells were harvested again by centrifugation at 3000 g for 5 min. The pellet was resuspended gently in 4 ml of ice-cold

0.1 M $CaCl_2$. Competent cells were either used immediately at this stage or frozen. For storage in a freezer, a sterile-filtered solution of 75 % (v/v) glycerol was added to give a final concentration of 15 % (v/v) glycerol and aliquots (50 µl) were stored at -80 °C until needed.

### 2.2.2. Transformation of DH5α and BL21 DE3

50 µl of competent *E. coli* cells were transformed as follows: DNA (1-5 µl) was added to the cells and incubated on ice for 30 minutes. The cell mixture was then heat shocked at 42 °C for 45 seconds and placed on ice for 1-2 min. Subsequently, 450 µl of LB media was added and the cultures incubated in a shaker at 37 °C for 60 min. Cultures were then spread onto LB agar plates containing selection antibiotic and incubated overnight at 37 °C.

## 2.3. Protein Production and Purification

### 2.3.1. Small-scale expression trial:

pET28a vector containing the construct $His_6$–ACA-01 was obtained from GenScript and competent BL21 (DE3) *E. coli* cells were transformed with the vector for the expression of N-terminally $His_6$-tagged ACA-01. To identify successful transformation of the bacterial colonies, thirteen colonies were selected and checked for their ability to express ACA-01.

Briefly, the colonies from the transformed plates were picked and inoculated each into 5 mL $LB^{Kan}$ (LB with Kanamycin) and allowed to grow overnight. After overnight growth, 1 mL of each starter culture was transferred into 100 mL of fresh $LB^{Kan}$ and grown until optimum density, $OD_{600}$ reached 0.6 and cells were induced with 1 mM IPTG to induce protein expression. After overnight growth post induction, 10 µL sample of each culture was centrifuged, and the expression of the protein tested by SDS-PAGE.

To test whether the protein was expressed in the soluble or insoluble fraction, briefly, small-scale starter cultures of 5 mL $LB^{Kan}$ were inoculated using the high-expressing colony identified. After overnight growth, 1 mL of each starter was transferred into 100 mL of fresh $LB^{Kan}$ and grown until the $OD_{600}$ approached 0.6. 1 mM IPTG was then added for induction of protein expression. 10 µL sample was collected at 4 hours post induction with IPTG and after overnight growth and were centrifuged at 10 000 rpm, for 5 min to collect pellets which were then resuspended in 4 mL of Lysis Buffer. The

supernatant was stored at 4 °C for further analysis, if needed. Suspensions were then sonicated with 3 x 60 sec bursts and the soluble fraction separated from the insoluble by centrifugation at 14 000 rpm for 20 min. 10 µL sample was analysed by SDS-PAGE to determine whether to collect soluble or insoluble fraction for protein purification.

For expression of $His_6$-SUMO-ACA-01 a small-scale expression trial was conducted to determine the optimum temperature and IPTG concentration. BL21 (DE3) *E. coli* cells were transformed with $His_6$-SUMO-ACA-01 and one colony was picked to inoculate small-scale starter cultures of 5 mL $LB^{Kan}$, which were grown overnight (all growth in liquid media at 37 °C, shaking at 180 rpm). After overnight growth, 25 µL of starter was transferred into fresh 50 mL $LB^{Kan}$ (1 in 100 dilution) and grown until optical density ($OD_{600}$) reached 0.6. Cells were then induced at three different concentrations of IPTG: 0.2 mM, 0.5 mM and 1 mM, and post-induction overnight growth temperatures of 18 °C, 25 °C, and 37 °C. After overnight expression, 100 µL of the cells were centrifuged at 13,000 rpm for 2 minutes to separate the media from the pellet. The pellets were analysed on SDS-PAGE after resuspension in 10 µL SDS loading buffer and heated at 100 °C for denaturation. 15% gels were prepared, and samples were run at 160 V for ~60 min. Protein bands were observed using Coomassie staining and compared with Precision Plus Protein™ Dual Color Standard. Using this small-scale expression trial, colonies that are high-expressing were selected for further use.

### 2.3.2. Large scale production of ACA-01: Expression and Harvest

BL21 (DE3) cells were transformed with $His_6$-SUMO-ACA-01 and plated on LB agar containing 50 µg/ml kanamycin. 50 ml of LB medium containing 50 µg/ml of kanamycin in a 250 ml conical flask was inoculated with a colony of BL21 (DE3) transformed with the $His_6$-SUMO-ACA-01 plasmid. The starter culture was grown in the shaking incubator overnight at 37 °C, 180 rpm. The next day 4 L LB media (500 ml in each 1 L flask) was inoculated with 5 ml of freshly prepared starter culture to each flask (containing with 50 µg/ml kanamycin). This was then incubated at 37 °C in a shaker incubator at 180 rpm until $OD_{600}$ reached between 0.4 - 0.6. Once the $OD_{600}$ was reached, 1 ml IPTG (final concentration 0.5 mM) was added to each flask and incubated in a shaking incubator for 16-18 hrs at 37 °C and 180 rpm.

Cells were harvested by centrifugation for 30 minutes at 4 $^{o}$C and 8500 rpm using SORVALL centrifugation rotor. 10 µL samples of supernatant and pellet were collected and analysed by SDS PAGE. The cell pellets were transferred to 50 ml Falcon tubes and resuspended in lysis buffer (for 5 ml of cells 25 ml of Lysis Buffer was used). From this point onwards, samples were maintained on ice to minimise aggregation. To facilitate cell lysis 100 ul of 10mg/ml lysozyme (final concentration 100 µg/ml) was added and incubated the cells on shaker at 30 $^{o}$C for 30 mins. The lysed cells were sonicated with 3 X 60 sec with 60 sec cooling intervals. The cells are then centrifuged (40 mins at 15000 rpm) to collect the supernatant and filtered through 0.45 µm filter.

The insoluble fraction was resuspended in 10 mL Lysis Buffer and 5mg/mL of DNAse was added and incubated at room temperature for 30 minutes. The suspension was then centrifuged at 15, 000 rpm for 40 minutes, and the pellet was resuspended in 10 mL Inclusion Body Wash Buffer. After centrifugation (same as above), the pellet was resuspended in Load/Equilibration Buffer (10 mL) and left to denature overnight at 4 °C. The protein was unfolded after overnight denaturation in Load/Equilibration Buffer.

After overnight denaturation, the protein was separated from bacterial proteins by Immobilized Metal Affinity Chromatography (IMAC) using a HisTrap column. Protein was eluted using an ÄKTA Purifier FPLC which was equipped with UV lamp at 280 using HisTrap Buffer A and HisTrap Buffer B. The flow-through contained bacterial proteins while the His-tagged protein was bound to the HisTrap column which was then eluted in HisTrap Buffer B.

### 2.3.3. Purification

At this stage, the protein had been unfolded through denaturation and maintained in the denatured state during previous purification steps. Thus, a refolding step was needed to refold the protein, which was achieved by a rapid dilution refolding method, in which the protein solution (~30 mL) was added slowly at ~0.1 mL/min into rapidly stirring refolding buffer (2 L). This method allowed the denatured protein to be rapidly diluted with minimal aggregation or precipitation. The refolding solution was then filtered with Whatman filter paper (pore size 25 µm) and loaded onto a HisTrap column at 5 mL/min. Protein was eluted using an ÄKTA Purifier FPLC connected to a UV lamp at 280 nm. Fractions were collected and analysed by SDS-PAGE. Fractions containing semi-pure protein were then pooled.

For $His_6$-SUMO-ACA-01, the recombinant protein was expressed in soluble fraction, and after partial purification using a HisTrap column using HisTrap Buffer A and HisTrap Buffer B (protein was eluted in 100% Buffer B), the eluted fractions were pooled and dialysed against PBS pH 7.4. Dialysis was done in a snake-skin dialysis membrane placed in 1L PBS overnight. ACA-01 was partially purified using HisTrap column using HisTrap Buffer A and HisTrap Buffer B. ACA-01 was eluted in 100% Buffer A. The partially purified protein was incubated with Ulp1 protease (1:100 = Ulp1: $His_6$-SUMO-ACA-01) for cleavage at 30 $^oC$ for 1 hr. The maintenance of temperature is crucial for Ulp1 protease activity. Slight precipitation was seen, which was removed by further centrifugation. Completion of cleavage was analysed by SDS PAGE. After cleavage, the protein was purified using a HisTrap column with HisTrap Buffer A and HisTrap Buffer B. The flow-through, which contained ~80% of the cleaved ACA-01, was collected. The HisTrap column contained the $His_6$-SUM- and the flow through contained cleaved ACA-01. 100 % HisTrap Buffer B was run for a further 20 minutes to elute any remaining proteins. The protein concentration was measured using UV spectroscopy and an SDS PAGE analysis was conducted at this stage. The flow through and the eluted protein were concentrated using a spin concentrator MW cut - off 3 KDa.

Final purification was done purified using gel filtration using a PSEC buffer. Pooled fractions were concentrated to a final volume of 2 mL and injected onto a Hi-Load 16/60 Superdex 75 prep grade SEC column which was attached to a ÄKTA Purifier FPLC and run at 0.3 mL/min with PSEC Buffer. Fractions containing protein were collected analysed by SDS-PAGE to assess purity.

The amount of protein present was determined using spectrophotometry (280 nm) and the Beer-Lambert law:

$$\text{mass (g)} = A / [\ \varepsilon\ (\text{mol.L}^{-1}\ \text{cm}^{-1})\ x\ l\ (\text{cm})\ ]\ x\ Mw\ (\text{gmol}^{-1})\ x\ V\ (\text{L})$$

Fractions containing the desired protein were pooled, concentrated, and snap frozen in liquid nitrogen and stored at -80 °C until further use.

## 2.4. Quality Control:

### 2.4.1. Analytical Size Exclusion Chromatography

For ASEC, a SEC Yarra™-2000 column was used. 20 µl of the purified protein was injected in the column and 0.1 M $NaH_2PO_4$ buffer (pH 7.5) was used to elute the protein at a flow rate of 0.35 ml/min. Protein elution was determined by the detector at 280 nm.

### 2.4.2. MALDI mass spectrometric analyses

For MALDI mass spectrometric analyses, samples were mixed 1:1 with matrix solution of 10mg/ml a-cyano-4-hydroxycinnamic acid (Laser BioLabs, Sophia-Antipolis**,** France) in 50% Acetonitrile 0.1% TFA and spotted onto an MTP anchorChip 800/384 TF MALDI target plate. The sample were analysed on a Bruker Daltonics (Bremen, Germany) ULTRAFLEX MALDI TOF/TOF in reflector mode with an m/z range of 5000 to 20000Da, using Smartbeam parameter set 4, and detector gain 2.5x for 1000 shots. The data was processed using flexAnalysis Version 3.4(build50). The spectra externally calibrated against Myoglobin peaks which was spotted on adjacent calibration wells. For internal calibration the Myoglobin was co-spotted with the sample.

## 2.5. Fluorescence Anisotropy Assay

### 2.5.1. Direct Binding Assay (DBA):

The method for Direct Binding Assay was previously developed in the lab, to determine the affinity of each chemokine for the Fl-R3D peptide. Duplicate assays were performed 3 times independently in a 96 well plate. Briefly, a solution of the chemokine was prepared at double the desired final concentration (1 µM for 500 nM final) and added to wells A1 and A2. A serial 2-fold dilution of the samples was conducted (in MOPS Buffer), with no chemokine solution added to the final row H (which provided the Yfinal value for Competitive Binding Assays, below). A solution of Fl-R3D was then prepared at double the desired final concentration (at 20 nM for 10 nM final) and overlayed in each well. A sample of free fluorescein (5 nM) was used in a separate well as a reference for solution height and intensity. A BMG Labtech PHERAstar FS plate reader was used to measure fluorescence anisotropy 5 minutes after plating, with excitation and emission wavelengths of 485 and 520 nm, respectively. GraphPad Prism v.6.0 software was used to plot the mean anisotropy and fit a non-linear regression line using an established equation that describes a simple equilibrium 1:1 binding model to determine the pKd ± SEM.

### 2.5.2. Competitive Binding Assay (CBA):

Competitive Binding Assays were conducted against a panel of 6 CC chemokines to screen for chemokine binding ability. 96 well plates were used for the initial screening. Duplicate assays were performed 3 times independently. Briefly, a solution of ACA-01 was prepared at double the desired final concentration (at 2 µM for 1 µM final); a serial 2-fold dilution was conducted with no ACA-01 solution added to the final row H; and a solution of Fl-R3D and the chemokine to be screened was then prepared at double the final concentration (at a ratio of 20 nM Fl-R3D: 200 nM chemokine for 10 nM: 100 nM final) and overlayed. As for the DBAs, free fluorescein was used as a reference and fluorescence anisotropy was measured 5 mins after plating. The anisotropy values were entered into GraphPad Prism v.6.0 software, which plotted the mean anisotropy and fitted a non-linear regression line using an established equation that describes a 1:1 competitive displacement curve. The pKd ± SEM for the binding of the Evasin to the chemokine was calculated with reference to the pKd for the binding of Fl-R3D to the chemokine (determined in the DBA).

### 2.5.3. Statistical Analysis:

The following equations are derived when considering the formation of a reversible 1:l complex between a receptor (R) and either labeled (L) or unlabeled (U) ligand.

$$R + L \rightleftharpoons R\,L \tag{1}$$

$$R + U \rightleftharpoons R\,U \tag{2}$$

$$KL = \frac{[R][L]}{[RL]}\ \frac{(RT - [RL] - [RU])(LT - [RL])}{[RL]} \tag{3}$$

$$KU = \frac{[R][U]}{[RU]}\ \frac{(RT - [RL] - [RU])(UT - [RU])}{[RU]} \tag{4}$$

$K_L$ and $K_U$ are dissociation constants; RT, LT, and UT represent total concentrations.

$$\frac{KL}{KU} = \frac{(LT-[RL])[RL]}{UT-[RU][RL]} \tag{5}$$

After solving equation 5 for [RU]

$$RU = \frac{(KL)(UT)[RL]}{(KU)(LT)+\Delta K[RL]} \tag{6}$$

where ΔK = KL – KU, substitution for R, in Equation 3 would obtain the following:

$$[RL]^3 + \frac{(KL)(UT)+(KU)(LT)-\Delta K(RT+LT+KL)}{\Delta K}[RL]^2 +$$

$$\frac{LT(RT\Delta K-(KU)(LT)-(KL)(UT)-(RT)(KU)-(KL)(KU))}{\Delta K}[RL] + \frac{(RT)(LT)_2(KU)}{\Delta K} = 0 \quad (7)$$

Further equation 7 was simplified by Olson et al. (1991), in cubic form:

$$x^3+a_1x^2+a_2x+a^3= 0 \quad (8)$$

whose roots are given by,

Assuming KU > KL, $[RL]= -2\sqrt{Q}\cos\frac{\theta}{3} - \frac{a1}{3}$ (9)

For KU<KL, $[RL]= -2\sqrt{Q}\cos\frac{\theta+4\pi}{3} - \frac{a1}{3}$ (10)

Where,

$\theta = \text{acos}\ (R / \sqrt{Q^3}))$, $Q = (a_1^2-3a_2)/9$ and $R = (2a_1^3-9a_1a_2+27a_3)/54$ (11)

Competitive Displacement data were fit to the equation below:

$$A=A_i+ \frac{(Af-Ai)[RL]}{LT} \quad (12)$$

In equation 12, A = the observed anisotropy, $A_i$ = is the anisotropy in the absence of any R, Af = is the maximum anisotropy that would be observed in the presence of saturating levels of R, and [RL] is the concentration of bound L. We fitted each set of displacement data using equation 9 when we have initial estimates of KU>KL and corresponding constraints and Equation 10 with initial estimates of KU<KL.

### 2.6. Stability Studies:

Purified ACA-01 was stored at -20 $^oC$ and prior to experiments, protein concentration was measured via UV absorbance at 280 nm. Frozen ACA-01 was thawed by holding the tube in the palm for 5 minutes, and $UV_{280}$ measured and recorded. The sample was re-frozen and re-thawed on three consecutive days and $UV_{280}$ measured.

### 2.6.1 Thermal Shift Assay:

For stability studies, a thermal shift assay was conducted. We prepared 48 different buffers based 6 different buffers; 50 mM sodium phosphate, 50 mM MOPS, 50 mM Bis-Tris, 50 mM HEPES and 50 mM Tris with a pH range of 7.0 – 8.0 in addition to a low and high concentration of salt in each of the buffers. Dilution buffer was added to the protein stock solution in a 15 ml conical tube to obtain a final volume of 5 ml, sufficient to screen one 96-well plate. 4 µl of SYPRO Orange dye (stock concentration: 5000X) was added to the protein solution such that the final concentrations of protein and dye in the mixture was 5 µM and 2X respectively. Protein, dye and dilution buffer were thoroughly mixed by inverting the tube several times and then the solution was placed in a multichannel pipette reservoir trough. A multichannel pipette was used to transfer 40 µl of solution into each well of a 96-well assay plate and centrifuged at room temperature 5× buffer screen plate at 800 × g for 2 min at 25 °C. 10 µl of the buffer screen stocks was added to the assay plate. The mix was then inverted several times and incubated for 10 minutes. The assay plate was centrifuged at 800 × g for 2 min at 25 °C to collect solutions in the bottom of the well and remove air bubbles. A real-time PCR instrument was used to perform the assay. We created a 2 min initial hold at 20 °C, then ramp temperature in 0.5 – 1.0 °C increments up to 95 °C, reading fluorescence at the end of a 1 min hold at each temperature.

### 2.6.2. Crystallisation trials:

For crystal trials, purified ACA-01 was submitted to the Monash Macromolecular Crystallisation Facility (MMCF) at concentrations of 8.5 mg/ml and 10 mg/ml in PSEC buffer. Different conditions that were used are: JCSG+, PACT, Peg Ion-4, Morpheus-4, Morpheus-II. Crystallisation trials were performed using the NT8 crystallisation robot (by Formulatrix). Briefly, 100 nL of protein was mixed with 100 nL of crystallisation buffer in each drop, in 96-well SWISSCI MRC 2 Lens Crystallisation Plates made of UVXPO polymer (Swissci). Plates were then sealed with 3-inch-wide Crystal-Clear Sealing Tape (Hampton Research) for incubation in Rock Imager incubators (Formulatrix) with automatic imaging on preset dates. The four screens used for crystallisation were: JCSG+ and PACT (from Nextal Biotech), PEG Ion-4 (from Hampton Research), Morpheus and Morpheus-II (from Molecular Dimensions).

# Chapter 3: Expression, Purification and Characterization of ACA 01

## Chapter 3: Expression, Purification, and Characterization of ACA 01

### *3.1. Expression and Purification of ACA-01 using $His_6$-ACA-01 construct*

The goal of this thesis was to characterize the putative novel chemokine-binding protein ACA-01. In order to achieve this goal, the first step was to overexpress ACA-01 in BL21 (DE3) *E. coli* cells and prepare it to a high level of purity. After obtaining sufficient amount of protein, our next aim was to test for chemokine-binding affinity and attempt to solve the three-dimensional crystal structure of ACA-01.

Previously, one of our lab members expressed ACA-01 in BL21 (DE3) *E. coli* cells and purified it using Immobilized Metal Affinity Chromatography (IMAC). Although the expression was considered to be reasonable, the yield of the protein was very poor due to the protein being expressed in inclusion bodies and loss of protein during subsequent refolding of the denatured protein obtained from inclusion bodies. Furthermore, PSEC was not conducted, and only partial purification of the protein was achieved through nickel affinity chromatography. This was therefore not suitable for biophysical analysis.

The first part of this chapter therefore focuses on the development of an effective overexpression and purification protocol for the production of pure ACA-01, and the second part focuses on increasing the yield of ACA-01 using an expression vector with a solubility tag.

### *3.2. Colony screening:*

For the purpose of obtaining a better yield of protein, I started with the overexpression of $His_6$-tagged ACA-01. A pET28a vector containing the construct $His_6$–ACA-01 was obtained from GenScript and competent BL21 (DE3) *E. coli* cells were transformed with the vector for the expression of N-terminally $His_6$-tagged ACA-01 as described in Materials and Methods section 2.2.2. In order to identify successful transformation of the bacterial colonies, thirteen colonies were selected and checked for their ability to express ACA-01.

Briefly, the colonies from the transformed plates were picked and cultured, followed by induction with 1 mM (IPTG) to induce protein expression. After overnight (ON) growth, a small sample of each culture was centrifuged and the expression of the protein tested by SDS-PAGE. $His_6$-tagged ACA-01 has a MW of 12,313 Da, and according to Figure 3.1, all the colonies showed overexpressed protein at ~15 kDa. Proteins might run at slightly higher MW than expected on SDS-PAGE because they may not be fully denatured prior to electrophoresis. Darker bands were observed for lanes 4 – 6 that are likely due to a higher amount of sample loaded. In terms of the overexpression of ACA-01 we did not notice any significant difference amongst the colonies, and hence we could select any of these colonies for large-scale production of ACA-01. We selected colony 5.

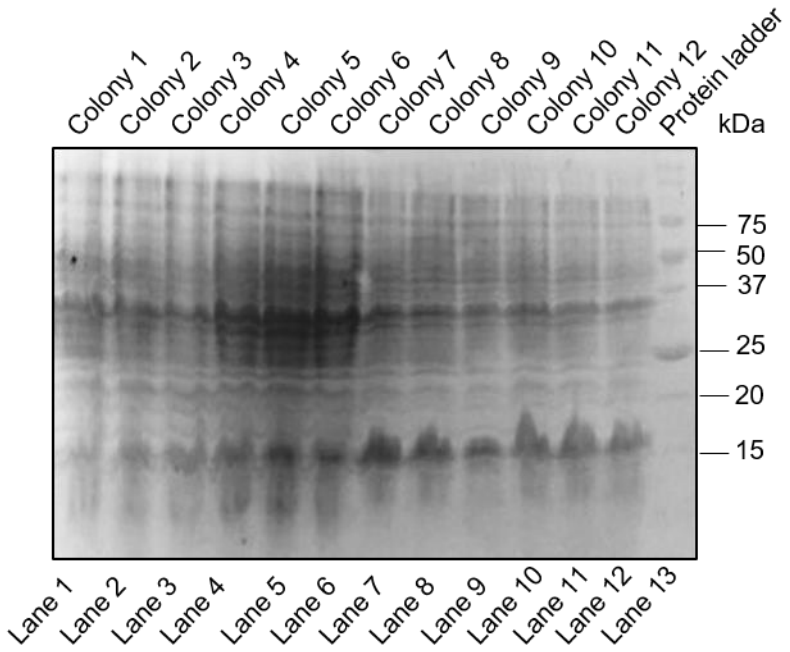


**Figure 3.1: SDS-PAGE analysis of small-scale colony screening of ACA-01 in BL21 (DE3) E. coli cells.** Lanes 1 – 12: Pellets collected from small-scale culture of colonies of BL21 (DE3) E. coli transformed with $His_6$ – ACA-01. Lane 13: Molecular weight marker. The Figure shows all the colonies had overexpressed ACA-01.

### *3.3. Large-scale production of recombinant protein*

With the intention of large-scale production of ACA-01, 4 X 1 L LB was inoculated with 10 ml starter culture, which was grown overnight. Cells were incubated at 37 $^{o}$C in a shaking incubator and induced with 1 mM IPTG once the $OD_{600}$ reached 0.6 absorbance units (AU). Cells were then harvested after ON expression, sonicated and the soluble fraction separated from the insoluble fraction by centrifugation. To analyse the overexpression of ACA-01, small samples before and after induction were examined using SDS-PAGE, under reducing and non-reducing conditions. Non-reducing conditions were used to separate proteins based only on the denaturing capabilities of SDS; this allows for the separation of protein subunits that are not linked by disulfide bonds (i.e. noncovalently linked proteins). Reducing conditions using β–mercaptoethanol, disrupt the disulfide bonds.

According to the gel image shown in Figure 3.2, we observed that the protein is overexpressed after induction with 1 mM IPTG. The over-expressed protein after induction was observed to run at ~15 kDa under both reducing and non-reducing conditions. Lane 2 and 5 shows ACA-01 in both reducing and non-reducing conditions. Since the protein appears in both reducing and non-reducing conditions, we assume that ACA-01 is not a disulfide-linked oligomer. After harvesting the cells, the difference in the intensity of the bands of soluble and insoluble fractions (lane 6 and 7 respectively) on SDS-PAGE was possibly because of unequal amounts of samples loaded on the gel. The insoluble fraction was collected since it contained protein at the expected MW and taken for further purification.

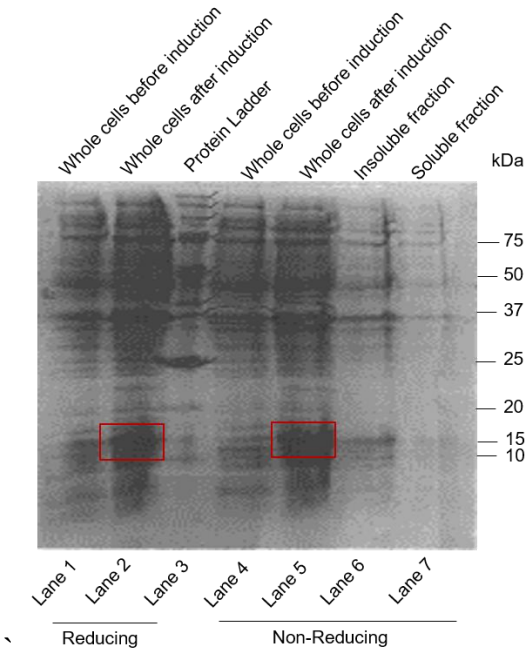


**Figure 3.2: SDS-PAGE analysis for expression of ACA-01**. Lane 1 – 2: Whole cells before and after induction with 1 mM IPTG (under reducing condition). Lane 3: Molecular weight marker. Lane 4 – 5: Whole cells before and after induction with 1 mM IPTG (under non-reducing condition). Lane 6: Insoluble fraction Lane 7: Soluble fraction. ACA-01 was overexpressed after induction and was observed to be mostly in the insoluble fraction.

### *3.4. Partial Purification of ACA-01 through Nickel Affinity Chromatography*

Since the protein was tagged with $His_6$, it could be solubilised and purified using nickel affinity chromatography. Solubilisation was achieved using Inclusion Body Wash buffer containing 0.5 % (v/v) Triton X-100. The $His_6$-tagged ACA-01 was then separated from other bacterial proteins using nickel affinity chromatography (details included in Materials and methods section 2.3.2). $His_6$-tagged ACA-01 bound to the nickel column while the bacterial proteins were removed as flow-through. $His_6$-tagged ACA-01 was then eluted from the column in a buffer with high concentration of imidazole (200 mM). The protein collected after HisTrap elution was allowed to refold overnight in a buffer containing a mixture of reduced and oxidized glutathione. This was done to allow the denatured protein to exchange disulfide bonds until the correct disulfide formation was achieved. Refolding was conducted by a rapid-dilution refolding method, in which ~30 mL of the protein solution was added slowly (~ 0.1 ml/min) into a rapidly stirred refolding buffer (2 L). This ensured that the denatured

protein was able to fold in a diluted condition with minimal aggregation or precipitation. However, after overnight refolding, the buffer was observed to be quite cloudy, which suggested that a degree of aggregate formation had occurred.

The cloudy protein solution was then filtered and loaded onto a HisTrap Nickel Affinity column as a concentrating step (at 5 ml/min). On the ÄKTA Purifier FPLC, the protein was eluted through isocratic elution using 200 mM imidazole. Fractions were collected and analysed by SDS-PAGE. Figure 3.3 shows the image for SDS-PAGE, under non-reducing conditions, for the fractions collected after elution from the HisTrap column. All the fractions show a consistent band at the expected MW range of 15 kDa, however, we can also see bands at ~25 kDa and 75 kDa which could possibly be dimers and multimers of ACA-01. The fractions containing semi-pure proteins were then pooled, concentrated and purified by PSEC.

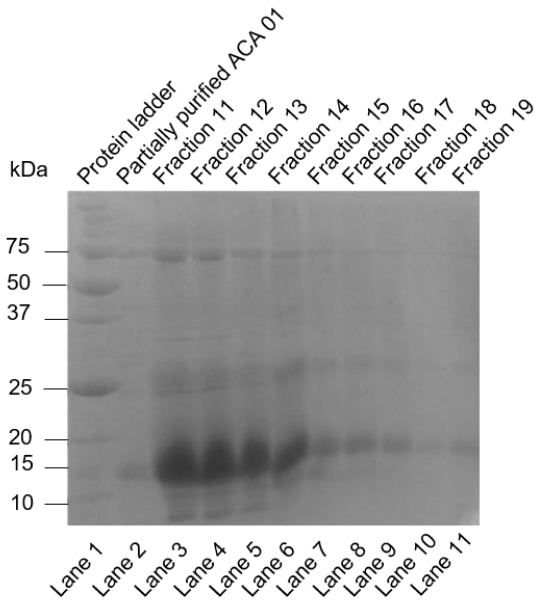


**Figure 3.3: SDS-PAGE analysis for partial purification of ACA-01 through Nickel Affinity Chromatography**. Lane 1: Molecular weight marker. Lane 2: Partially purified ACA-01 by previous lab member. Lane 3 – 19: Fractions collected after HisTrap elution for partial purification of ACA-01 after dropwise refolding. All the samples were run on the gel under non-reducing conditions.

### *3.5. Preparative Size Exclusion Chromatograohy and Analysis of Purity and Homogeneity*

The final step of purification involved PSEC. Pooled fractions of semi-pure ACA01 after Nickel Affinity purification were concentrated to 2 ml and injected onto a Hi-Load 16/60 Superdex 75 prep grade SEC column attached to the ÄKTA Purifier FPLC and eluted at 0.3 ml/min with PSEC Buffer containing 10 mM HEPES. As shown in Figure 3.4 (A) two distinct peaks were observed; fractions from both the peaks were collected and analysed by SDS-PAGE under reducing and non-reducing conditions Figure 3.4 (B). Sample treatment for SDS-PAGE breaks down intermolecular non-covalent bonds, while intramolecular disulfide bonds remain intact. Sample containing intermolecular disulfide bonds, will appear as multimers under non-reducing condition, and monomers under reducing conditions since intermolecular disulfide bonds will be reduced by the presence of β- mercaptoethanol under reducing conditions. Two peaks were observed in Figure 3.4 (A) PSEC Chromatogram. Fractions 17-18 corresponding to the first peak, showed a laddering pattern in both reducing and non-reducing conditions. ACA-01 is clearly present at the expected MW, but so are larger MW species that appear at multiples of this MW that are suggestive of multimer formation – although multimers would not really be expected to be seen in SDS-PAGE. Under reducing conditions, these intramolecular covalent bonds are expected to be reduced by the presence of β- mercaptoethanol and since reduction did not happen, it could mean that β- mercaptoethanol has gone bad. The other possibility might be that these are non-covalent multimers which appear in the higher MW due to incomplete heating of samples prior to SDS-PAGE analysis. Contaminants present in the sample might also appear in the higher MW range. Fractions 29-31 corresponding to the second peak, shows monomeric ACA-01 under reducing conditions. Under non-reducing conditions, the presence of a protein band at a molecular weight corresponding to dimeric ACA-01 was observed for fraction 29. Bands corresponding to monomeric ACA-01 was observed for fractions 30-31 in both reducing and non-reducing conditions which were then pooled and concentrated for further use.

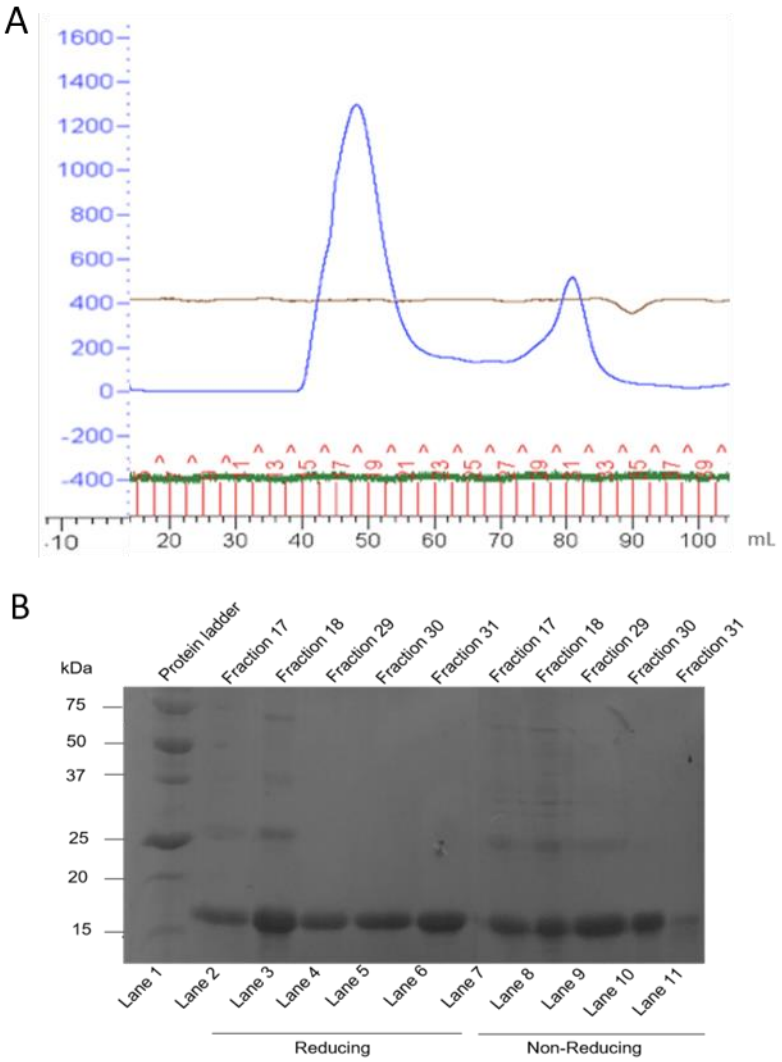


**Figure 3.4: Purification by PSEC and SDS-PAGE analysis of ACA-01.** A: Preparative Size Exclusion Chromatogram (A280; absorbance at 280 nm) showing the purification of ACA-01. The two other parameters observed on the chromatogram are conductivity (depends on salt concentration and remains constant during elution) and pressure (maintained at a constant pressure of 0.3 MPa) of the column. B: SDS-PAGE analysis of the purified fractions of ACA-01 by SEC. Samples for SDS-PAGE were run under reducing and non-reducing conditions. Two peaks were observed after purification by SEC. SDS-PAGE analysis illustrates fractions 17 – 18 from peak 1 of SEC containing a mixture of monomer and non-covalently bonded multimers, while fractions 29 – 31 of peak 2 containing mostly monomer with a trace of non-covalently bonded dimer observed only in fraction 29.

So far, we observed that ACA-01 runs at ~15 kDa on SDS-PAGE although the expected MW of ACA-01 is 12313 Da. Hence, it was important to identify the protein. Mass spectrometry was used to assess the purified protein for its expected molecular weight. 20 µl of 1.4 mg/ml was submitted to Monash Biomedical Proteomics Facility for Matrix Assisted Laser Desorption Ionization (MALDI), a technique used for mass analysis. The method is described in Materials and Methods Section 2.4.2.

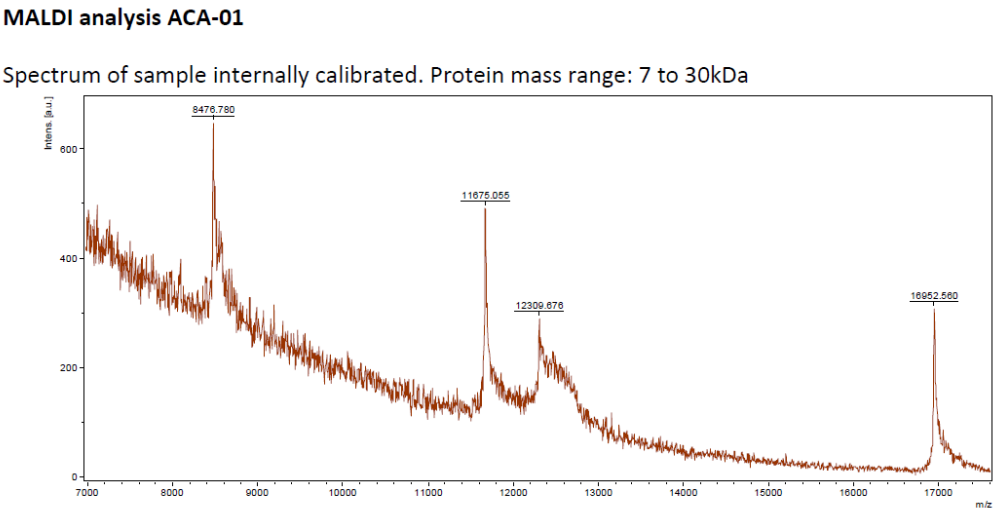


**Figure 3.5: MALDI Analysis of ACA-01.** 12309.7 Da mass observed. Peaks at 8476, 11675 and 16952 are protein standards for internal calibration.

According to Expasy Protparam the N-terminally $His_6$-tagged ACA-01 has an expected MW of 12313.7 Da. It contains 4 intra-molecular disulfide bonds, and hence the MW of ACA-01 will appear 8 Da less than this with an expected MW of 12305.7 Da. The observed mass on Mass Spec was 12309.7 Da (Figure 3.5), which is within the level of accuracy of MALDI (5 to 10 Da). Thus, we confirmed that we obtained ACA-01 with the correct MW.

Once the protein was analysed by Mass spectrometry, it was essential to determine the purity and homogeneity of ACA-01. This was conducted using ASEC which is a separation technique for proteins and other compounds based on the size (or more specifically the Stokes radii) of the analytes in solution. A calibration curve can be derived from a set of unknown analytes, through size-based separation, which can be

used to estimate the molecular weight of an unknown analyte (Striegel 2009, Guo 2003, Vander Heyden 2000). Typical calibration curves are based on proteins or polymers of known molecular weight. By plotting the log M (log molecular weight) versus retention volume Ve/Vo, we generated the expected MW (Table 1.2 Appendix I).

For the evaluation of purity and homogeneity of ACA-01, a Yarra 3 µm SEC-2000 column was used. 0.1 M sodium-phosphate buffer pH 7.5, was used as mobile phase at 0.35 ml/min flow rate. A series of protein standards, 7 µg each, was used to establish a calibration curve for the column. The data are provided in Appendix I. Protein standards were selected for a range that would include both large and small MW. However, we obtained an acceptable linear region for apparent MW ~50 to 10 kDa, and ACA-01 is within this MW range.

To analyse the purity of ACA-01 we injected 17.5 µg of the protein in the column and obtained the chromatogram in Figure 3.6. According to the chromatogram, we observed three distinct peaks. The first peak was eluted at 5.5 min which was beyond the linear region of column calibration. This molecule was possibly an aggregate with a high MW. The second (and major) peak observed was eluted at 9.2 min, which was within the linear region (according to Table 1.2 Appendix I) and had an apparent MW of ~19 kDa. The expected MW of ACA-01 is 12 kDa and mass spec analysis had confirmed this. The difference in MW supports the possibility of ACA-01 existing in a shape that might allow it to elute in the higher MW range. Dimerization could be a possibility; however, we could not run a native gel that would confirm the presence of dimers.

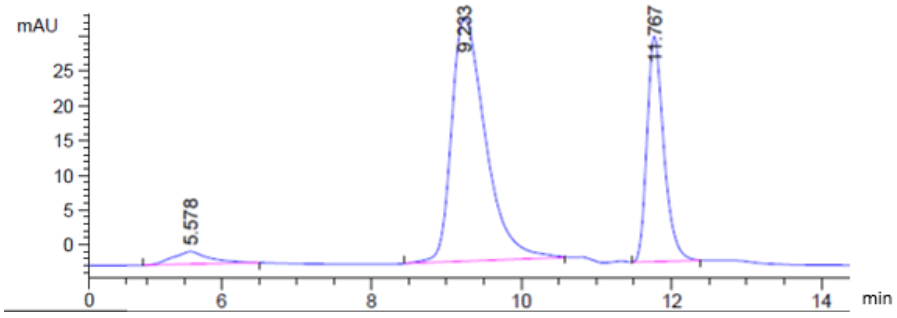


**Figure 3.6: Analytical Size Exclusion Chromatogram of ACA-01.** Sample was analysed through Yarra 3 µm SEC-2000 column and $NaH_2PO_4$ was used as mobile phase buffer. Flow rate was maintained at 0.35 ml/min. Elution of protein was

detected at 280 nm (monitored as mAU). Three distinct peaks were observed; first peak (at 5.5 min) was that of aggregates, the second peak corresponds to ACA-01(at 9.2 min) and the third peak could be that of HEPES (at 11.7 min) from previous purification step. ACA-01 eluted at 9.23 min with an apparent MW ~19 kDa.

The final yield of ACA-01 was only 1.67 mg from 4 L culture total. The low yield and presence of aggregates drove us to find an expression system that would allow us to obtain soluble expression and subsequent production of pure ACA-01.

A new construct was designed for ACA-01 with a soluble SUMO–tag as well as a $His_6$-tag at the N-terminus that could facilitate soluble expression of ACA-01 in *E coli*. This would also avoid the need for refolding, which contributes to protein aggregation. SUMO is a small ubiquitin-like modifier that facilitates functional protein production in prokaryotic and eukaryotic expression systems, based upon significantly improved protein stability and solubility. Following the expression and purification of the fusion protein, the SUMO-tag can be cleaved by specific (SUMO) proteases via their endopeptidase activity *in vitro* to generate the desired N-terminus of the released protein partner (Panavas 2009). With the aim of soluble expression of ACA-01 we decided to use the SUMO-tag and hence ordered the construct $His_6$-SUMO-ACA-01 in pET28a from GeneScript.

### *3.6. Small-scale expression trial for SUMO-tagged ACA-01*

Initially, a small-scale expression trial was conducted to determine the optimum temperature and IPTG concentration for expression of $His_6$-SUMO-ACA-01. BL21 (DE3) *E. coli* cells were transformed with $His_6$-SUMO-ACA-01 and a colony was cultured in a small scale of 10 ml of $LB_{Kan}$. Cells were induced at three different concentrations of IPTG: 0.2 mM, 0.5 mM and 1 mM, and post-induction overnight (ON) growth temperatures of 18 $^oC$, 25 $^oC$, and 37 $^oC$. After ON expression, the pellets were analysed on SDS-PAGE (Figure 3.7).

Overexpression of $His_6$-SUMO-ACA-01 was observed at ~30 kDa, which was consistently observed across all the conditions (Figure 3.7). Lanes 4 and 8, corresponding to 0.5 mM IPTG at 37 $^oC$ and 1 mM IPTG at 25 $^oC$ respectively, showed

lighter bands due to low amount of sample loaded. The other consistently overexpressed band was observed at ~15 kDa, which could possibly be of *E. coli* protein. The expected MW of $His_6$-SUMO-ACA-01 is ~23 kDa, and this is discrepancy could be due to highly cationic nature of $His_6$-SUMO- which might lower its mobility on SDS-PAGE. Alternatively, the conformation of $His_6$-SUMO-ACA-01 might be such as to lower its mobility on SDS-PAGE.

Since $His_6$-SUMO-ACA-01 was overexpressed in all different conditions, including 18 $^oC$, we selected 18 $^oC$ as the optimum temperature for post-induction overexpression of the SUMO-tagged recombinant protein post-induction. This was done considering that a low cultivation temperature is most likely to reduce protein aggregation due to slowing down of the rate of protein synthesis, which in turn would reduce self-aggregation (Schumann 2004). In addition to this, we selected 0.5 mM IPTG concentration for large-scale production of protein. Although for economic purpose 0.2 mM IPTG concentration could have been selected, 0.2 mM could be too low a concentration at a larger scale and we did not want to risk future experiments.

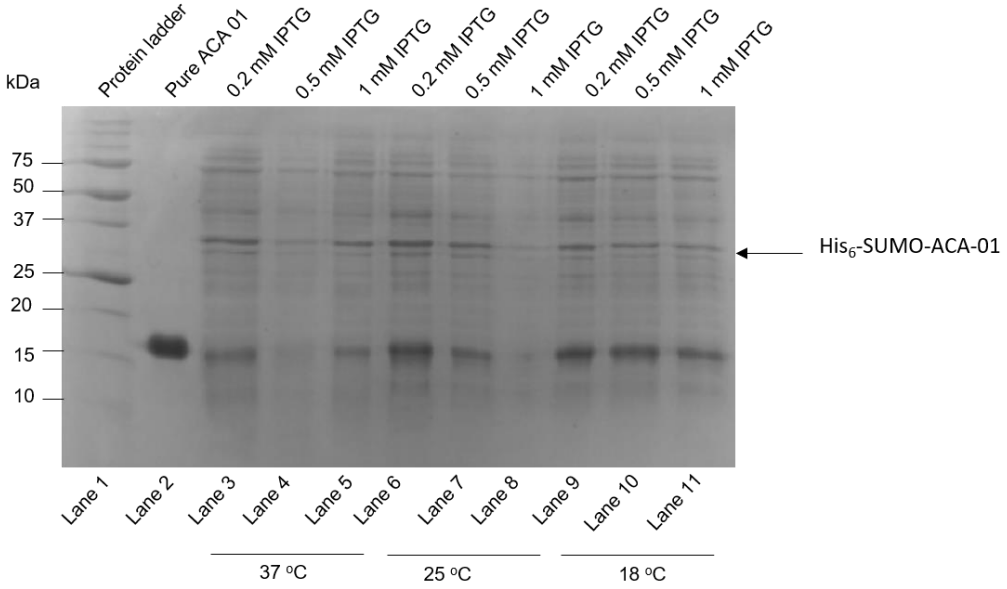


**Figure 3.7: SDS-PAGE analysis for small-scale expression trials of ACA-01**. Lane 1: Molecular weight marker. Lane 2: Pure ACA-01 from previous construct. Lane 3 – 5: *E. coli* grown at 37 $^oC$ and induced with 0.2 mM, 0.5 mM and 1 mM IPTG respectively. Lane 6 – 8: *E. coli* grown at 25 $^oC$ and induced with 0.2 mM, 0.5 mM and 1 mM IPTG respectively. Lane 9 – 11: *E. coli* grown at 18 $^oC$ and induced with 0.2 mM, 0.5 mM and 1 mM IPTG respectively.

### *3.7. Large-scale expression and purification of ACA-01 from $His_6$-SUMO-ACA-01*

For large-scale overexpression of soluble ACA-01, 4 X 1L LB cultures were grown at 37 $^oC$ pre-induction and 0.5 mM IPTG was added when the $OD_{600}$ reached 0.6. Cells were harvested after post-induction overnight incubation at 18 $^oC$ in a shaking incubator. Small samples of insoluble and soluble fractions were analysed on SDS-PAGE. Similar to small-scale expression trial results, large-scale overexpression of $His_6$-SUMO-ACA-01 was also observed to run at ~30 kDa (higher than its expected MW of ~23 kDa) in the soluble fraction (lane 2) of the culture (Figure 3.8). Lane 3 shows pre-induced whole cells. Lane 4 and 5 corresponds to insoluble fractions, which do not show the presence of the recombinant protein. Thus $His_6$-SUMO-ACA-01 was successfully expressed in the soluble fraction.

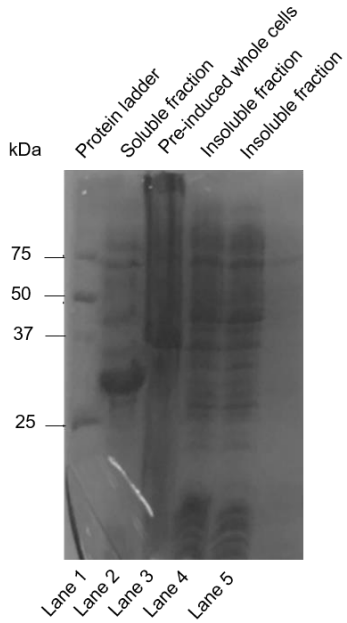


**Figure 3.8 SDS-PAGE analysis of soluble expression of ACA and partial purification after cleavage.** Lane 1: Molecular weight marker. Lane 2: Soluble Fraction. Lane 3: Pre-induced whole cells. Lane 4 – 5: Insoluble fraction. ACA-01 is observed to be largely expressed in soluble fraction.

The soluble fraction of the harvested protein was then filtered and separated from bacterial proteins via a nickel affinity purification step conducted using a HisTrap

column and ÄKTA FPLC. $His_6$-SUMO-ACA-01 bound to the nickel column while the bacterial proteins were removed as a flow through from the column. Figure 3.9 shows the chromatogram of the HisTrap partial purification of ACA-01. The curve for the removal of bacterial protein is not shown in the graph. Gradient elution was used to elute $His_6$-SUMO-ACA-01, with an increasing concentration of imidazole.

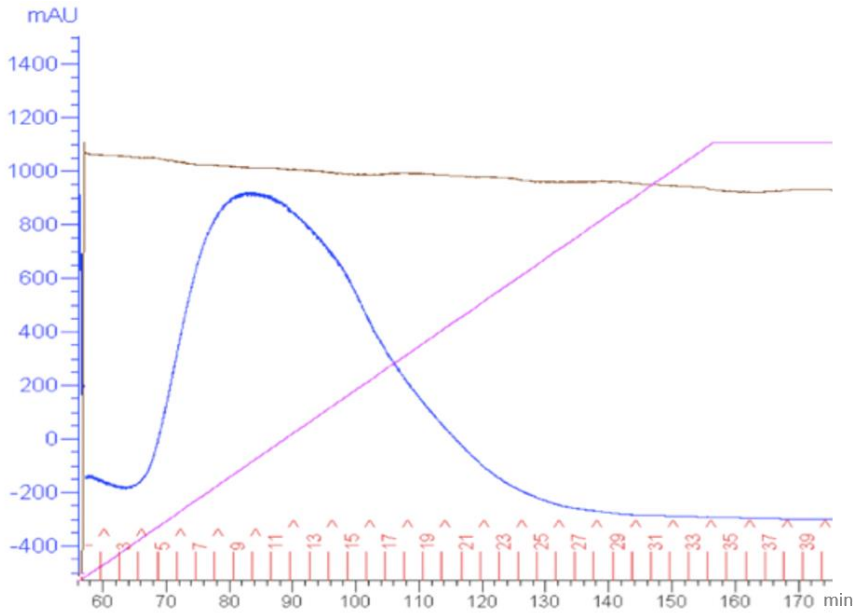


**Figure 3.9: Nickel Affinity Chromatogram for partial purification of ACA-01 prior to cleavage.** Chromatogram (A280; absorbance at 280 nm represented by mAU) showing the partial purification of ACA-01. The two other parameters observed on the chromatogram are conductivity represented by the brown curve (depends on salt concentration and remains constant during elution) and % Buffer B containing 200 mM Imidazole (increased slowly from 0 – 100% at 1 ml/min). Histagged bound ACA-01 was thus dissociated from the nickel column.

In order to obtain untagged ACA-01, it was important to cleave off the $His_6$-SUMO tag. Before cleaving the protein, it was buffer exchanged into PBS for 3 hours, for efficient cleavage of $His_6$-SUMO from ACA-01 by Ulp1. Cleavage was undertaken using Ulp1 protease at 18 $^oC$ on a rocker for 1 hour. Ulp1 cleaves the peptide bond C-terminal to a Gly-Gly site in the SUMO tag . At this stage, the efficiency of cleavage was checked by SDS-PAGE. Figure 3.10 confirms the apparent MW of the protein after cleavage. A small amount of the mix of $His_6$ -SUMO-ACA-01 and Ulp1 was

loaded onto lane 2 and 3, which shows two crisp bands for ACA-01 at ~10 kDa and for $His_6$ -SUMO- at ~15 kDa. After successfully cleaving the $His_6$-SUMO-ACA-01, the next step was partial purification of the cleaved ACA-01 from the free $His_6$-SUMO tag and any remaining uncleaved $His_6$–SUMO–ACA-01. This was achieved using a HisTrap column and ÄKTA FPLC, and a concentration of 20 mM imidazole. The elution pattern is shown in Figure 3.11. Fractions 6 – 17 correspond to the elution of cleaved ACA-01, while the $His_6$-SUMO is eluted by increasing the concentration of imidazole to 200 mM which dissociates bound $His_6$-SUMO from the nickel column. Cleaved fractions of ACA-01 were pooled and analysed by SDS-PAGE, under non - reducing conditions (Figure 3.10). Lane 4-5 corresponds to flow-through collected and pooled from the nickel column and confirms complete cleavage of ACA-01 as observed by the band at MW ~11 kDa. Lane 6 is the elution from the nickel column after it was washed with 200 mM imidazole. It contained $His_6$ -SUMO- and was observed to run at ~15 kDa.

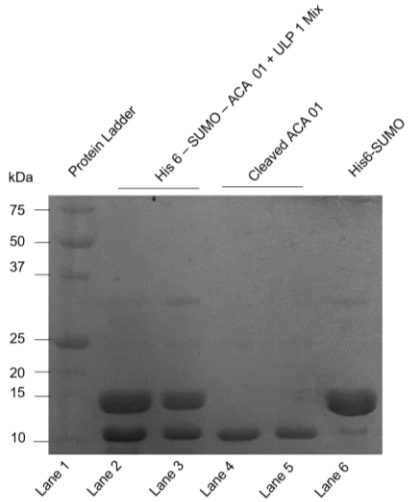


**Figure 3.10: SDS-PAGE analysis of cleavage of $His_6$ – SUMO – ACA-01.** Lane 1: Molecular weight marker. Lane 2 – 3: $His_6$ – SUMO – ACA + Ulp1 mix. Lane 4 – 5: Cleaved ACA-01. Lane 6: $His_6$ – SUMO. ACA-01 was successfully cleaved and appeared at the expected MW at 11 kDa.

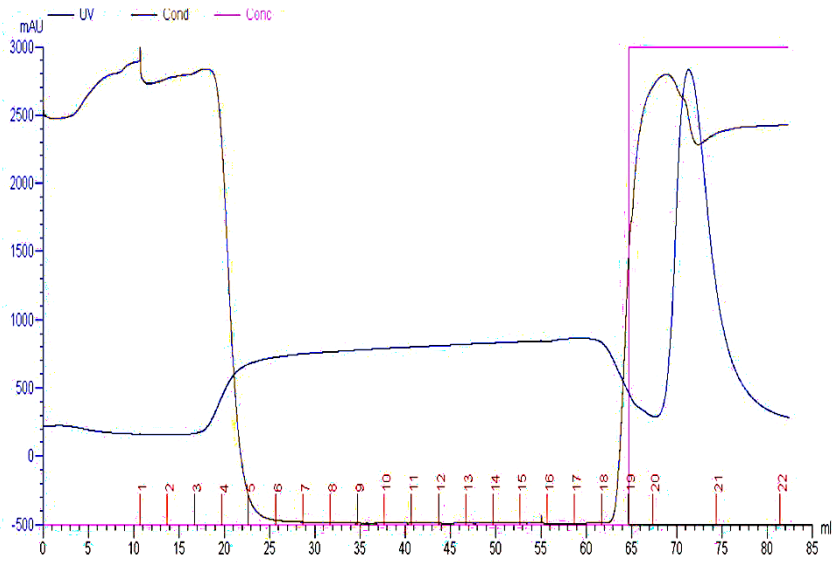


**Figure 3.11: Nickel Affinity Chromatogram for partial purification of cleaved ACA-01.** Purification profile of ACA-01 was observed with absorbance (mAU) detected at 280 nm (solid blue line) he two other parameters observed on the chromatogram are conductivity (brown line) which depends on salt concentration and remains constant during elution and % Buffer B (pink line) containing 200 mM imidazole (increased slowly from 0 – 100% at 1 ml/min). Histagged bound ACA-01 was thus dissociated from the nickel column.

In order to obtain pure ACA-01, the next step was to purify the protein by PSEC. The eluted ACA-01 from Nickel Affinity Chromatography was collected, pooled and concentrated to 2 ml and injected onto a Hi-Load 16/60 Superdex 75 prep grade SEC column attached to the ÄKTA Purifier FPLC and run at 0.3 ml/min with PSEC Buffer containing 10 mM HEPES pH 7.4. According to the chromatogram shown in Figure 3.12, elution of a broad shoulder of a peak started at ~42.5 ml which indicates the presence of aggregates. A significant peak is observed to begin at ~72.5 ml. The fractions of this peak 26 – 28 were collected and analysed using SDS-PAGE. The purified ACA-01 appeared to run at an apparent MW of ~10 kDa and the expected MW is 11,117.44 Da. Thus, we can confirm that we were able to successfully obtain pure ACA-01.

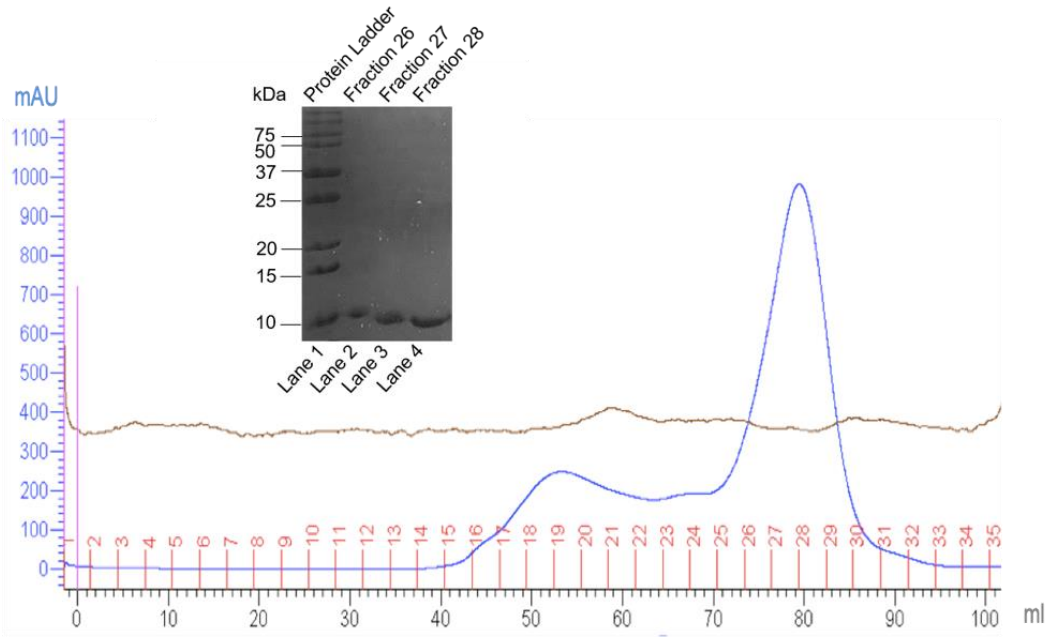


**Figure 3.12: Illustration of the purification of ACA-01 by PSEC.** The separation is detected by A280; absorbance at 280 nm depicted by the solid blue line. The other parameter observed on the chromatogram is conductivity of the column (depends on salt concentration and remains constant during elution) depicted by the brown line. ACA-01 was eluted at ~72.5 ml. SDS-PAGE analysis (under non-reducing condition) of the fractions 26 – 28 collected from PSEC is shown in inset. The fractions were observed to run at ~10 kDa MW.

### *3.8. Evaluation of Purity and homogeneity of ACA – 01*

After ACA-01 was purified by PSEC, the identification of the protein and its purity analysis was essential. We used MALDI to identify the protein. The sample was submitted to Monash Biomedical Proteomics Facility. According to Expasy Protparam the MW of ACA-01, without any tags is 11117.44 Da. It contains 4 intra-molecular disulfide bonds, and hence the MW of ACA-01 with all Cys residues considered is 11109.44 Da. The observed mass on Mass Spec was 11106.6 Da (Figure 3.13), which is 4 Da less than the expected mass but is within the accuracy of the MALDI method. Thus, we confirmed that we obtained ACA-01 with the correct MW.

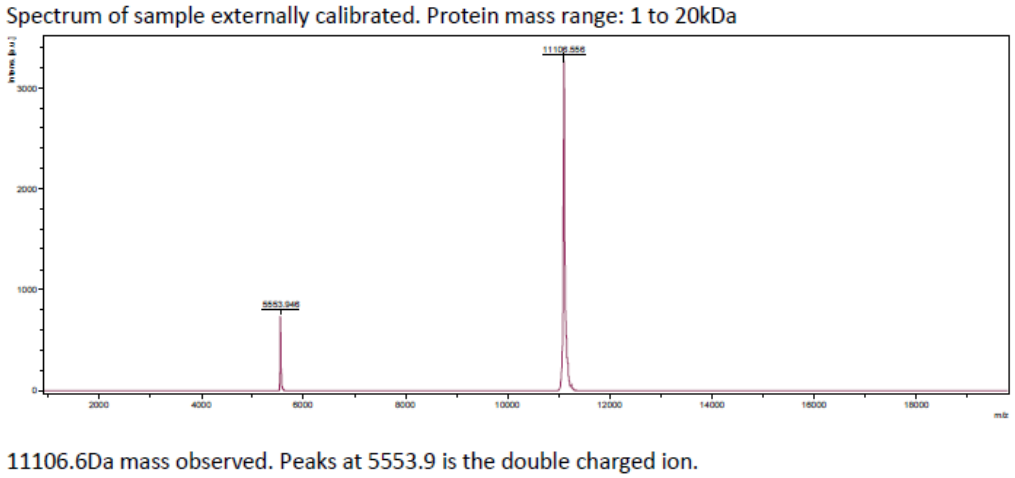


**Figure 3.13: De-convoluted spectrum showing the [M]+ masses observed.** The primary mass observed was 11110.6 Da, which is within the level of accuracy of MALDI (5 to 10 Da). Thus, we confirmed that we obtained ACA-01 with the correct MW.

Once the protein species was identified, further confirmation of purity and homogeneity of the protein was analysed by ASEC. Figure 3.14 shows the chromatogram for ASEC, and a single peak of the protein is observed at ~9.10 min, which according to the calibration of the Yarra 3 µm SEC-2000 column (Appendix I) has a MW of ~19 kDa. This is nearly double the expected MW of the monomer which is ~11 kDa. It is possible that the ACA-01 exists as a dimer in equilibrium with a monomeric form to give rise to the averaged elution time and the appearance of a shoulder of the peak as seen in Figure 3.14. In comparison to the ASEC data of ACA-01 from the previous construct, we did not see any aggregates or small molecules in the elution profile. Hence, we can say that with the new $His_6$-SUMO-ACA-01 construct we obtained a protein with higher level of purity compared to the previous construct and yield of 2.5 mg/ L.

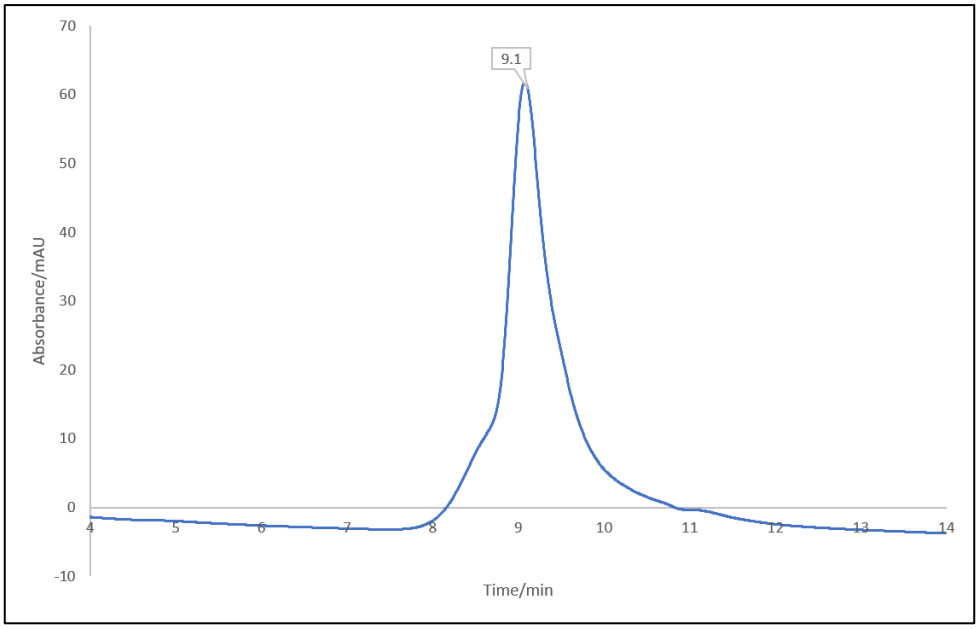


**Figure 3.14: Analytical Size Exclusion Chromatogram of ACA-01.** Sample was loaded on Yarra 3 µm SEC-2000 column and $NaHPO_4$ was used as mobile phase buffer. Flow rate was maintained at 0.35 ml/min. Elution of protein was detected at 280 nm (monitored as mAU). ACA-01 was eluted as a mixture of monomer and dimer (~19 kDa) at 9.23 min.

### *3.10. Discussion:*

ACA-01 is an 8-cysteine containing novel tick Evasin found in *Amblyomma cajanennse*. ACA-01 was previously expressed as $His_6$-ACA-01 and was expressed in the insoluble fraction. The yield of the protein was also very poor. Hence, we decided to initially obtain some protein from the previous construct and improve on the preparation.

The $His_6$-ACA-01 protein was overexpressed after induction with 1 mM IPTG and large-scale production was conducted in 4X 1 L LBKan. After harvest and analysis of the expression, $His_6$– ACA-01 was expressed in the insoluble fraction. The pellet from the insoluble fraction was harvested, denatured and sonicated to collect the protein which at that stage was also denatured. Hence, the denatured protein was refolded overnight by drop-wise refolding in a continuously stirring buffer, containing oxidized and reduced glutathione. This provided an environment for the denatured protein for

disulfide exchange until the protein folds into a form that is more stable. This could include some correctly folded or misfolded proteins. A large portion of ACA-01 had also aggregated during refolding which resulted in poor yield of ACA-01. This method of refolding could be improved by control of temperature, speed of stirring, speed of dropwise addition of the protein into the buffer and changing buffer at least 2 times. The final step of purification was by PSEC and we collected $His_6$-ACA-01 as mostly monomer. Mass Spectrometry was used to assess the purified protein for its expected molecular weight. The expected MW for N-terminally $His_6$-tagged ACA-01 was 12305.7 Da (with 4 disulfide bonds) and the observed mass on Mass Spec was 12309.7 Da, which is within the level of accuracy of MALDI (5 to 10 Da). Thus, we confirmed that we obtained ACA-01 with the correct MW.

The purity of $His_6$-tagged ACA-01 was finally checked using ASEC. According to the elution time, the apparent MW of ACA-01 was 19 kDa (Figure 3.6), which is higher than the monomeric MW (12 kDa) and is thus suggestive of a mixture of monomer and dimer. The ASEC chromatogram also shows the presence of aggregates and smaller molecules, which indicates the protein sample analysed by ASEC was not pure. The protein was stored at -20 $^{o}$C and thawed at room temperature, which is often a cause of protein aggregation. The small molecule at 11.8 min is most likely to be imidazole. One limitation to this method was that, fresh protein was not analysed and hence we could not make a definitive conclusion of whether the aggregates were formed during the purification process or after freeze-thawing. The yield of $His_6$-ACA-01 was poor and not enough for further analysis and thus we decided to stretch our research to find a soluble expression system.

A new construct was designed for ACA-01 with a soluble SUMO – tag as an N-terminal tag that could facilitate soluble expression of ACA-01 in *E coli*. Through small-scale trial, we selected 18 $^{o}$C post-induction growth temperature and 0.5 mM IPTG concentration for culture of BL21 (DE3) cells. After successful expression of $His_6$ – SUMO – ACA-01 in the soluble fraction, we partially purified the protein by Nickel Affinity Chromatography and cleaved the N- terminally tagged $His_6$ – SUMO- using Ulp1 protease. The tag was cleaved efficiently and the uncleaved ACA-01 was

further purified by Nickel Affinity Chromatography and PSEC. PSEC and subsequent SDS PAGE analysis of the purified fractions showed that ACA-01 had an apparent MW of ~10 kDa (the expected MW is 11117.44 Da). Thus, we can confirm that we were able to successfully obtain pure ACA-01. The new construct with the SUMO – tag proved to be very promising, which improved the soluble expression of ACA-01 and resulted in a yield of 2.5 mg/ L (with a total of ~6 mg) ACA-01. Identification of the correct MW of ACA-01 was conducted by Mass Spectrometry MALDI. Analysis of the purity and homogeneity of ACA-01 was conducted by ASEC and we observed elution of ACA-01 at ~19 kDa, which is nearly double to the expected MW. We assume that ACA-01 possibly exists as an equilibrium of monomer and dimer to give rise to the averaged elution time and the appearance of a shoulder of the peak observed. From the outcome of this analysis, it was important to run the protein sample on a native gel and perform analytical ultracentrifugation, which would give us an idea of whether ACA-01 exists as a non-covalently bonded dimer. But due to time constraints we were not able to conduct these assays. We also observed a higher level of purity as opposed to the ASEC chromatogram of the previous $His_6$-ACA-01 construct.

We obtained a better yield and purity of ACA-01 since SUMO-tag enhances expression of protein. The exact mechanism of how SUMO-tag enhances protein expression is unknown, yet it is assumed that ubiquitin is the most rapidly folding protein. Therefore, the compact, rapidly folded structure of Ub initiates the folding of its C-terminally fused protein (Makhalov MP, 2004). It is also known that Ub and SUMO proteins are very stable and can withstand heat and proteolysis, therefore, addition of a highly stable species at the N-terminus of a protein facilitates in the stabilization and yield of the recombinant protein.

The highly pure ACA-01 obtained would be used for performing binding studies with a panel of CC chemokines.

# Chapter 4: Chemokine Binding Studies of ACA-01

### *4.1. Chemokine Binding Studies of ACA-01:*

One of the aims of this thesis was to determine the chemokine-binding selectivity of ACA-01. Having produced sufficiently pure ACA-01 we then screened the protein for chemokine-binding activity against a panel of 6 human CC chemokines using a Fluorescence Anisotropy (FA) competition-binding Assay. The chemokines selected were CCL11/eotaxin-1, CCL24/eotaxin-2, CCL26/eotaxin-3, CCL/2/MCP-1, CCL8/MCP-2 and CCL7/MCP-3. Previously Hayward *et al.* (2017) reported binding of ACA-01 with CC chemokines, however, the ACA-01 samples were only partially purified and possibly not folded properly. Deruaz *et al* (2019) also reported the selectivity of Evasin-1 and -4 for CC chemokines. Evasin-1 is rather selective, binding to several CC chemokines – CCL3, CCL3L1, CCL4, CCL4L1, CCL14, and CCL18. Evasin-4 also binds only CC chemokines but is less selective, binding around 20 CC chemokines (Déruaz 2013). For the ease of this thesis, we will address each of the chemokines by its common name, for instance, eotaxin-1 or Eotaxin-1 instead of CCL11.

Figure 4.1 shows the basic principle of the Fluorescence Anisotropy Assay. The fluorescence anisotropy technique, also known as fluorescence polarization, is based on the observation that when a fluorescently labelled molecule is excited by polarized light, it emits light with a degree of anisotropy (closely related to polarization) that is inversely proportional to the rate of molecular rotation (Moerke, 2009). The FA assay used in this thesis is designed with the detection of a small fluorescently labelled peptide (Fl-R3D) that can bind to the chemokine protein. When the small peptide (~ <1500 Da) is covalently attached to a fluorophore, in solution, depolarization of the emitted light is very high. This occurs due to the reorientation of the fluorophore during its excited state. If this labelled peptide is bound to a protein (~ >10 kDa), the fluorophore reorients to a much smaller degree during the lifetime of the excited state, because the rotational speed of the complex decreases. Thus, the emitted light will still be polarized to a significant degree. The observed anisotropy in a mixture of labelled ligand and receptor is proportional to the fraction of bound ligand. This feature of FA can be used to develop the technique for measurement of ligand binding.

Moreover, a competition binding assay can easily be established by measuring the decrease in FA signal produced when an inhibitor of the interaction is added to the mixture of labelled ligand and receptor.

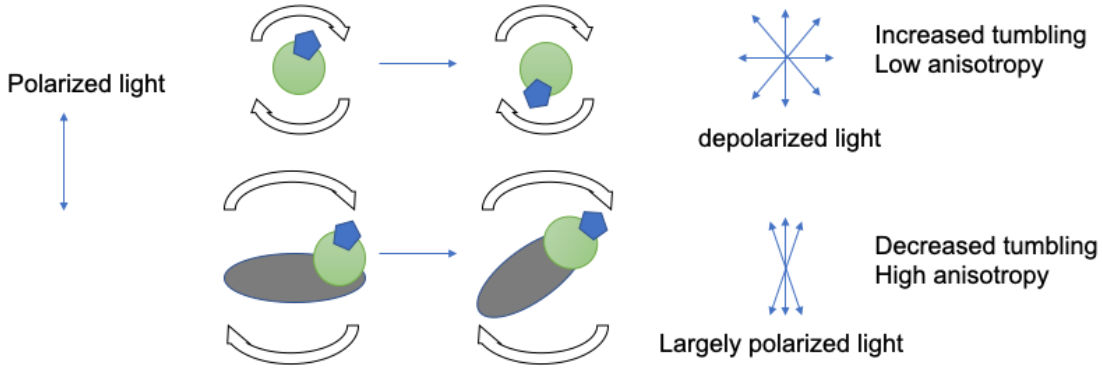


**Figure 4.1. Basic illustration of principle of Fluorescence Anisotropy.** When a small peptide (pastel circle) bound to a fluorescently label molecule (blue pentagon) is excited by polarized light at the excitation wavelength of the fluorophore, the ligand reorients to a significant degree due to molecular tumbling which occurs during its excited state. Thus, large depolarization of emitted light occurs. If the ligand is bound to a protein (grey ellipse), the resulting bigger complex tumbles much slower, and the emitted light retains its anisotropy (or polarization). Higher molecular tumbling results in low anisotropy while decreased tumbling results in high anisotropy.

### *4.2. Direct Binding Assay:*

Initially for FA, the direct binding of the chemokines and the fluorescent peptide Fl-R3D was conducted. Fl-R3D is a fluorescently labelled, doubly-sulfated peptide corresponding to the N-terminus of chemokine receptor CCR3 (Wang, 2017). Details of the method are explained in Materials and Methods section 2.4.1. Through the direct binding assay, we wanted to determine the equilibrium dissociation constant ($K_d$) for the complex between each chemokine and the fluorescent peptide, which is required in the analysis of the competitive binding assay data (see below). In addition, we wanted to establish the concentrations of chemokines required to give ~50-80% saturation of the fluorescent peptide Fl-R3D, so that the decreases in these signals would be readily detectable in the competitive binding assay.

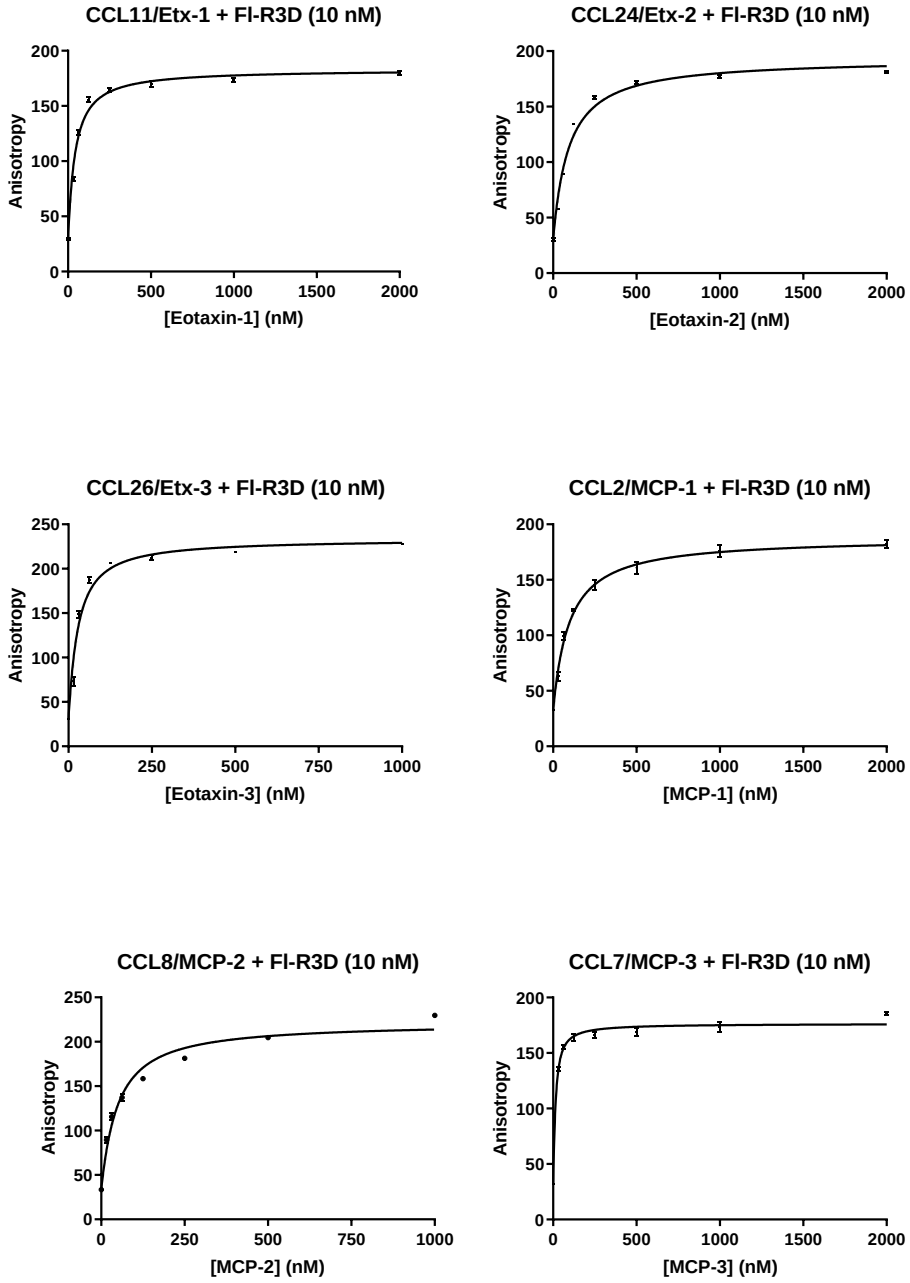


| **Chemokine** | Eotaxin-1 | Eotaxin-2 | Eotaxin-3 | MCP-1 | MCP-2 | MCP-3 |
|---|---|---|---|---|---|---|
| $K_D$ (nM) | 35.8 | 86.9 | 23.2 | 90.4 | 43.8 | 9.8 |

**Figure 4.2: Fluorescence Anisotropy assay to determine the affinity of six CC chemokines for the Fl-R3D peptide.** Direct binding curve for Fl-R3D with Eotaxin-1, Eotaxin-2, Eotaxin-3, MCP-1, MCP-2 and MCP-3 respectively showing the concentration of chemokine at which it tightly binds to Fl-R3D peptide. Binding of MCP-3 with Fl-R3D is the tightest with an observed $K_D$ of 9.8 nM. MCP-1 had the highest $pK_d$ of 7 and hence less tightly bound. Data are the mean ± SEM of three independent measurements.

Figure 4.2 shows the anisotropy of the Fl-R3D as each of the 6 CC chemokines is added. From the shape of the curves, we can see that all the chemokines bind tightly with Fl-R3D with MCP-3 forming the tightest complex. Using Graphpad Prism v8.0.2, the data were analysed for the direct binding assay. The $K_D$ values obtained are tabulated in Figure 4.2. As speculated earlier, CCL7/MCP-3 has a higher affinity for Fl-R3D with a $K_D$ of 9.8 nM while MCP-1 had the a lowest affinity with a $K_D$ of 90.4 nM.

### *4.3. Competitive Binding Assay:*

After determining the $K_D$ (in nM) from the direct binding assay of the fluorescent peptide with each of the 6 CC chemokines, this was used to design the FA competitive-binding assay (CBA) to screen ACA-01 for chemokine-binding activity against the 6 human CC chemokines. For successful competitive displacement, we expect to observe a decrease in fluorescence anisotropy which represents the release of the fluorescent peptide. So, the strongest binding interaction of ACA-01 would result in the steepest initial drop in anisotropy. The method is explained in Materials and Methods section 2.4.2. Figure 4.3 shows the competitive binding results for ACA-01 when bound to each of the chemokines. To generate these curves, Graphpad prism v8.0.2 was used, which plotted the mean anisotropy and fitted a non-linear regression line using an established equation that describes a 1:1 competitive displacement model (Huff *et al.*, 1994). In this model, the chemokine can bind to either the fluorescent peptide or ACA-01 but not to both simultaneously. We fitted each set of displacement data using equation 9 when we have initial estimates of KU>KL and corresponding constraints and Equation 10 with initial estimates of KU<KL. The equations for statistical analysis are described in Materials and Methods section 2.5.3.

The $pK_d$ (negative logarithm of $K_d$ in molar) for the binding of the Evasin to the chemokine was calculated with reference to the $K_d$ for the binding of FL-R3D to the chemokine (determined in the DBA). $pK_d$ is used instead of $K_d$ because its error is more readily interpretable as the error distribution for $pK_d$ has a Gaussian distribution whereas the error distribution for $K_d$ does not.

**Table 4.1: Summary of competitive binding of ACA-01 with 6 CC chemokines:**

| Chemokine | Eotaxin-1 | Eotaxin-2 | Eotaxin-3 | MCP-1 | MCP-2 | MCP-3 |
|---|---|---|---|---|---|---|
| $pK_d$ ± SEM | 8.2 ± 0.2 | 6.6 ± 0.2 | 7.5 ± 0.1 | 7.7 ± 0.1 | 8.0 ± 0.1 | 8.6 ± 0.3 |
| $K_d$ (nM) | 10 | 268 | 29 | 22 | 11 | 2.7 |

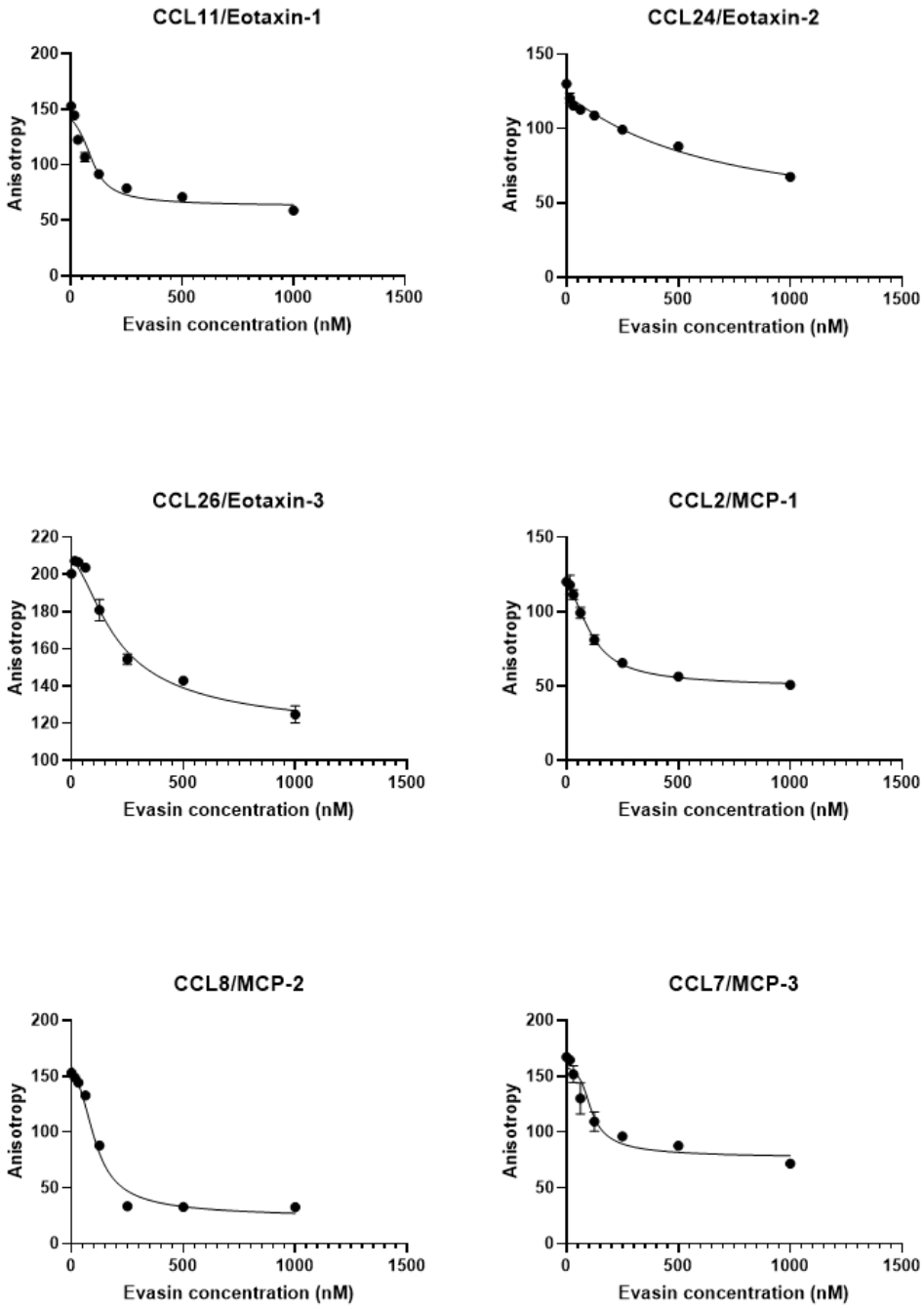


**Figure 4.3: Competitive binding of ACA-01.** A comparison of competition displacement curves for chemokine binding by ACA-01 for each of the CC chemokines. Each point represents mean anisotropy ± SEM from duplicate assays performed three

times independently. ACA-01 was observed to have the strongest interaction with CCL7/MCP-3 with $pK_d$ of 8.6 ± 0.3, and the lowest with CCL24/Eotaxin-2 with $pK_d$ of 6.6 ± 0.2.

Although the initial anisotropy value should theoretically be the same for all the chemokines when Fl-R3D is bound to the chemokine, however, some discrepancies are observed which could result from different proportion of Fl-R3D bound to chemokine, different sizes or shapes of chemokines, and differences in the restriction of fluorophore movement upon binding. According to Figure 4.3 and summary table 4.1, we observe that ACA-01 binds to all 6 CC human chemokines with most of the $K_D$ in nM range. MCP-3 shows the strongest binding with $pK_d$ of 8.6 ± 0.3 and the weakest binding was with Eotaxin-2 with $pK_d$ of 6.6 ± 0.2. SEM is within ± 0.2 which indicates the errors are small in comparison to the range of $K_d$ values observed.

### *4.4. Discussion:*

For the purpose of studying the chemokine-binding activity of ACA-01 we conducted a competitive fluorescence anisotropy assay. Other techniques that could be used to detect chemokine-binding include Biolayer Interferometry and Surface Plasmon Resonance (SPR). SPR can be configured as a fairly high-throughput technique and is very commonly used. However, the method for Evasin-chemokine binding is challenging, since the concentration of Evasin and chemokine need to be optimized, in addition to ensuring non-specific binding does not occur. Hence, we chose FA, the method of which was already developed and optimized in our lab by Julie Sanchez (Xiaoyi Wang *et al.*, 2017). The FA technique uses the feature of anisotropy where the observed anisotropy in a mixture of labelled ligand and receptor is proportional to the fraction of bound ligand. This is very effective to develop a technique for measurement of ligand binding. In addition to it, a competition binding assay can easily be established by measuring the decrease in FA signal produced when an inhibitor of the interaction is added to the mixture of labelled ligand and receptor.

Initially, we performed a direct binding assay to determine the concentration of chemokine needed to bind to the fluorescent peptide Fl-R3D completely. $K_D$ values were

generated by Graphpad Prism software, using a one-site total equation. Through direct binding assay, we determined the concentration of chemokine and fluorescent peptide that would form a stable complex. A higher anisotropy indicated formation of the chemokine:Fl-R3D complex. In addition, direct binding assay also allowed us to determine the equilibrium constant $K_D$ for binding of chemokine to the fluorescent peptide Fl-R3D, which was later used in the calculations of competitive binding assay.

Once the concentration of chemokine for binding to Fl-R3D was determined by the direct binding assay, we conducted a competitive displacement assay, whereby, once ACA-01 was added to the chemokine-peptide mixture, it would displace the fluorescent peptide and hence we would observe a fall in anisotopy. ACA-01 was able to bind to all the six CC chemokines tested and the strongest binding of ACA-01 was observed with CCL7/MCP-3 with a pKU of 8.56, and the lowest with CCL24/Eotaxin-2 with $pK_D$ of 6.57. It was interesting to observe the difference in selectivity of chemokine-binding by ACA-01; ACA-01 being more selective to CCL7/MCP-3 than CCL24/Eotaxin-2.

Here we have successfully shown that most of the chemokines bind to ACA-01 with Kd in nM range, while in comparison, R. sanguineus Evasins-1 and -4 have been reported to bind various chemokines with KD values ranging from ~30 pM to ~200 nM, although the reported values varied somewhat depending on the experimental methods used and may also be dependent on expression systems used due to variable post-translational modifications. The differences in affinity and selectivity could be due to the sequence variation among the Evasins and chemokines tested. The selectivity of Class A Evasins for CC chemokines can be rationalized based on the interactions of CCL3 Cys-11 and Cys-12, as well as their disulfide bond partners (Cys-35 and Cys-51, respectively), with residues in EVA-1. In addition, the chemokine sequences differ substantially in the regions that interact with the Evasins, such as the flexible N terminal region. The differences in affinity and selectivity could be due to the sequence variation among the Evasins and chemokines tested. The selectivity of Class A Evasins for CC chemokines can be rationalized based on the interactions of CCL3 Cys-11 and Cys-12, as well as their disulfide bond partners (Cys-35 and Cys-51, respectively), with residues in EVA-1. In addition, the chemokine sequences differ substantially in the regions that interact with the Evasins, such as the flexible N terminal region. Sequence alignment of the 6 CC chemokines when ranked according to their binding affinity, shows similar amino acid residues in the N-terminal region, for instance amino acids Ala-53 and Lys-58, are

present in CCL2, CCL7, CCL8 and CCL11, all of which bind tightly with ACA-01. However, CCL24 and CCL26 that bind weakly to ACA-01 have a varied N-terminal amino acid sequence.

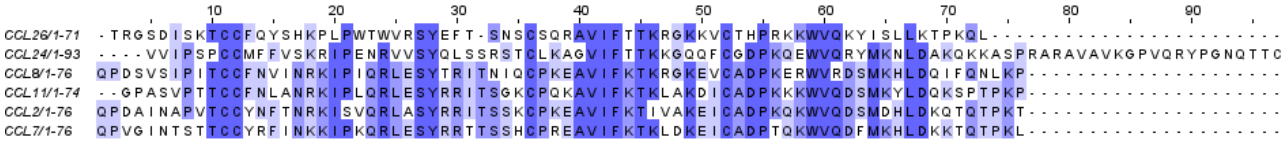


**Figure 6.1: Sequence alignment of six human CC chemokines.** Sequences of the six human CC chemokines which were used for binding studies with ACA-01, were analysed by Clustal Omega 2.1. Sequence similarity shows differences in the N-terminal region of the chemokines.

Based on the binding results of ACA-01 and 6 CC chemokines, we are now confident that ACA-01 is a chemokine-binding Evasin and has the potential to be used as a treatment for chemokine-mediated inflammatory diseases. For instance, ACA-01 showed some selectivity for CCL7/MCP-3 over CCL24/Eotaxin-2, and considering that the eotaxins and CCL7/MCP-3 are agonists of chemokine-receptor CCR3, which is expressed exclusively on eosinophils (Nagase, 2001), ACA-01 may be useful in the treatment of allergic diseases whose pathology is dependent on the recruitment of these immune cells.

# Chapter 5: Trials for Structure Determination of ACA-01

## Chapter 5: Crystallisation Trials of ACA 01

After we were able to express, purify and characterize the chemokine-binding of ACA-01 we aimed to elucidate the 3-D crystal structure of ACA-01 through X-Ray crystallography. The only reported crystal structure of Class A Evasins is EVA-1 with which ACA-01 shares a sequence identity of 41.76% and similarity of 65.2%, (as shown below) and hence the predicted folding would also be similar. Thus, we were optimistic to obtain protein crystals.

```
Percent Identity Matrix - created by Clustal2.1

1: Evasin-1    100.00   41.76
2: ACA-01       41.76  100.00

Sequence Similarity - created by Clustal2.1

Evasin-1  EDDEDYGDLGGCPFLVAENKTGYPTIVACKQDCNGTTETAPNGTRCFSIGDEGLRRMTAN  60
ACA-01    EQDYDYGT-DTCPFPVLANKTNKAKFVGCHQKCNGGDQKLTDGTACYVVERKVWDRMTPM  59
          *:* ***  . *** *  ***.  .:*.*:*.***  :.  :** *: :  :   ***

Evasin-1  LPYDCPLGQCSNGDCIPKETYEVCYRRNWRDK 92
ACA-01    LWYECPLGECKNGVCEDLRKKEDCRKGNGEEK 91
          * *:****:*.** *   .. * * : * .:*
```

### *5.1. Stability Studies*

Protein stability is a pre-requisite for crystallization and functional studies. Presence of denaturants, changes in temperature during purification, might result in protein degradation. For the second aim of this thesis - to obtain crystals of ACA-01, it was important to find out the condition in which the protein was stable, thus can be purified and stored without causing protein denaturation, and the buffer would assist with crystallisation.

Until this point the choice of buffer for protein purification and storage was 10 mM HEPES at pH 7.5, however, we observed the concentration of protein decreased after longer duration of storage at -20 $^{o}$C. This was assessed by storing an aliquot of ACA-01 at 8 mg/ml and subsequently thawing it and measuring the absorbance of protein at $A_{280}$. Each time we observed a lower $A_{280}$. This gave rise to the question of whether the storage condition of the protein needed to be improved.

To find the condition at which the protein might best be stored, we used a thermal shift assay to study the stability of the protein in a wide range of conditions. The stability of

the protein is indicated by it requiring more heat for denaturation. The basic principle of a thermal shift assay involves incubation of natively folded proteins with SYPRO Orange dye and a systematic increase in temperature and concurrent monitoring of SYPRO Orange fluorescence emission with a thermocycler. It is thus possible to monitor thermal denaturation of the protein in many conditions simultaneously. When the temperature is increased, the protein slowly unfolds exposing its hydrophobic regions to which the SYPRO Orange dye interacts thus increasing their fluorescence emission intensities. Thermal shift assay (also known as differential scanning fluorimetry or ThermoFluor™) generates an ideal melt curve as fluorescence response unit (RFU) which exhibits a flat pretransition baseline and a steep transition on unfolding (Huynh *et al.*, 2015).

We used this high-throughput technique to study the stability of purified ACA 01 in 48 different buffers. Table 5.1 shows the 48 different conditions used for the thermal shift assay. The design of the experiment was based primarily on 6 different buffers; 50 mM sodium phosphate, 50 mM MOPS, 50 mM Bis-Tris, 50 mM HEPES and 50 mM Tris with a pH range of 7.0 – 8.0 in addition to a low and high concentration of salt in each of the buffers. ACA-01 was incubated with SYPRO Orange dye (explained in Materials and Methods 2.5.1.) and heated; fluorescence intensity of the dye was measured as Fluorescence Response Unit. Figure 5.1 shows the melt curves obtained for ACA 01 under 48 different conditions.

The melt curve in Figure 5.1 shows a pattern of two melting transitions – first one appearing at ~40 $^{o}$C (+/- 4 $^{o}$C), and the second was at ~80 $^{o}$C (+/- 4 $^{o}$C). The melting temperature $T_m$ °C is determined as the temperature at the mid-point of the transition. Much of the same melting pattern was observed for all the different conditions. Multiple melting temperatures are observed in misfolded species or multimeric proteins (Wang, 1999). Presence of different thermostable domains may also result in the intact protein to melt in two distinct temperature regions. From what we concluded in Section 3.8 ACA-01 could either exist as monomer and a dimer in equilibrium, or differently folded monomers. The first $T_m$ could be the dimer separating while the second $T_m$ was possibly the melting of the monomer. Capillaries 18 (50 mM Bis-Tris pH 7.0 + 250 mM NaCl), 19 (50 mM Bis-Tris pH 7.5 + 50 mM NaCl) and 35 (50 mM HEPES pH 7.5 + 50 mM NaCl) showed the highest inflection point ($T_m$) of ~84 $^{o}$C, which is very high and is often seen in proteins containing disulfide bonds (Zabetakis 2014). Table 5.1 shows the inflection points ($T_m$) for the different conditions. As for the primary objective of this

experiment – to find the optimum condition at which ACA-01 is most stable, we observed in Figure 5.1. three conditions at which the melting temperature was highest (50 mM Bis-Tris pH 7.0 + 250 mM NaCl; 50 mM Bis-Tris pH 7.5 + 50 mM NaCl; 50 mM HEPES pH 7.5 + 50 mM NaCl), hence from these three conditions we selected 50 mM HEPES pH 7.5 50 mM NaCl for purification and storage.

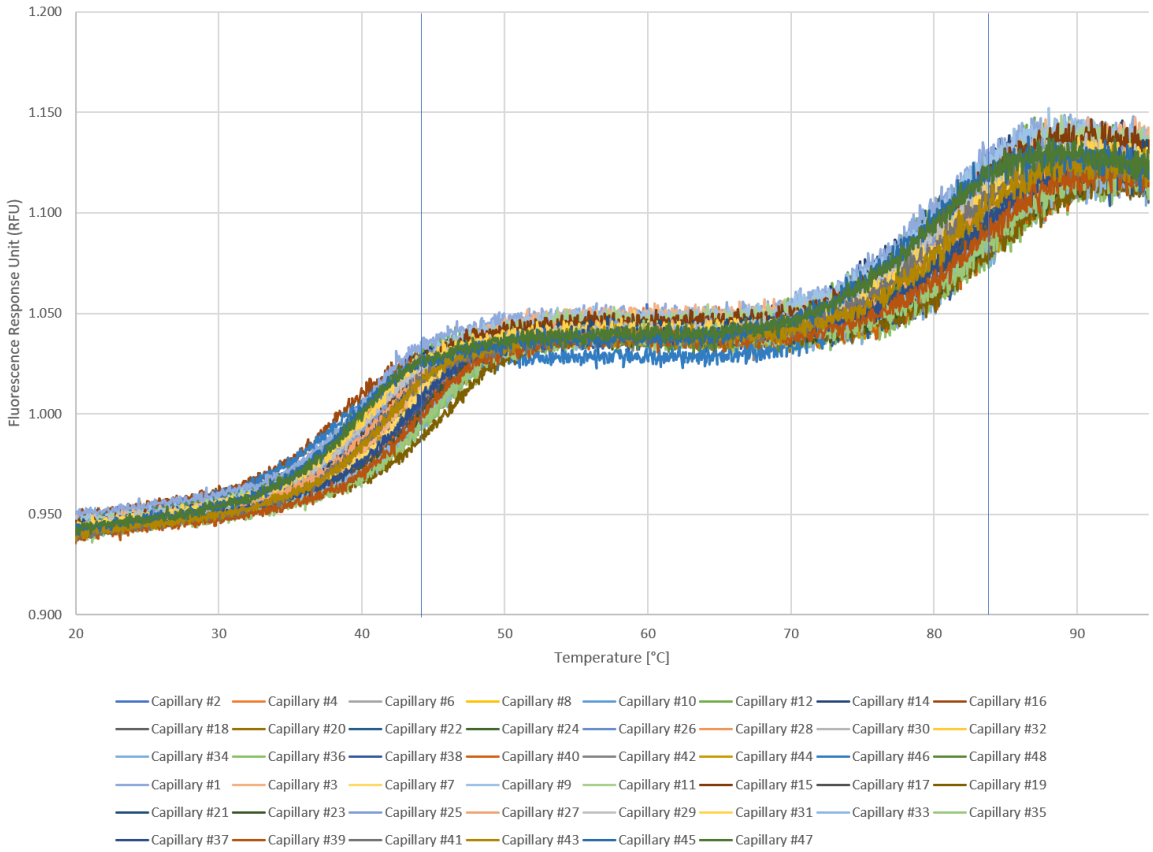


**Figure 5.1: Thermal melt curve to analyse stability of ACA 01.** 48 different conditions are used for the thermal shift assay which is demonstrated by each of the different colours on the graph. SYPRO Orange was added to the protein at a 100-fold dilution from stock. The capillary number refers to the different conditions tabulated in table 5.1. Inflection point in the curve is the melting temperature $T_m$ °C. Capillaries 18 (50 mM Bis-Tris pH 7.0 + 250 mM NaCl), 19 (50 mM Bis-Tris pH 7.5 + 50 mM NaCl) and 35 (50 mM HEPES pH 7.5 + 50 mM NaCl) shows the highest inflection point ($T_m$) of ~84 $^oC$.

**Table 5.1: Conditions used to study the stability of ACA 01 using DSF**

| Capillary | Sample ID | Start Temp | End Temp | Inflection Point #1 | Inflection Point #2 |
|---|---|---|---|---|---|
| 1 | 50 mM Sodium Phosphate pH 7.0 + 50 mM NaCl | 20°C | 95°C | 40.3°C | 80.1°C |
| 2 | 50 mM Sodium Phosphate pH 7.0 + 250 mM NaCl | 20°C | 95°C | 39.7°C | 80.3°C |
| 3 | 50 mM Sodium Phosphate pH 7.5 + 50 mM NaCl | 20°C | 95°C | 43.1°C | 81.8°C |
| 4 | 50 mM Sodium Phosphate pH 7.5 + 250 mM NaCl | 20°C | 95°C | 43.1°C | 82.2°C |
| 5 | 50 mM Sodium Phosphate pH 8.0 + 50 mM NaCl | 20°C | 95°C | 40.9°C | 81.8°C |
| 6 | 50 mM Sodium Phosphate pH 8.0 + 250 mM NaCl | 20°C | 95°C | 41.3°C | 82.9°C |
| 7 | 50 mM Sodium Phosphate pH 8.5 + 50 mM NaCl | 20°C | 95°C | 43.3°C | 59.7°C |
| 8 | 50 mM Sodium Phosphate pH 8.5 + 250 mM NaCl | 20°C | 95°C | 43.4°C | 61.7°C |
| 9 | 50 mM Sodium Citrate pH 7.0 + 50 mM NaCl | 20°C | 95°C | 41.5°C | 57.8°C |
| 10 | 50 mM Sodium Citrate pH 7.0 + 250 mM NaCl | 20°C | 95°C | 41.4°C | 80.4°C |
| 11 | 50 mM Sodium Citrate pH 7.5 + 50 mM NaCl | 20°C | 95°C | 42.1°C | 81.2°C |
| 12 | 50 mM Sodium Citrate pH 7.5 + 250 mM NaCl | 20°C | 95°C | 42.2°C | 59.4°C |
| 13 | 50 mM Sodium Citrate pH 8.0 + 50 mM NaCl | 20°C | 95°C | 41.5°C | 58.3°C |
| 14 | 50 mM Sodium Citrate pH 8.0 + 250 mM NaCl | 20°C | 95°C | 41.4°C | 60.8°C |
| 15 | 50 mM Sodium Citrate pH 8.5 + 50 mM NaCl | 20°C | 95°C | 41.5°C | 81.5°C |

| | | | | | |
|---|---|---|---|---|---|
| 16 | 50 mM Sodium Citrate pH 8.5 + 250 mM NaCl | 20°C | 95°C | 41.6°C | 80.9°C |
| 17 | 50 mM Bis-Tris pH 7.0 + 50 mM NaCl | 20°C | 95°C | 44.2°C | 63.4°C |
| 18 | 50 mM Bis-Tris pH 7.0 + 250 mM NaCl | 20°C | 95°C | 44.2°C | 83.7°C |
| 19 | 50 mM Bis-Tris pH 7.5 + 50 mM NaCl | 20°C | 95°C | 46.0°C | 83.9°C |
| 20 | 50 mM Bis-Tris pH 7.5 + 250 mM NaCl | 20°C | 95°C | 46.2°C | 66.1°C |
| 21 | 50 mM Bis-Tris pH 8.0 + 50 mM NaCl | 20°C | 95°C | 41.9°C | 60.1°C |
| 22 | 50 mM Bis-Tris pH 8.0 + 250 mM NaCl | 20°C | 95°C | 42.0°C | 82.5°C |
| 23 | 50 mM Bis-Tris pH 8.5 + 50 mM NaCl | 20°C | 95°C | 44.2°C | 63.0°C |
| 24 | 50 mM Bis-Tris pH 8.5 + 250 mM NaCl | 20°C | 95°C | 44.1°C | 64.0°C |
| 25 | 50 mM MOPS pH 7.0 + 50 mM NaCl | 20°C | 95°C | 40.9°C | 59.5°C |
| 26 | 50 mM MOPS pH 7.0 + 250 mM NaCl | 20°C | 95°C | 40.6°C | 81.5°C |
| 27 | 50 mM MOPS pH 7.5 + 50 mM NaCl | 20°C | 95°C | 41.5°C | 59.1°C |
| 28 | 50 mM MOPS pH 7.5 + 250 mM NaCl | 20°C | 95°C | 41.4°C | 60.0°C |
| 29 | 50 mM MOPS pH 8.0 + 50 mM NaCl | 20°C | 95°C | 40.7°C | 80.7°C |
| 30 | 50 mM MOPS pH 8.0 + 250 mM NaCl | 20°C | 95°C | 40.1°C | 60.5°C |
| 31 | 50 mM MOPS pH 8.5 + 50 mM NaCl | 20°C | 95°C | 40.6°C | 60.3°C |
| 32 | 50 mM MOPS pH 8.5 + 250 mM NaCl | 20°C | 95°C | 40.4°C | 81.4°C |
| 33 | 50 mM HEPES pH 7.0 + 50 mM NaCl | 20°C | 95°C | 44.4°C | 83.4°C |
| 34 | 50 mM HEPES pH 7.0 + 250 mM NaCl | 20°C | 95°C | 44.4°C | 83.6°C |
| 35 | 50 mM HEPES pH 7.5 + 50 mM NaCl | 20°C | 95°C | 44.7°C | 83.7°C |
| 36 | 50 mM HEPES pH 7.5 + 250 mM NaCl | 20°C | 95°C | 44.6°C | 64.1°C |

| | | | | | |
|---|---|---|---|---|---|
| 37 | 50 mM HEPES pH 8.0 + 50 mM NaCl | 20°C | 95°C | 43.2°C | 82.3°C |
| 38 | 50 mM HEPES pH 8.0 + 250 mM NaCl | 20°C | 95°C | 42.9°C | 82.4°C |
| 39 | 50 mM HEPES pH 8.5 + 50 mM NaCl | 20°C | 95°C | 44.0°C | 82.9°C |
| 40 | 50 mM HEPES pH 8.5 + 250 mM NaCl | 20°C | 95°C | 43.8°C | 63.8°C |
| 41 | 50 mM Tris pH 7.0 + 50 mM NaCl | 20°C | 95°C | 41.5°C | 61.7°C |
| 42 | 50 mM Tris pH 7.0 + 250 mM NaCl | 20°C | 95°C | 41.3°C | 81.4°C |
| 43 | 50 mM Tris pH 7.5 + 50 mM NaCl | 20°C | 95°C | 41.7°C | 60.4°C |
| 44 | 50 mM Tris pH 7.5 + 250 mM NaCl | 20°C | 95°C | 41.5°C | 81.6°C |
| 45 | 50 mM Tris pH 8.0 + 50 mM NaCl | 20°C | 95°C | 39.2°C | 79.7°C |
| 46 | 50 mM Tris pH 8.0 + 250 mM NaCl | 20°C | 95°C | 38.8°C | 59.3°C |
| 47 | 50 mM Tris pH 8.5 + 50 mM NaCl | 20°C | 95°C | 39.7°C | 80.3°C |
| 48 | 50 mM Tris pH 8.5 + 250 mM NaCl | 20°C | 95°C | 39.1°C | 80.2°C |

### *5.2. Crystallization trials of ACA 01*

To perform crystallization trials of ACA 01, purified protein was concentrated to 8.5 mg/mL and 10 mg/ml. The protein was submitted to Monash Molecular Crystallisation Facility (MMCF), for initial crystal trials using the sitting drop vapour diffusion method.

In the sitting drop vapour diffusion method, crystals are formed when a supersaturated state of the protein solution is reached. To achieve this state, the sitting drop is composed of protein and half reservoir solution. The reservoir therefore has higher concentration of the precipitant than the drop, and due to this concentration gradient, water vapor migrates slowly from the drop to the reservoir, thus creating a supersaturated state of the drop. At some point, considering the conditions, such as pH, ionic strength, types of buffers and additives are appropriate, protein crystals start to form.

Several different conditions were selected for the crystal trial. Each of these conditions had different salt concentrations, pH and crystallants. Table 5.2 lists the screens used for crystal trials of ACA-01.

Table 5.2 Conditions used for crystal trials of ACA -01

| **Conc (mg/ml)** | **Screen** | **Temp (°C)** | **Drop Vol (nl)** | **Sample %** | **Well Vol ( µl)** |
|---|---|---|---|---|---|
| 10 | PACT | 4 | 300 | 50 | 50 |
| 8.5 | PACT | 4 | 300 | 50 | 50 |
| 10 | JCSG+ | 4 | 300 | 50 | 50 |
| 8.5 | JCSG+ | 4 | 300 | 50 | 50 |
| 10 | PEG Ion -4 | 4 | 300 | 50 | 50 |
| 8.5 | PEG Ion -4 | 4 | 300 | 50 | 50 |
| 10 | Morpheus-4 | 4 | 300 | 50 | 50 |
| 8.5 | Morpheus-4 | 4 | 300 | 50 | 50 |
| 10 | Morpheus-II | 4 | 300 | 50 | 50 |
| 8.5 | Morpheus-II | 4 | 300 | 50 | 50 |

### *5.3. Preliminary data for crystal trials of ACA-01*

After 7-14 days of setting the crystal trays we observed the images through Rockmaker® web. Some representative images observed are shown in Figure 5.2. We used two different concentrations, because often a higher concentration of protein increases the chance of crystallization since supersaturation would drive nucleation (McPherson 2014). However, it did not make much of a difference in our observed results.

We observed some general patterns in each of the trays, as seen in Figure 5.2. Clear drops are free of crystals, precipitate, phase separation, or another insoluble outcome. Clear drops suggest that the relative supersaturation (protein and reagent concentration) did not reach the point of saturation which would nucleate and grow crystals. We have also seen amorphous precipitate that are yellow or brown without an edge, are often heavy and clumped and was an indication of denatured protein which would not crystallize. We also observed phase separation which appears as few large or many small droplets. The droplets are often considered a protein-rich phase that separates from the original drop

solution. Protein-based phase separation was identified on Rockmaker® image using the UV-visible setting set at 280 nm.

In PACT-4, 48 out of 96 drops in the tray showed some precipitates. These could either be from protein or PEG present as a precipitant. In JCSG+ we observed precipitates in 28 drops, mostly containing Bis-Tris and HEPES buffer. The most promising result was observed in drop B6 (Figure 5.3). Rhys Colson, a fellow PhD student carried out X-ray crystallography of the needles at the Australian Synchrotron, however, no diffraction was observed. This is most likely due to the very small size of the needles. Some debris was observed in Drop F10 (Appendix II Figure 2.2), and amorphous precipitate was observed in F2. All 96 drops in the tray of PEG Ion-4 condition were clear which suggests that protein concentration was not enough for phase separation to occur (Appendix II). In Morpheus-4 we observed 28 drops with phase separation and precipitate but no nucleation was observed even after 4-5 weeks. Amorphous precipitate images were observed in 14 drops when material such as glass, dust, or debris was present in the plate, sample, or reagent when the experiment was set and sealed. In Morpheus-II we observed precipitates in 27 drops. Drops E5-E7 (Appendix II Figure 2.5) had precipitates with denatured protein in them.

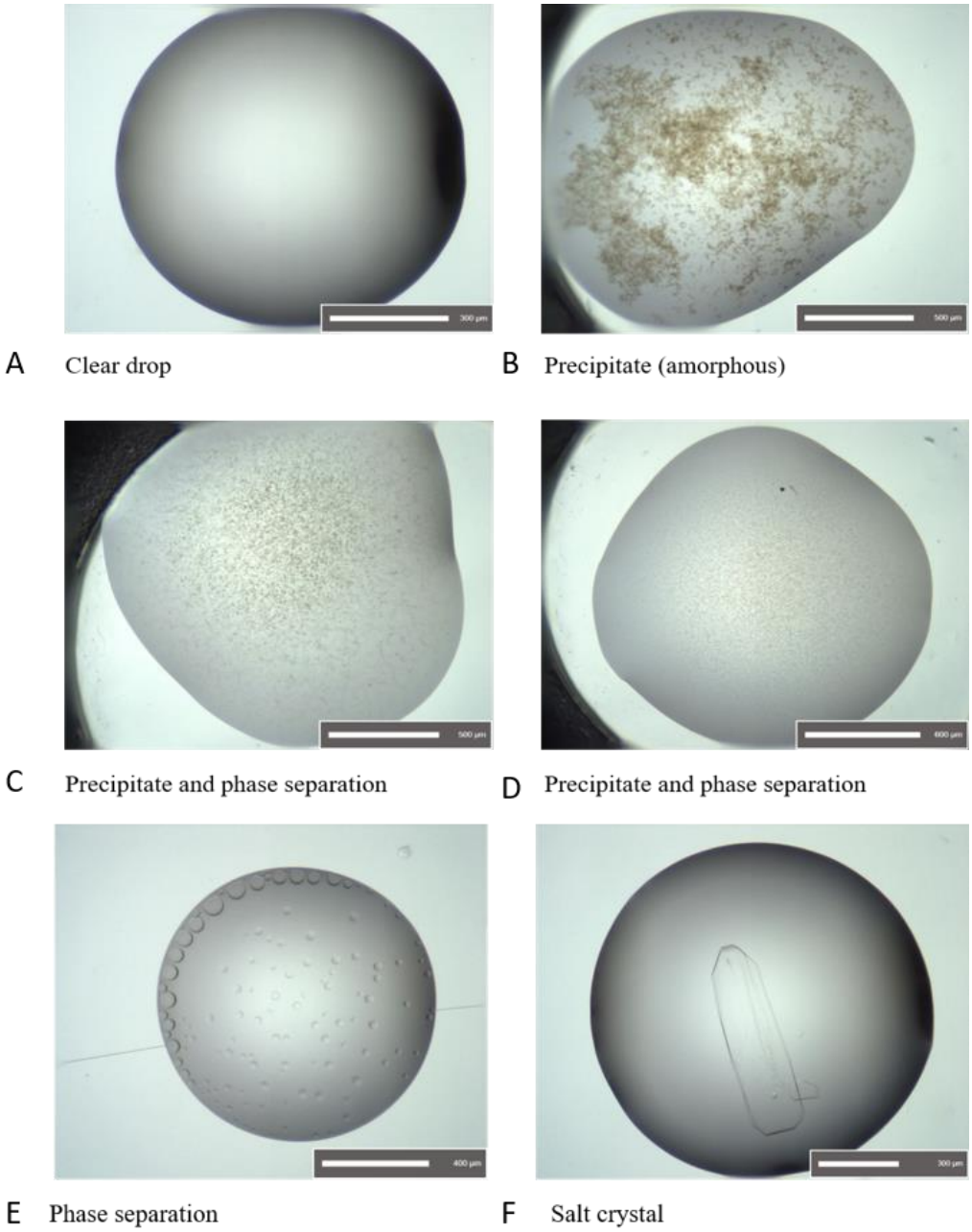


**Figure 5.2: Images obtained from Rockmaker web® for crystallization trials. A:** Clear drop was observed in 20 %w/v PEG 3350 (Polymer) and 0.2 M NaF (Salt); **B:** Amorphous precipitate was in 0.002 M Lanthan (Additive) 50 %v/v MPM6 (Precipitant) 0.1 M MB5 7.5 pH (Buffer).; **C and D:** Precipitate and phase separation were observed 2.4 M $Na_2$ Malon (Salt); **E:** Phase separation was observed in 0.2 M $LiSO_4$ (Salt) 0.1 M Na Acet 4.5 pH (Buffer) 50 %v/v PEG 400 (Precipitant); **F:** Salt crystal was observed in 20 %w/v PEG 3350 (Polymer) and 0.2 M K2SO4 (Salt).

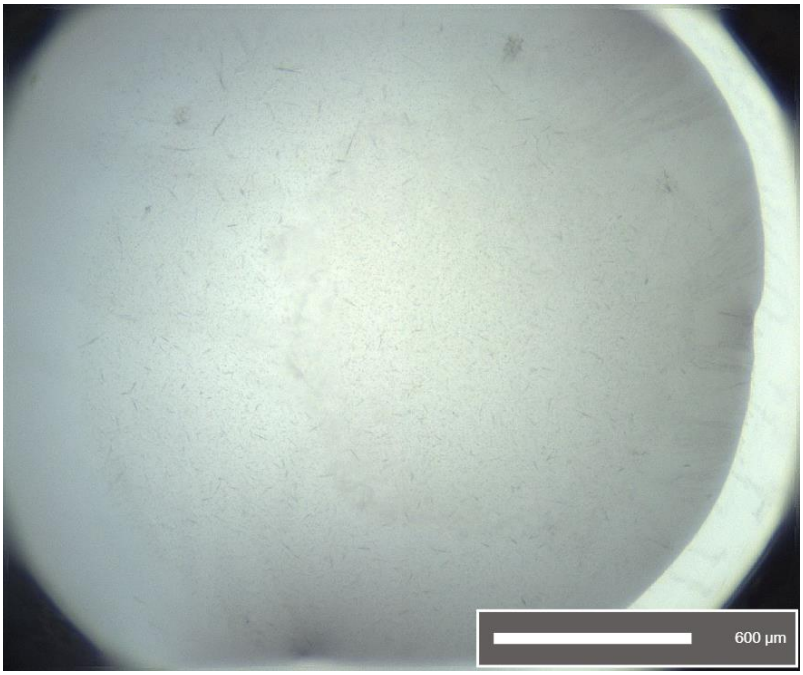


**Figure 5.3: Rockmaker web® image of needles formed of ACA-01**: Needles were observed at a concentration of 8.5 mg/mL under the conditions of 0.1 M Phosphate Citrate pH 4.2, 40% v/v EtOH, 5% w/v PEG 1K.

### *5.4. Discussion*

After we successfully expressed and purified ACA-01 and determined its chemokine-binding affinities, we aimed to solve its crystal structure of ACA-01. We first undertook to determine the buffer in which the protein is most stable. Hence, we performed stability studies for ACA-01 in 48 different conditions using a thermal shift assay. From the results we found out that 50 mM Bis-Tris pH 7.0 + 250 mM NaCl, 50 mM Bis-Tris pH 7.5 + 50 mM NaCl and 50 mM HEPES pH 7.5 + 50 mM NaCl showed the highest inflection point ($T_m$) of ~84 $^oC$. From these three conditions we selected 50 mM HEPES pH 7.5 + 50 mM NaCl for purification and storage. Once the buffer for purification and storage was selected, we then set up crystal trays to attempt the crystallisation of ACA-01. To perform crystallization trials of ACA 01, purified protein was concentrated at 8.5 mg/mL and 10 mg/ml and conditions used were, Morpheus, JCSG+, PACT, PEG Ion-4 based on different salt concentrations, pH, crystallants. We observed needles of ACA-01 crystals, and after checking with X-ray crystallography, we did not observe a diffraction for protein crystals. We assumed that the size of the needles was too small for a definitive outcome.

Since we are very optimistic now that we can easily express and purify ACA-01, we can now take a number of different steps towards obtaining the crystal structure of ACA-01. First step is optimization of the condition in which we obtained the needles of ACA-01. The optimization process would entail sequential, incremental changes in the chemical parameters that influence crystallization, such as pH, ionic strength and precipitant concentration as well as physical parameters including temperature and sample volume. Another way to possibly obtain crystal is seeding, whereby needles would be crushed and seed stock prepared which would be seeded as sitting drops on reservoir solutions of reagent composition identical to that used to obtain the initial seed crystals (Luft 1999). We could also attempt crystal trials of a ACA-01:chemokine complex. This could be done by purifying complex of ACA-01 with one chemokine such as CCL7/MCP-3. Solving the crystal structure of ACA-01 would be a huge assistance to the targeted design of anti-inflammatory drugs, whereby a chemokine antagonist could selectively target its receptor agonists while leaving other chemokines free to interact as part of normal immune surveillance

# Chapter 6: Discussion

***Discussion:***

Researchers have increasingly been interested to find chemokine-binding proteins for the treatment of inflammatory and autoimmune diseases. The chemokine receptors are important targets for therapeutic interference in several inflammatory, autoimmune, and infectious diseases, but due to the complex nature of chemokine-receptor interactions, receptor-targeted anti-inflammatory therapies are yet to be found. Although some chemokine-receptor antagonists have been developed to block leukocyte recruitment to treat chemokine-mediated diseases, most chemokine receptor antagonists have failed to show efficacy. Therefore, it is necessary to adopt an alternative approach to target chemokine-receptor interactions.

In nature, ticks have developed a strategy to interfere with the chemokine signalling network, which helps them to remain undetected by the host immune system (Deruaz, 2008). Genome and transcriptome analyses of ticks have led to the discovery of a family of chemokine-binding proteins called Evasins in the tick species *Rhipicephalus sanguineus* (Frauenschuh, 2007).

Since their discovery, Evasins have shown promising results as potential chemokine antagonists in several mouse models of inflammatory diseases (Deruaz 2008). Deruaz *et al*. (2008), reported that Evasin-1, which is highly selective to CCL3 and CCL4, successfully reduced the leukocyte influx, fibrosis, and death in CCL3- dependant bleomycin-induced pulmonary injury in murine models. They also reported that Evasin-3 bound to CXCR2 and thus reduced neutrophil influx into the joint in a model of antigen-induced arthritis. Deruaz *et al* (2013) later reported the chemokine-binding activity of Evasin-4, which is selective to some CC chemokines, however, has a broad specificity and can recognize about 20 different proteins. An attempt to identify an exclusive motif within the amino acid sequence of Evasin-4 to explain its selectivity profile, remains unsuccessful.

In recent years discovery of homologues of Evasins were achieved by Hayward *et al.,* (2017) and Singh *et al* (2017) in separated studies. The last couple of years witnessed the discovery of a number of new Evasins and their new nomenclature was reported by Bhusal *et al*, (2020). They reported two classes of Evasins, Class A Evasins with sequence identity to EVA-1 and -4, and Class B Evasins with sequence identity to Evasin-3.

The current project initially aimed to express and purify ACA-01 a Class A $C_8$-Evasin from the species *Amblyomma cajennense.* ACA-01 was expressed as $His_6$-ACA-01 in insoluble fractions. Expression, purification, and qualitative analysis of His-tagged ACA-01 indicated the protein sample was not homogeneous. The poor yield and quality of $His_6$-ACA-01 produced encouraged us to design a new construct for ACA-01 with a soluble SUMO-tag as an N-terminal tag that could facilitate soluble expression of ACA-01 in *E coli*. After successful expression of $His_6$-SUMO-ACA-01 in the soluble fraction, partial purification was done by IMAC followed by cleavage of the N- terminally tagged $His_6$-SUMO using Ulp1 protease and further purification by IMAC and PSEC. Qualitative analyses by MS and ASEC showed SUMO-tag successfully improved the soluble expression of ACA-01 and resulted in a yield of 2.8 mg/L. From FA binding assays we determined the chemokine-binding activity of ACA-01. ACA-01 was able to bind to all six human CC chemokines tested and the strongest binding of ACA-01 was observed with CCL7/MCP-3 with $pK_d$ of 8.56 ± 0.26 ($K_d$ = 3 nM), and the lowest with CCL24/Etx-2 with $pK_d$ of 6.57 ± 0.2 ($K_d$ = 270 nM). Through FA we have successfully shown that most of the tested chemokines bind to ACA-01 with $K_D$ in nM range. We then aimed to solve its crystal structure. Although we were able to obtain crystal needles of ACA-01, the size of the needles was far too small for X-ray diffraction.

From the outcome of this analysis, we speculated that ACA-01 exists as an equilibrium between a monomer and a dimer. Studies in the future could include analyses of ACA-01 through native gel and analytical ultracentrifugation (AUC) to understand the monomer-dimer equilibrium of ACA-01, i.e., to assess self-association. We have previously used SDS gel which requires the use of SDS (sodium dodecyl sulfate), an anionic detergent. SDS disrupts the tertiary and quaternary structure of the protein. However, native gel is performed by preparing samples in non-denaturing (and non-reducing) buffer which does not denature the structure of the protein. Thus, the protein subunit interactions can be retained, and we can use it to analyse quaternary structures of the protein. To quantify protein self-association, AUC can be used to determine the monomer-dimer equilibrium constant. Sedimentation equilibrium is obtained through AUC which accurately determines native molecular weight of the protein and therefore the stoichiometry of the species in its native form by comparing the native molecular weight with the theoretical molecular weight of the monomeric species (Laue, 1990) (Lebowitz, 2002). If purified ACA-01 is predominantly a single species (all monomer or

all dimer), then dividing the apparent molecular weight by the theoretical molecular weight will provide the stoichiometry. Alternatively, if it exists in equilibrium between monomer and dimer species, the AUC data can be fitted using a model of this equilibrium, thus yielding the $K_d$ for dimerisation.

Another major area of interest could be the structure-function analysis of ACA-01. The only Class A Evasin structure solved till now is Evasin 1:CCL3 (Dias, 2009) in which Evasin-1 binds to CCL3 with 1:1 stoichiometry and the regions of CCL3 that interact with Evasin-1 are the same regions required for binding and activation of chemokine receptors. Based on the published structure of the Evasin-1:CCL3 complex, there are three regions within the Evasin sequence which interact with CCL3. (i) N-terminal, (ii) C- terminal and (iii) the "middle" region (Figure 6.1A). Figure 6.1B and C shows stick and space-filling representation of the four Cys residues of CCL3 (magenta) which forms two conserved disulfide bonds and the corresponding residues of Evasin-1, with which they interact directly. Hydrophobic interactions are formed by each of the CCL3 disulfide bonds, within the CC motif, with Evasin-1 side chains (V-16, P-24, and P-13). Each of these side chains are conserved or substituted by other hydrophobic residues in most other Evasin sequences, including ACA-01 (Figure 6.4). Based on these observations and sequence similarity of Evasin-1 to ACA-01, mutagenesis studies can be designed, whereby chemokine-binding regions of ACA-01 could be truncated and/or mutated including P-18 and F-19, and the chemokine-binding studies of these mutants would give us important insights to selectivity differences.

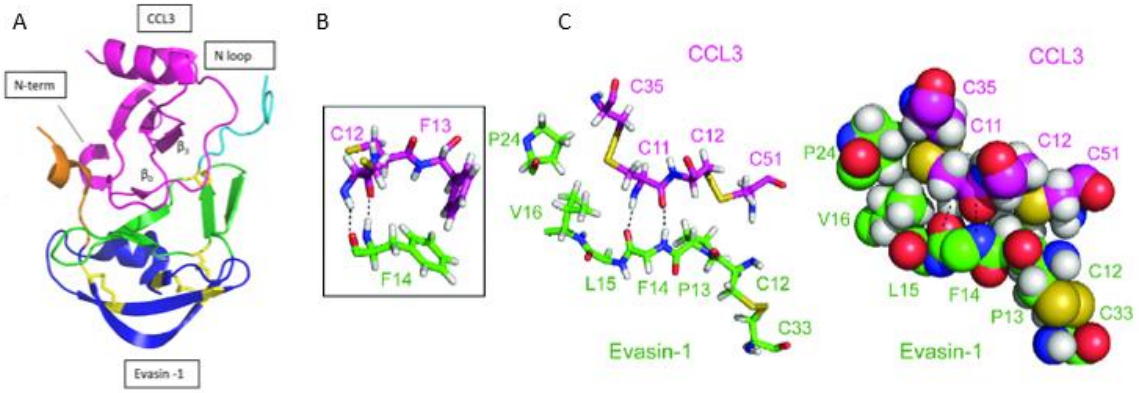


**Figure 6.1: Interface between evasin-1 and the conserved cysteine residues of CCL3.** (A) Ribbon representation illustrating the interacting interface of Evasin-1 with CCL3

(PDB ID: 3FPR). Stick (B) and space-filling (C) representation showing the four Cys residues of CCL3 (designated by magenta carbon backbone and labels) which forms two conserved disulfide bonds and the residues of Evasin-1 (designated by green carbon backbone and labels) with which they directly interact. The first disulfide bond of Evasin-1 (Cys-12 to Cys-33) is also shown as yellow stick. Dashed lines are used to indicate two hydrogen bonds from CCL3 Cys-11 to Evasin-1 Phe-14.

```
Evasin-1        ------EDDEDYGDLGGCPFLVAENKTGYPTIVACKQDCNGTTETAPNGTRCFSIGDEGL  54
ACA-01          ENTQQEEQDYDYG-TDTCPFPVLANKTNKAKFVGCHQKCNGGDQKLTDGTACYVVERKVW  59
                      *:* ***  . *** *  ***.  .:*.*:*.***  :.  :** *: :  :

Evasin-1        RRMTANLPYDCPLGQCSNGDCIPKETYEVCYRRNWRDKKN  94
ACA-01          DRMTPMLWYECPLGECKNGVCEDLRKKEDCRKGNGEEK-- 97
                 ***  * *:****:*.** *   .. * * : * .:*
```

**Figure 6.4: Sequence alignment of Evasin-1 and ACA-01**. Sequence alignment of Evasin-1 and ACA-01 generated from Clustal Omega showing the conserved Cys residues and the corresponding P-18 and F-19 residue in ACA-01.

FA assay was carried out for the purified ACA-01 with 6 human CC chemokines, however, it is not sufficient for understanding chemokine-binding selectivity of ACA-01. Hence future studies could include selection of all 20 human chemokines. Binding studies of ACA-01 could also be done with chemokines from mouse. Although mouse model is usually considered to be important for studying human diseases, research found divergence of human and mouse chemokine clusters (Nomiyama, 2003). One of the important differences is that some chemokines are present in mouse and not in humans and vice versa. In the CXC subfamily, CXCL8 does not have a mouse counterpart, whereas CXCL15 exists in the mouse but not in human. Among the CC subfamily, CCL13 and CCL18 are present in human but not in mouse. Further studies could also include cell-based assays, whereby chemokine signalling via chemokine receptor can be measured by assays which determines the ability of chemokines to inhibit cAMP production. Chemokines bound to ACA-01 would exhibit reduced cAMP production.

For structure elucidation, Circular Dichroism (CD) can be used to analyse the secondary structure of ACA-01. This method measures the difference in absorbance of right- and left-circularly polarized light and can be analysed for the different secondary structural types: alpha helix, parallel and antiparallel beta sheet, and turn. Optimization of the buffer in which we obtained crystal needles of ACA-01 would possibly increase the size

and quality of crystals obtained. In addition, since we can now easily express and purify ACA-01, we can increase the concentration of the protein for crystallization attempts, since increasing concentration of the protein increases the possibility for saturation. We could also attempt to perform crystal trials of ACA-01:chemokine complexes using the chemokines(s) that have high binding affinity for ACA-01, such as CCL7/MCP-3.

In summary, the studies carried out in the expression and purification of ACA-01 have resulted in the successful production of pure soluble ACA-01 which has been shown to bind to 6 human CC chemokines. ACA-01 binds most strongly to CCL7/MCP-3, which is an important regulator in tumorigenesis (Liu, 2018). Neutralization of CCL7 by ACA-01 could be a therapeutic approach for tumour growth. Thus, ACA-01 has the potential to be engineered into a chemokine-antagonist to selectively neutralise the chemokine subsets that contribute to the pathology of inflammatory and autoimmune diseases.

**References:**


Alcami, A. and M. Saraiva (2009). Chemokine binding proteins encoded by pathogens. Pathogen-Derived Immunomodulatory Molecules, *Springer*: 167-179.

Amanda, E. I. P., et al. (2016). "Evasins: therapeutic potential of a new family of chemokine binding proteins from ticks." *Frontiers in Immunology* 7.

Bai, N., et al. (2019). "Isothermal Analysis of ThermoFluor Data can readily provide Quantitative Binding Affinities." *Scientific Reports* 9(1): 2650.

Bannert, N., et al. (2001). "Sialylated O-glycans and sulfated tyrosines in the NH2-terminal domain of CC chemokine receptor 5 contribute to high affinity binding of chemokines." *J. Exp. Med.* 194(11): 1661-1673.

Bhusal, R. P., et al. (2020). "Evasins: Tick Salivary Proteins that Inhibit Mammalian Chemokines." *Trends in Biochemical Sciences* 45(2): 108-122.

Blanchard, C., et al. (2006). "Eotaxin-3 and a uniquely conserved gene-expression profile in eosinophilic esophagitis." *The Journal of clinical investigation* 116(2): 536-547.

Bonvin, P., et al. (2014). "Identification of the pharmacophore of the CC chemokine-binding proteins Evasin-1 and -4 using phage display." *J Biol Chem* 289(46): 31846-31855.

Braunersreuther, V., et al. (2013). "Treatment with the CC chemokine-binding protein Evasin-4 improves post-infarction myocardial injury and survival in mice." *Thromb Haemost* 110(4): 807-825.

Castor, M. G., et al. (2010). "The CCL3/macrophage inflammatory protein-1α–binding protein evasin-1 protects from graft-versus-host disease but does not modify graft-versus-leukemia in mice." *The Journal of Immunology* 184(5): 2646-2654.

Franck, C., et al. (2020). Semisynthesis of an evasin from tick saliva reveals a critical role of tyrosine sulfation for chemokine binding and inhibition. *Proceedings of the National Academy of Sciences*, *117*(23), pp.12657-12664.

Copin, J.-C., et al. (2013). "Treatment with Evasin-3 reduces atherosclerotic vulnerability for ischemic stroke, but not brain injury in mice." *Journal of Cerebral Blood Flow & Metabolism* 33(4): 490-498.

Coussens, L. M., & Werb, Z. (2002). Inflammation and cancer. *Nature*, 420(6917), 860–867.

Crump, M. P., et al. (1997). "Solution structure and basis for functional activity of stromal cell-derived factor-1 dissociation of CXCR4 activation from binding and inhibition of HIV-1." *Embo J.* 16(23): 6996-7007.

Das, A. M., et al. (2006). "Selective inhibition of eosinophil influx into the lung by small molecule CC chemokine receptor 3 antagonists in mouse models of allergic inflammation." *Journal of Pharmacology and Experimental Therapeutics* 318(1): 411-417.

Dell'Agnola, C. and A. Biragyn (2007). "Clinical utilization of chemokines to combat cancer: the double-edged sword." *Expert review of vaccines* 6(2): 267-283.

Denisov, S.S., et al. (2019). Tick saliva protein Evasin-3 modulates chemotaxis by disrupting CXCL8 interactions with glycosaminoglycans and CXCR2. *Journal of Biological Chemistry*, *294*(33), pp.12370-12379.

Deruaz, M., et al. (2008). "Ticks produce highly selective chemokine binding proteins with antiinflammatory activity." *J. Exp. Med.* 205(9): 2019-2031.

Déruaz, M., et al. (2013). "Evasin-4, a tick-derived chemokine-binding protein with broad selectivity can be modified for use in preclinical disease models". *The FEBS journal*, *280*(19), pp.4876-4887.

Deshaies, R. J. (2005). Ubiquitin and Protein Degradation, Part B, Academic Press.

Dias, J. M., et al. (2009). "Structural basis of chemokine sequestration by a tick chemokine binding protein: the crystal structure of the complex between Evasin-1 and CCL3." *PLoS One* 4(12): e8514.

Duma, L., et al. (2007). "Recognition of RANTES by extracellular parts of the CCR5 receptor." *J. Mol. Biol*. 365(4): 1063-1075.

Eaton, J. R., et al. (2018). "The N-terminal domain of a tick evasin is critical for chemokine binding and neutralization and confers specific binding activity to other evasins." *Journal of Biological Chemistry: jbc*. RA117. 000487.

Farrens, D., et al. (1996). "Requirement of Rigid-body motion of transmembrane helices for light activation of rhodopsin." *Science* 274(5288): 768-770.

Frauenschuh, A., et al. (2007). "Molecular cloning and characterization of a highly selective chemokine-binding protein from the tick Rhipicephalus sanguineus." *Journal of Biological Chemistry* 282(37): 27250-27258.

Fujiwara, H., et al. (2002). "Infiltrating eosinophils and eotaxin: their association with idiopathic eosinophilic esophagitis." *Annals of Allergy, Asthma & Immunology* 89(4):

429-432.

Fulkerson, P. C., et al. (2006). "A central regulatory role for eosinophils and the eotaxin/CCR3 axis in chronic experimental allergic airway inflammation." *Proceedings of the National Academy of Sciences* 103(44): 16418-16423.

Georgiou, G. and L. Segatori (2005). "Preparative expression of secreted proteins in bacteria: status report and future prospects." *Current Opinion in Biotechnology* 16(5): 538-545.

González-Motos, V., et al. (2016). "Chemokine binding proteins: An immunomodulatory strategy going viral." *Cytokine & Growth Factor Reviews* 30: 71-80.

Griffith, J. W., et al. (2014). Chemokines and Chemokine Receptors: Positioning Cells for Host Defense and Immunity. *Annu. Rev. Immunol*. 32: 659-702.

Guo, X., et al. (2003). "Determination of molecular weight of heparin by size exclusion chromatography with universal calibration." *Analytical biochemistry* 312(1): 33-39.

Hajnicka, V., et al. (2001). "Anti-interleukin-8 activity of tick salivary gland extracts." *Parasite immunology* 23(9): 483-489.

Han, J. and R. J. Ulevitch (2005). "Limiting inflammatory responses during activation of innate immunity." *Nat Immunol* 6(12): 1198-1205.

Hayward, J., et al. (2017). "Ticks from diverse genera encode chemokine-inhibitory evasin proteins." *J. Biol. Chem.* 292(38): 15670-15680.

Heidarieh, H., et al. (2015). "Immune modulation by virus-encoded secreted chemokine binding proteins." *Virus research* 209: 67-75.

Hong, P., et al. (2012). "A review size-exclusion chromatography for the analysis of protein biotherapeutics and their aggregates." *Journal of liquid chromatography & related technologies* 35(20): 2923-2950.

Huttner, W. B. (1982). "Sulphation of tyrosine residues—a widespread modification of proteins." *Nature* 299: 273.

Huynh, K. and C. L. Partch (2015). "Analysis of protein stability and ligand interactions by thermal shift assay." *Current protocols in protein science* 79(1): 28.29. 21-28.29. 14.

Kaburagi, Y., et al. (2001). "Enhanced production of CC-chemokines (RANTES, MCP-1, MIP-1α, MIP-1β, and eotaxin) in patients with atopic dermatitis." *Archives of dermatological research* 293(7): 350-355.

Kobilka, B. K. and X. Deupi (2007). "Conformational complexity of G-protein-coupled receptors." *Trends in pharmacological sciences* 28(8): 397-406.

Larose, M.-C., et al. (2015). "Correlation between CCL26 production by human bronchial epithelial cells and airway eosinophils: Involvement in patients with severe eosinophilic asthma." Journal of Allergy and Clinical Immunology 136(4): 904-9

Laue, T.M. and Rhodes, D.G., (1990). Determination of size, molecular weight, and presence of subunits. In *Methods in enzymology* (Vol. 182, pp. 566-587). Academic Press.

Lebowitz, J., et al. (2002). Modern analytical ultracentrifugation in protein science: a tutorial review. *Protein science*, *11*(9), pp.2067-2079.

Lee, A. W., et al. (2019). "A knottin scaffold directs the CXC-chemokine–binding specificity of tick evasins." *Journal of Biological Chemistry* 294(29): 11199-1121

Lee, C.-D., et al. (2008). "An improved SUMO fusion protein system for effective production of native proteins." *Protein science: a publication of the Protein Society* 17(7): 1241-1248.

Lee, R. W. and W. B. Huttner (1983). "Tyrosine-O-sulfated proteins of PC12 pheochromocytoma cells and their sulfation by a tyrosylprotein sulfotransferase." *J Biol Chem* 258(18): 11326-11334.

Liu, J., et al. (2008). "Tyrosine Sulfation Is Prevalent in Human Chemokine Receptors Important in Lung Disease." *American Journal of Respiratory Cell and Molecular Biology* 38(6): 738-743.

Liu Y, et al. (2018). Crucial biological functions of CCL7 in cancer. *PeerJ* 6:e4928

Lodowski, D. T., et al. (2009). "Comparative Analysis of GPCR Crystal Structures†." *Photochemistry and Photobiology* 85(2): 425-430.

Loutsios, C., et al. (2014). "Biomarkers of eosinophilic inflammation in asthma." *Expert review of respiratory medicine* 8(2): 143-150.

Ludeman, J. P. and M. J. Stone (2014). "The structural role of receptor tyrosine sulfation in chemokine recognition." *British Journal of Pharmacology* 171(5): 1167-1179.

Mackay, C. R. (2008). "Moving targets: cell migration inhibitors as new anti-inflammatory therapies." *Nat Immunol* 9(9): 988.

Mierke, C. T. (2018). Inflammation and cancer. *Physics of Cancer*, Volume 1 (Second Edition), IOP Publishing: 2-1-2-51.

Millard, C. J., et al. (2014). "Structural basis of receptor sulfotyrosine recognition by a CC chemokine: the N-terminal region of CCR3 bound to CCL11/eotaxin-1." *Structure* 22(11): 1571-1581.

Montecucco, F., et al. (2010). "Single administration of the CXC chemokine-binding protein Evasin-3 during ischemia prevents myocardial reperfusion injury in mice." *Arteriosclerosis, thrombosis, and vascular biology* 30(7): 1371-1377.

Montecucco, F., et al. (2014). "Treatment with Evasin-3 abrogates neutrophil-mediated inflammation in mouse acute pancreatitis." *European Journal of Clinical Investigation* 44(10): 940-950.

Morokata, T., et al. (2006). "A novel, selective, and orally available antagonist for CC chemokine receptor 3." *Journal of Pharmacology and Experimental Therapeutics* 317(1): 244-250.

Moser, B. and P. Loetscher (2001). "Lymphocyte traffic control by chemokines." *Nat Immunol* 2(2): 123-128.

Mueller, S. N., et al. (2007). "Regulation of homeostatic chemokine expression and cell trafficking during immune responses." *Science* 317(5838): 670-674.

Nagase, H., et al. (2001). "Regulation of chemokine receptor expression in eosinophils." *International archives of allergy and immunology* 125(Suppl. 1): 29-32.

Nguyen, L. T. and H. J. Vogel (2012). "Structural perspectives on antimicrobial chemokines." *Frontiers in Immunology* 3: 384-384.

Nomiyama H, Egami K, Tanase S, et al. (2003). "Comparative DNA sequence analysis of mouse and human CC chemokine gene clusters". *J Interferon Cytokine Res*.;23(1):37-45.

Panavas, T., et al. (2009). SUMO fusion technology for enhanced protein production in prokaryotic and eukaryotic expression systems. SUMO protocols, *Springer*: 303-317.

Park, S. H., et al. (2012). "Structure of the chemokine receptor CXCR1 in phospholipid bilayers." *Nature* 491(7426): 779-783.

Pawig, L., et al. (2015). "Diversity and Inter-Connections in the CXCR4 Chemokine Receptor/Ligand Family: Molecular Perspectives." *Front Immunol* 6: 429.

Proudfoot, A. E., et al. (2010). "Anti-chemokine small molecule drugs: a promising future?" *Expert opinion on investigational drugs* 19(3): 345-355.

Proudfoot, A. E. I. (2002). Chemokine receptors: Multifaceted therapeutic targets. *Nat. Rev. Immunol.* 2: 106-115.

Punchard Neville, A., et al. (2004). "The Journal of Inflammation." *Journal of Inflammation* 1(1): 1.

Qin L, Kufareva I, Holden LG, et al. Structural biology. Crystal structure of the chemokine receptor CXCR4 in complex with a viral chemokine. *Science*. 2015;347(6226):1117-1122

Rajagopal, S., et al. (2013). "Biased agonism as a mechanism for differential signaling by chemokine receptors." J Biol Chem 288(49): 35039-35048.

Rajagopalan, L. and K. Rajarathnam (2006). Structural basis of chemokine receptor function - A model for binding affinity and ligand selectivity. *Biosci. Rep*. 26: 325-339.

Roth, N., et al. (2011). "Distinct eosinophil cytokine expression patterns in skin diseases–the possible existence of functionally different eosinophil subpopulations." *Allergy* 66(11): 1477-1486.

Russo, R. C., et al. (2011). "Therapeutic effects of evasin-1, a chemokine binding protein, in bleomycin-induced pulmonary fibrosis." *Am J Respir Cell Mol Biol* 45(1): 72-80.

Sabroe, I., et al. (2000). "A small molecule antagonist of chemokine receptors CCR1 and CCR3 potent inhibition of eosinophil function and CCR3-mediated HIV-1 entry." *Journal of Biological Chemistry* 275(34): 25985-25992.

Schumann, W. and L. C. S. Ferreira (2004). "Production of recombinant proteins in Escherichia coli." *Genetics and Molecular Biology* 27(3): 442-453.

Schwarz, M. K. and T. N. Wells (2002). "New therapeutics that modulate chemokine networks." *Nature Reviews Drug Discovery* 1(5): 347-358.

Seet, B. T. and G. McFadden (2002). "Viral chemokine-binding proteins." *Journal of leukocyte biology* 72(1): 24-34.

Senthilkumar, B. and Rajasekaran, R., 2017. Analysis of the structural stability among cyclotide members through cystine knot fold that underpins its potential use as a drug scaffold. *International Journal of Peptide Research and Therapeutics*, *23*(1), pp.1-11.

Simon, D., et al. (2010). "Organ-specific eosinophilic disorders of the skin, lung, and gastrointestinal tract." *Journal of Allergy and Clinical Immunology* 126(1): 3-13.

Singh, K., et al. (2017). "Yeast surface display identifies a family of evasins from ticks with novel polyvalent CC chemokine-binding activities." *Sci Rep* 7(1).

Skelton, N. J., et al. (1999). "Structure of a CXC chemokine-receptor fragment in complex with interleukin-8." *Structure* 7(2): 157-168.

Smith, P., et al. (2005). "Schistosoma mansoni secretes a chemokine binding protein with antiinflammatory activity." *The Journal of experimental medicine* 202(10): 1319-1325.

Steven, F. M. and J. B. Martin (2005). "Mechanisms of Disease: inflammation and the origins of cancer." *Nature Clinical Practice Oncology* 2(2): 90.

Stone, K. D., et al. (2010). "IgE, mast cells, basophils, and eosinophils." *Journal of Allergy and Clinical Immunology* 125(2): S73-S80.

Stone, M., et al. (2009). Tyrosine sulfation: an increasingly recognised post-translational modification of secreted proteins. *New Biotech*. 25: 299-317.

Stone, M. J., et al. (2017). "Mechanisms of Regulation of the Chemokine-Receptor Network." *Int J Mol Sci* 18(2).

Stone, M. J. and R. J. Payne (2015). "Homogeneous sulfopeptides and sulfoproteins: Synthetic approaches and applications to characterize the effects of tyrosine sulfation on biochemical function." *Accounts of chemical research* 48(8): 2251-2261.

Striegel, A., et al. (2009). Modern size-exclusion liquid chromatography: practice of gel permeation and gel filtration chromatography, John Wiley & Sons.

Studier, F. W. and B. A. Moffatt (1986). "Use of bacteriophage T7 RNA polymerase to direct selective high-level expression of cloned genes." *Journal of Molecular Biology* 189(1): 113-130.

Stulk, K., et al. (2003). "Some potentialities and drawbacks of contemporary size-exclusion chromatography." *Journal of biochemical and biophysical methods* 56(1-3): 1-13.

Szpakowska, M., et al. (2012). "Function, diversity and therapeutic potential of the N-terminal domain of human chemokine receptors." *Biochem. Pharmacol*. 84: 1366-1380.

Tan, J., et al. (2013). "Tyrosine Sulfation of Chemokine Receptor CCR2 Enhances Interactions with Both Monomeric and Dimeric Forms of the Chemokine Monocyte Chemoattractant Protein-1 (MCP-1)." *J. Biol. Chem*. 288(14): 10024-10034.

Terpe, K. (2006). Overview of bacterial expression systems for heterologous protein production: from molecular and biochemical fundamentals to commercial systems. K. Terpe. 72: 211-222.

Thiele, S. and M. M. Rosenkilde (2014). "Interaction of Chemokines with their Receptors - From Initial Chemokine Binding to Receptor Activating Steps." *Curr. Med. Chem*. 21(31): 3594-3614.

Vander Heyden, Y., et al. (2002). "Evaluation of size-exclusion chromatography and size-exclusion electrochromatography calibration curves." *Journal of Chromatography* A 957(2): 127-137.

Veldkamp, C. T., et al. (2006). "Recognition of a CXCR4 sulfotyrosine by the chemokine stromal cell-derived factor-1 alpha (SDF-1 alpha/CXCL12)." *J. Mol. Biol*. 359(5): 1400-1409.

Veldkamp, C. T., et al. (2008). "Structural basis of CXCR4 sulfotyrosine recognition by the chemokine SDF-1/CXCL12." *Science signaling* 1(37): ra4-ra4.

Vieira, A. T., et al. (2009). "Treatment with a novel chemokine-binding protein or eosinophil lineage-ablation protects mice from experimental colitis." *The American journal of pathology* 175(6): 2382-2391.

Wang, W., 1999. Instability, stabilization, and formulation of liquid protein pharmaceuticals. *International journal of pharmaceutics*, *185*(2), pp.129-188.

Wang, X., et al. (2017). Sulfation of the human cytomegalovirus protein UL22A enhances binding to the chemokine RANTES. *Angewandte Chemie International Edition*, *56*(29), pp.8490-8494.

Wells, T. N., et al. (2006). "Chemokine blockers–therapeutics in the making?" *Trends in pharmacological sciences* 27(1): 41-47.

Wise, E. L., et al. (2007). "Small molecule receptor agonists and antagonists of CCR3 provide insight into mechanisms of chemokine receptor activation." *Journal of Biological Chemistry* 282(38): 27935-27943.

Wittchen E. S. (2009). Endothelial signaling in paracellular and transcellular leukocyte transmigration. *Frontiers in bioscience* (Landmark edition), 14, 2522–2545.

Yan, L., et al. (2006). "Therapeutic potential of cytokine and chemokine antagonists in cancer therapy." *European journal of cancer* 42(6): 793-802.

Zabetakis, D., et al. (2014). "Evaluation of disulfide bond position to enhance the thermal stability of a highly stable single domain antibody." *PLoS One* 9(12): e115405.

Zheng, D., et al. (2012). "Virus-derived anti-inflammatory proteins: potential therapeutics for cancer." *Trends in molecular medicine* 18(6): 304-310.

Zlotnik, A. and O. Yoshie (2012). "The chemokine superfamily revisited." *Immunity* 36(5): 705-716.

# Appendix I

## Calibration data for Yarra SEC 2000

Table 1.1: Elution times for different protein standards used for development of calibration of Yarra SEC – 2000 column

| Component | Elution Time/ min | Elution Volume/ ml | Molecular Weight/ Da | Log Mr |
|---|---|---|---|---|
| Thyroglobulin bovine | 5.6 | 2.0 | 670000 | 5.83 |
| γ- globulin from bovine blood | 7.1 | 2.5 | 150000 | 5.18 |
| Albumin chicken grade VI | 8.1 | 2.8 | 44300 | 4.65 |
| Ribonuclease A type-A from bovine pancreas | 9.8 | 3.4 | 13700 | 4.14 |
| pABA | 11.8 | 4.1 | 137 | 2.14 |

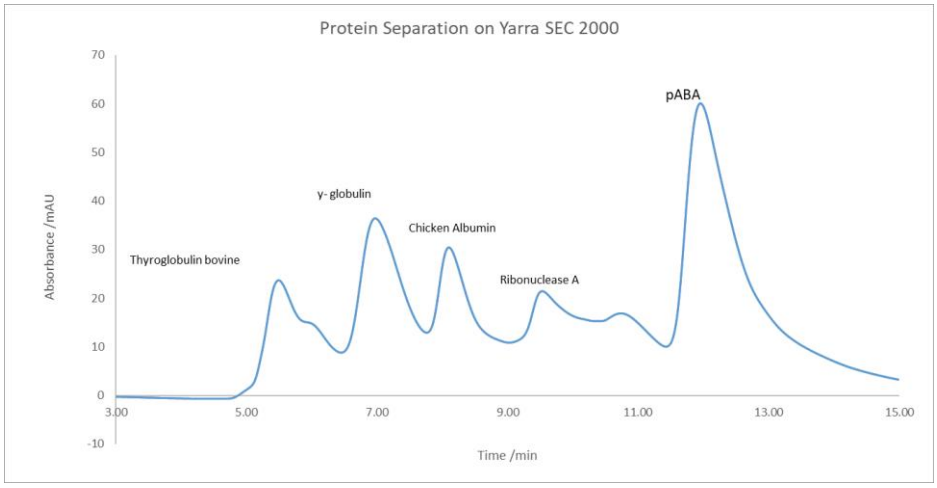


**Figure 1.1: ASEC chromatogram showing normalized elution time for protein standards used.** A series of five protein standards was analysed by ASEC. The column used was Yarra SEC-2000 µm; phosphate buffer was used as mobile phase at a flow rate of 0.35 ml/min. Protein elution was observed over time. Bovine thyroglobulin with the highest MW was eluted earliest while pABA with the lowest MW was eluted at last. This column was the same that is used for all the ASEC analysis for the purpose of this thesis.

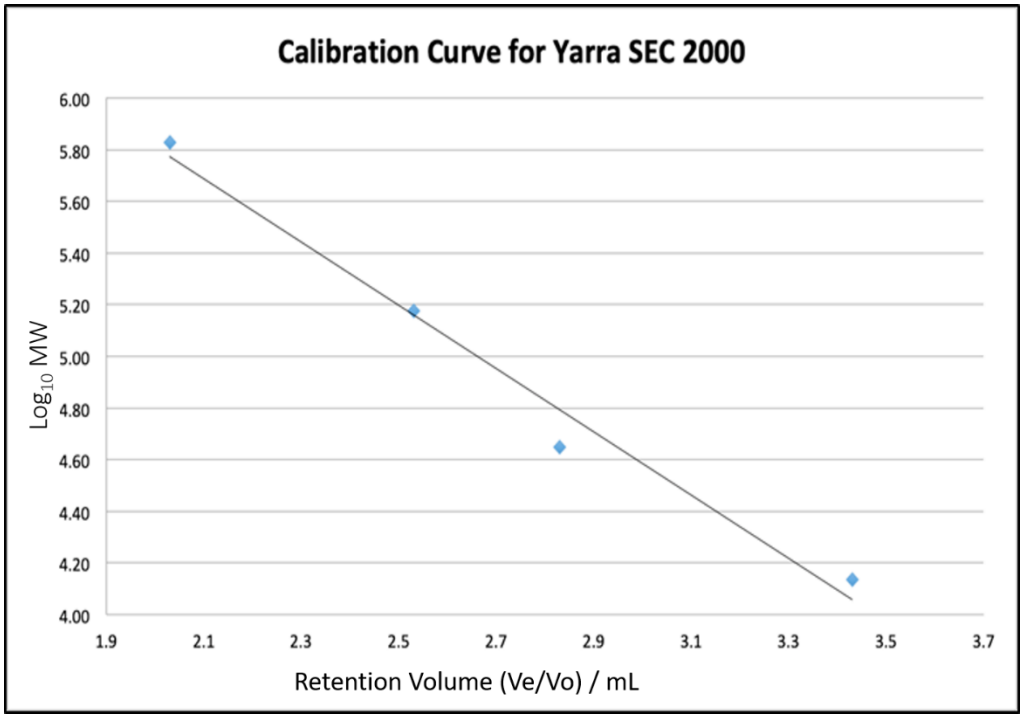


**Figure 1.2: Calibration Curve for Yarra SEC-2000.** Retention Volume (Ve/Vo) vs log MW from the chromatogram in Figure 1.1 was plotted to generate a calibration curve. Since pABA is too small, it was excluded from the calibration curve. Four data points were considered that were mostly relevant to the MW of ACA-01 (11 kDa). The equation generated was y = -1.1904x + 8.0856, which was used to prepare table 1.2 for estimation of the apparent MW of proteins.

Table 1.2: Look up table for estimation of the apparent molecular weight of proteins

| Elution Time (min) | Elution Vol-Ve (mL) | Retention Vol-Ve/Vo (mL) | Apparent MW |
|---|---|---|---|
| 8.9 | 31.29 | 3.12 | 25553 |
| 9 | 31.59 | 3.15 | 23152 |
| 9.1 | 32.00 | 3.19 | 20975 |
| 9.2 | 32.30 | 3.22 | 19004 |
| 9.3 | 32.60 | 3.25 | 17218 |
| 9.4 | 33.00 | 3.29 | 15599 |
| 9.5 | 33.30 | 3.32 | 14133 |
| 9.6 | 33.70 | 3.36 | 12805 |
| 9.7 | 34.00 | 3.39 | 11601 |
| 9.8 | 34.40 | 3.43 | 10511 |
| 9.9 | 34.70 | 3.46 | 9523 |

## APPENDIX II

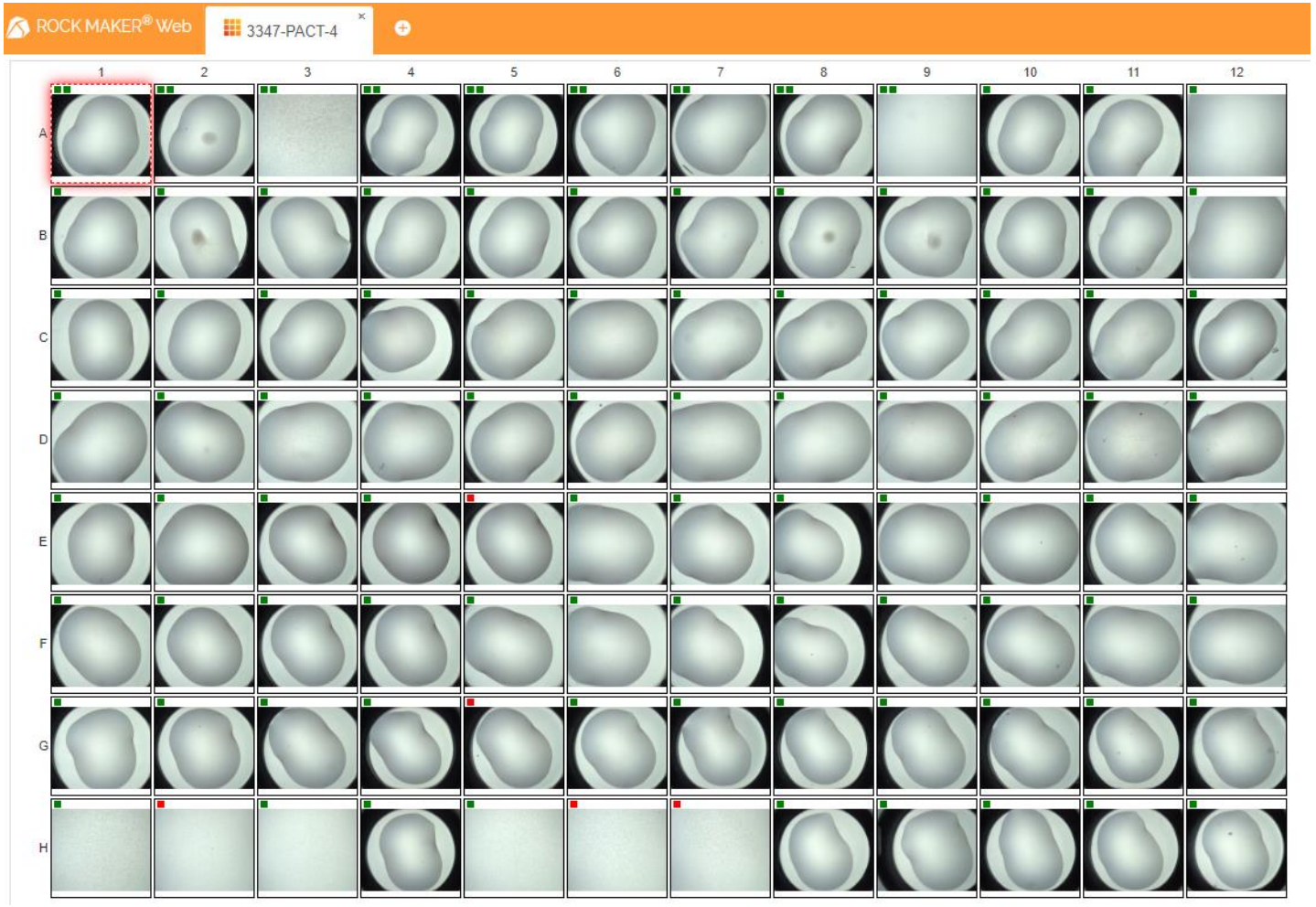


**Figure 2.1: Images from Rockmaker® for crystal trials of ACA-01 in PACT-4**: 28 drops showed some precipitate formation. PACT-4 contains PEG as the precipitant. Drops A2, B2, B8-9 shows precipitates which were most likely debris

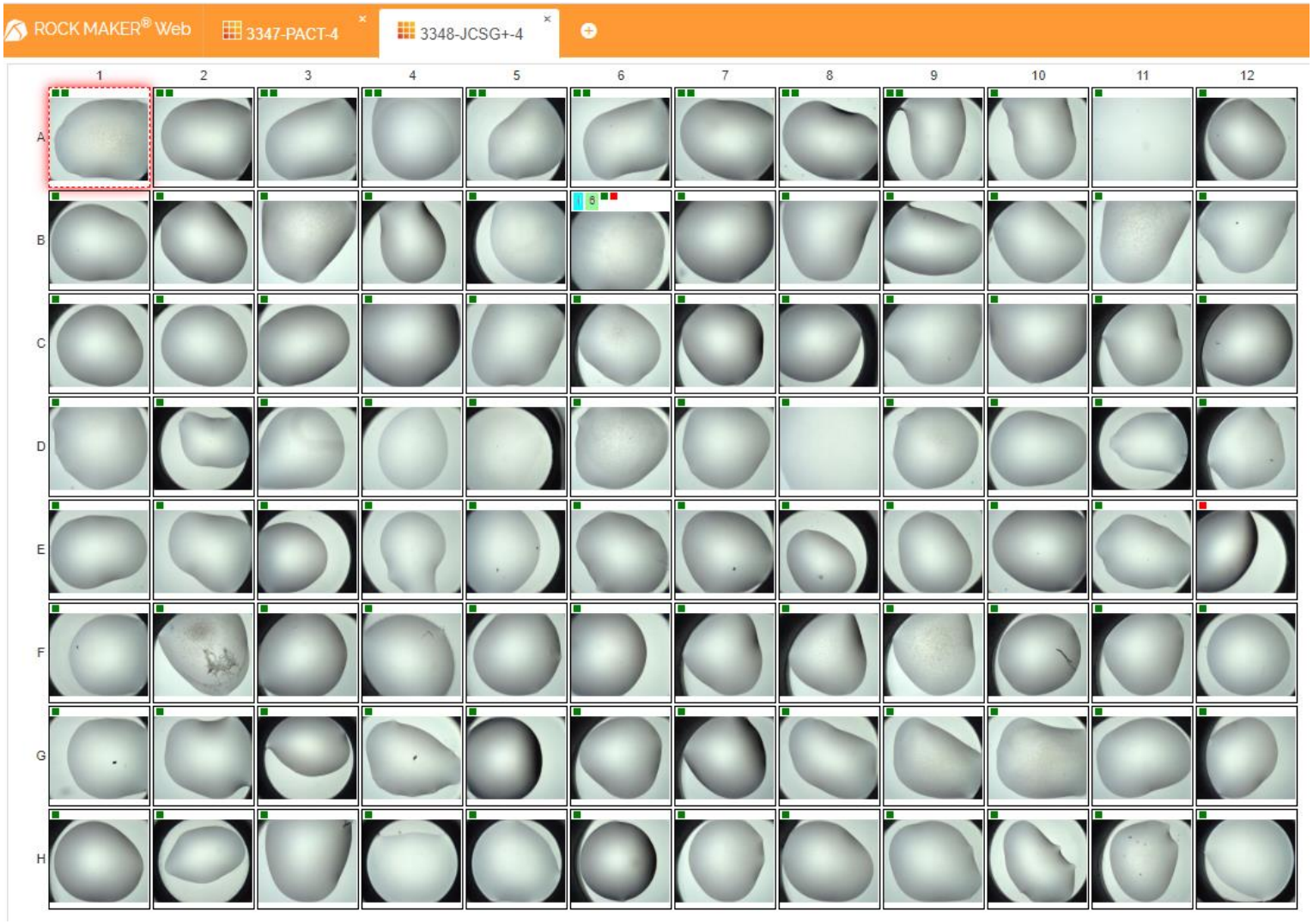


**Figure 2.2: Images from Rockmaker® for crystal trials of ACA-01 in JCSG+**. In JCSG+ we observed precipitates in 28 drops, mostly containing Bis-Tris and HEPES buffer. B6 drop image showed needle formation of ACA-01.

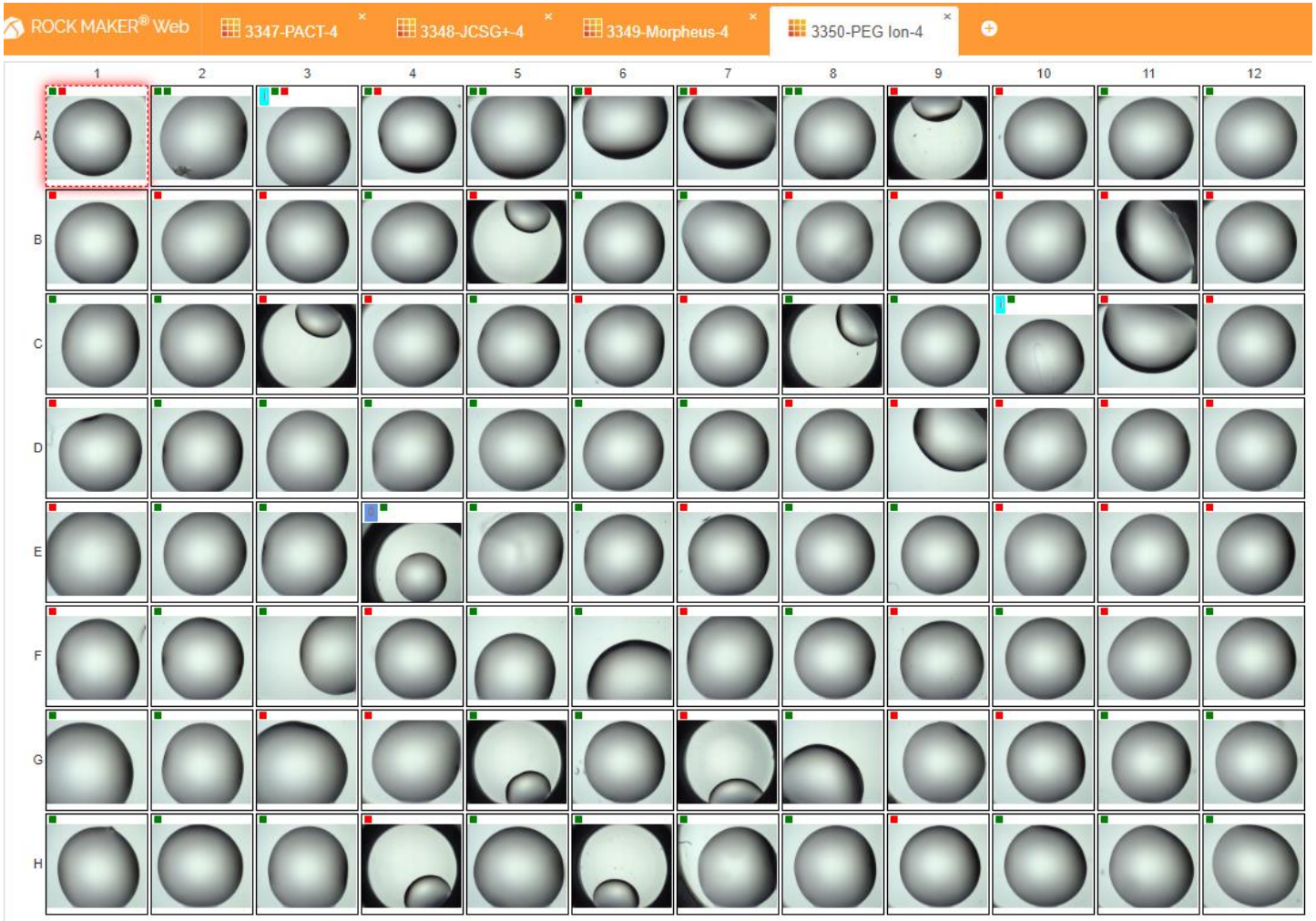


**Figure 2.3: Images from Rockmaker® for crystal trials of ACA-01 in Morpheus-4:** All 96 drops in the tray of PEG Ion-4 condition were clear.

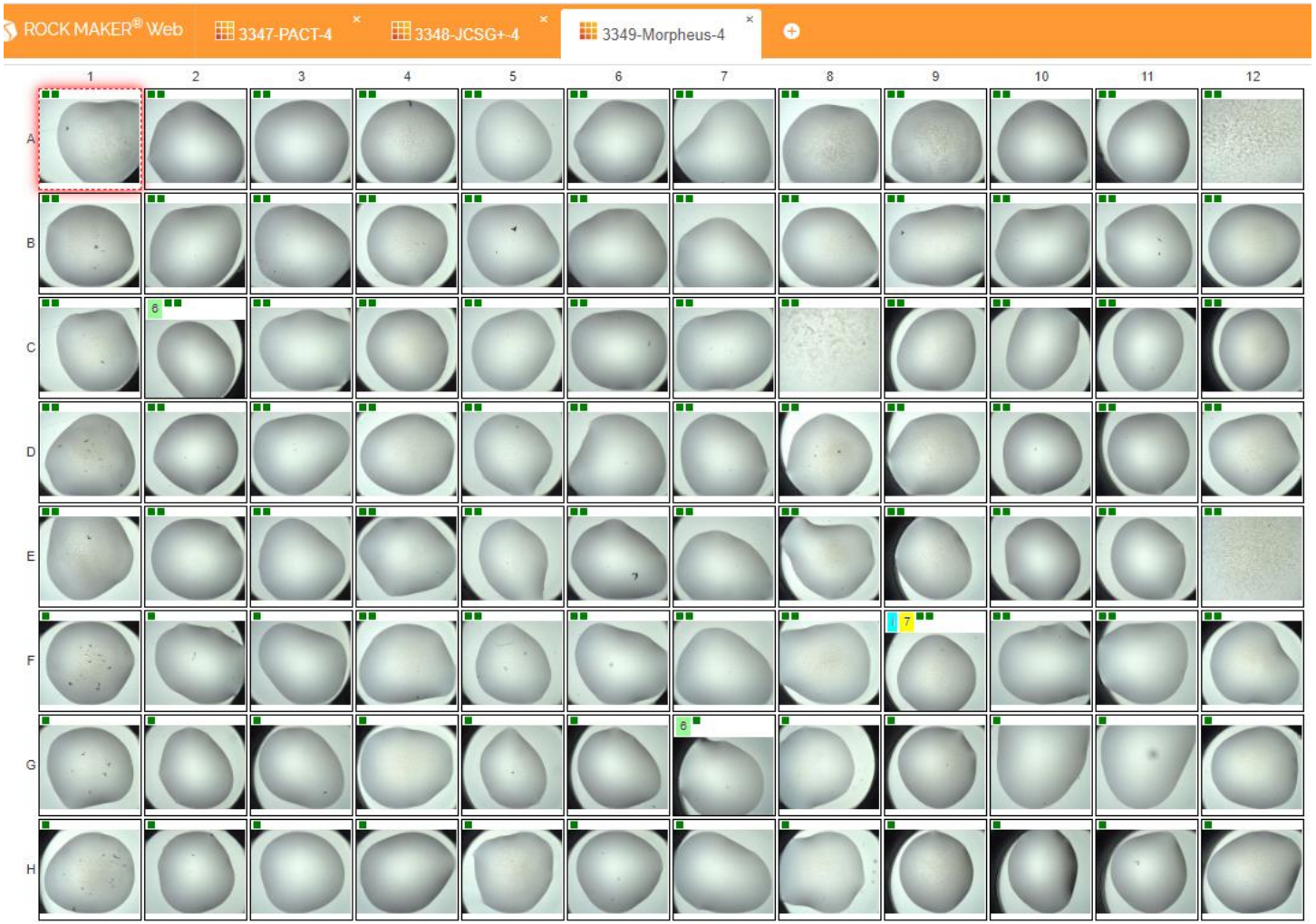


**Figure 2.4: Images from Rockmaker® for crystal trials of ACA-01 in Morpheus-4:** In Morpheus-4 we observed 28 drops with phase separation and precipitate but no nucleation. Amorphous precipitate images were observed in 14 drops, which could be dirt, glass or debris.

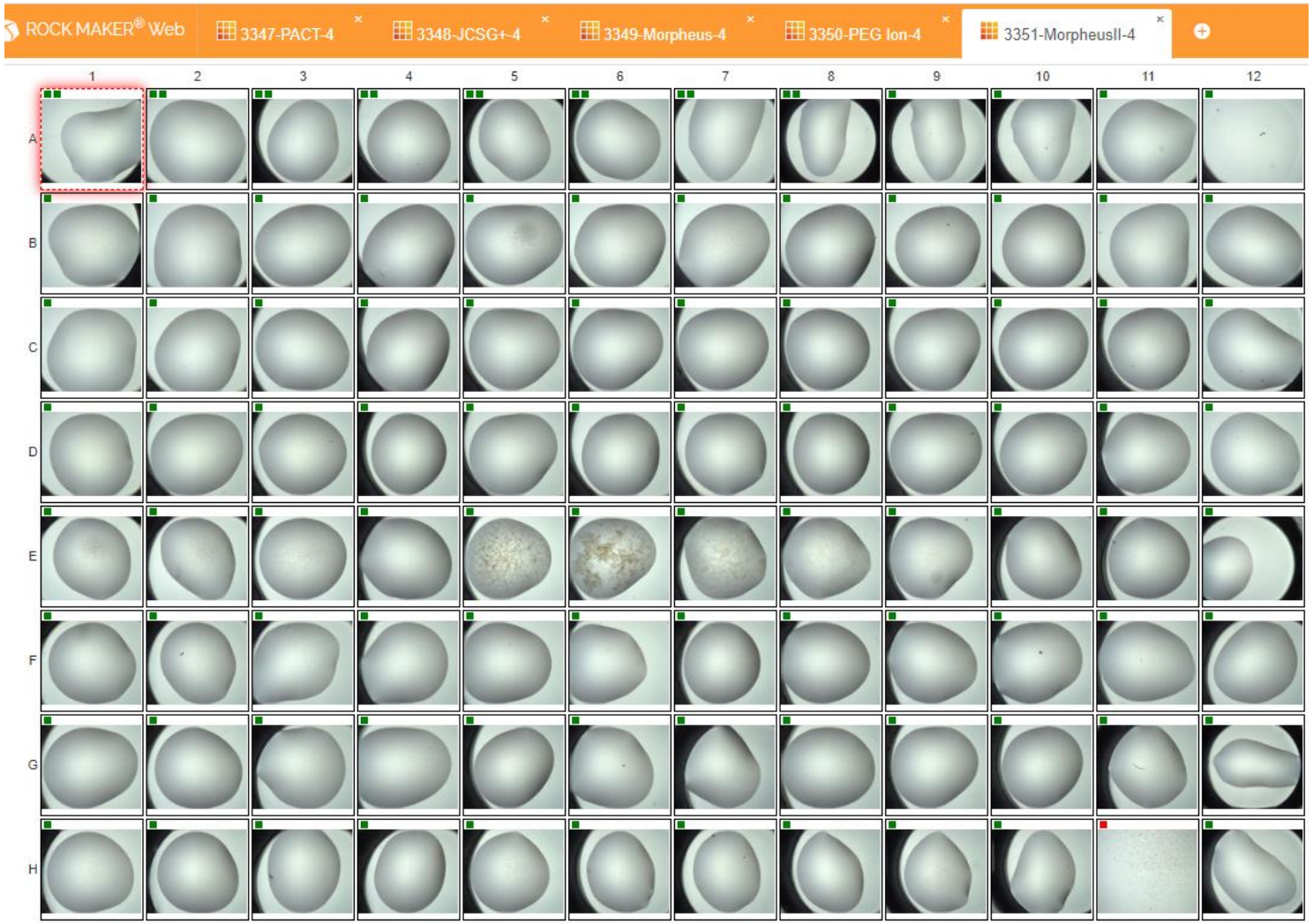


**Figure 2.5: Images from Rockmaker® for crystal trials of ACA-01 in Morpheus-II:** In Morpheus-II we observed precipitates in 27 drops. Drops E5-E7 had precipitates with denatured protein in them.